Kochi University of Technology Academic Resource Repository

Title	Evidence for adaptation at multi-levels for stereo-curvature aftereffects
Author(s)	YAN, Pengfei
Citation	高知工科大学, 博士論文.
Date of issue	2015-03
URL	http://hdl.handle.net/10173/1276
Rights	
Text version	ETD

Kochi, JAPAN
http://kutarr.lib.kochi-tech.ac.jp/dspace/

Evidence for adaptation at multi-level for stereo-curvature aftereffects

Pengfei YAN

A dissertation submitted to the Kochi University of Technology
for the degree of

Doctor of Philosophy

Hiroaki SHIGEMASU, Chair
Keizo SHINOMORI
Hiroshi KADOTA
Kiyoshi NAKAHARA
Shinichi YOSHIDA

Engineering Course,

Department of Engineering,

Graduate School of Engineering

Kochi University of Technology

February 2015

Copyright © 2015 Pengfei YAN

All Rights Reserved

ABSTRACT

Evidence for adaptation at multi-level for stereo-curvature aftereffects

Pengfei YAN
Department of Information System
Doctor of Philosophy

As one of most accurate cue for 3D depth percetion, binocular disparity has been widely used to make visual stimuli in stereopsis field. As a visual phenomenon for disparity-defined stereoscopic surfaces curved in depth, Stereo-curvature aftereffect (sCAE) is due to stereo-curvature adaptation. Specifically, after prolonged inspection of binocular surfaces curved in depth, stereo-curvature adaptation gives rise to shifts in perceived curvature for afterwards shown 3D surfaces. Furthermore, there have been neural evidences to support influence of the adaptation on extraction of depth structure from disparity.

However, previous studies have not agreed on whether stereo-curvature adaptation occurs to single or multiple sources along visual processing level. There should be disparity- or percept-related sources, which decide distinct dependency of sCAE on retinal position. We predicted multi-level adaptation for sCAE, based on results of previous studies on stereo-depth and stereo-slant aftereffects. In our study, both phychophysical (Experiment 1 and Experiment 2) and hemodynamical methods (Experiment 3) were used to probe multi-level adaptation of sCAE.

Experiment 1 investigated whether sCAE is dependent on retinal position and stimulus size, by dynamically altering location or size of adaptation stimuli with static fixation. Experiment 2, including three sub-experiments, aimed to clarify what shape properties are adapted for disparity-defined 3D surfaces. Experiment 2.1 examined how eccentricity influenced adaptation strength using static adaptation stimuli with different eccentricities; Experiment 2.2 tested a hypothesis about adaptation to percept-related primitive shape index (PSI) by dynamically scaled adaptation stimuli; and Experiment 2.3 tested another hypothesis on adapting disparity-specified average disparity information (ADI) using dynamic adaptation stimuli with changing PSI. The results showed retinal-position dependent and scale independent sCAE. In addition to possible eccentricity effect, the retinal-position dependence can result from ADI adaptation. And the scale independence can be attributed to PSI adaptation. These findings show that sCAE is caused by adaptation at both disparity-specified and percept-specified stages and that there are two parallel adapting processes with opposite dependency on retinal position.

The subsequent Experiment 3, using fMRI adaptation paradigm, provided neural evidences to multi-level stereo-curvature adaptation. We probed adaptation to both disparity-related (disparity & ADI) and percept-related (shape curvature & PSI) sources across 13 ROIs selective to disparity or for 3D shape. To separately investigate adaptation to distinct sources, adaptation stimuli involved dynamic change on size and PSI. Unlike psychophysical

study, adaptation to both disparity and ADI was smeared by moving fixation along Lissajous path in depth. We found adaptation to size-variant shape curvature in POIPS region as well as adaptation to size-invariant PSI in early region (VP), ventro-lateral areas (hV4, LO) and IPS regions (VIPS/V7*, DIPS). This is largely consistent of the widely accepted viewpoint that dorsal visual pathway encodes depth structure metrically while ventral pathway does this categorically. Results also showed disparity adaptation in early areas (V1-V2) and middle dorsal area (KO/V3B), as well as ADI adaptation in high dorsal area (V7) and IPS areas (VIPS/V7*, POIPS and DIPS), suggesting that high dorsal areas may involve a low-order calculation of disparity averaging compared with early and middle dorsal areas. Therefore, multi-level stereo-curvature adaptation, found in the psychophysical study, can be further verified in our fMRI study.

Keywords: disparity, stereo-curvature adaptation, fMRI adaptation, 3D shape perception

ACKNOWLEDGMENTS

First and foremost, I am deeply indebted to my advisor Dr. SHIGEMASU Hiroaki. Thank you to allow me to join our laboratory and to provide me with the opportunity to psychophysical field and to touch brain science. Also you always promoted me with expertise and insightful suggestion for my Ph.D study, from establishment of research topic through experiment designs to data analysis, especially in retinotopic mapping experiment.

Thanks to all subjects of my psychophysical and fMRI experiments. I would never have been able to finish my experiments without your participants.

Besides my advisor, I would like to express great appreciation to my sub-advisors, Dr. SHINOMORI Keizo, Dr. KADOTA Hiroshi, Dr. NAKAHARA Kiyoshi and Dr. YOSHIDA Shinichi, who spent precious time on supervising my research. Especially for Dr. KADOTA, who also provided technical assistance on data acquisition in my fMRI experiment.

Acknowledge also goes to all members in the lab of mine. You helped a lot during my doctorate career, so I have a happy lab life. Here, I would like to express my sincere gratitude to YABE Yoshiko sensei, who provided essential help in experiment design of our EEG study.

A special appreciation and thank to my close friends including GAO Yang, WANG Pengyu, AN Tingyu, SHEN Bo, WANG Yina, WANG Lingling, HOU Liyuan, LI Zhiwei, MA Ruiqing and ZHANG Yang. You usually provided me with much convenience and comfort in daily life.

Last but not the least, I will be forever grateful to my families, including my parents, elder sister and little brother. You always support me spiritually throughout my life.

Contents

List of Figures

List of Tables

Chapter 1

Outline

There are numerous cues for depth perception. As one of most accurate cues, binocular disparity provides important means to investigate stereopsis on primate. Absolute disparity assists us to perceive single dot somewhere in depth, disparity gradient to 3D slant surfaces and disparity curvature to 3D curved surfaces. Usually, we make disparity-defined object stimuli to investigate 3D shape perception, even though the objects do not exist in real world.

Stereo-curvature aftereffects (sCAE) is a visual phenomenon, mostly investigated when viewing disparity-defined 3D shapes. After prolonged inspection of stereoscopic surfaces curved in depth, stereo-curvature adaptation gives rise to shifts in perceived curvature for subsequently shown 3D surfaces. Although sCAE may not be perceptible for real objects involving multiple depth cues other than binocular disparity, the adaptation has been confirmed to affect estimation of depth structure from disparity. However, there has been no agreement on whether the adaptation occurs at a disparity-specified stage, a percept-specified stage, or both. Moreover, the related studies have not drawn definite conclusions on the dependency of sCAE on retinal-position and scale so far. For these reasons, it is worth investigating the adapting mechanism of stereo-curvature aftereffects in order to find

out more about how a 3D shape is perceived.

In our study, sCAE was predicted to be due to multi-level adaptation - not solely to shape-curvature adaptation - based on previous findings of multi-stage adaptation found for stereo-depth aftereffects (sDAE) and stereo-slant aftereffects (sSAE). A major challenge for the prediction is to separately examine each possible adaptation source. Unlike previous studies, we did not directly isolate adaptation to disparity and shape curvature. Instead, two new 3D shape properties, namely, disparity-specified ADI (Average Disparity Information) and percept-specified PSI (Primitive Shape Index), were originally investigated as possible adaptation sources of sCAE. The purpose of our study is to find psychophysical and neural evidences to support the prediction of multi-level stereo-curvature adaptation. To this end, two psychophysical experiments and one fMRIa experiment were conducted in our study.

The main content of the dissertation includes six chapters divided into two parts, with Part I including Chapter 3 - 6 and with Part II containing the following chapter 7 - 8. Part I provides detailed information for our psychophysical study, and Part II for our fMRI study. Lastly, the conclusion of our study is drawn in Chapter 9.

This dissertation begins, in Chapter 1, with introducing research background, objectives and dissertation organization. Thereafter, we listed and ranked, in Chapter 2, all possible adaptation sources when adapted with disparity-defined 3D shapes. Chapter 2 lists all possible adaptation sources for sCAE, including those examined in previous studies and two other our-defined sources. These newly-defined sources include disparity-specified ADI and percept-specified PSI. Besides, all of the adaptation sources are ranked into different adaptation levels, in terms of disparity order and their dependence on dynamic changes mentioned above.

Part I, covering Chapter 3 - 6, details our psychophysical study including two main experiments. Chapter 3 firstly reviews previous psychophysical studies on stereoscopic aftereffects

(including sDAE, sSAE and sCAE) from the aspects of adapting mechanism as well as dependency on retinal-position and sale. For adapting mechanism, the review showed disagreement on what adaptation sources were adapted, disparity, shape curvature or both. To tackle this question, multi-level adaptation was predicted for sCAE in our study. Moreover, we suggested to use dynamically-presented surfaces as adaptation stimuli, for one reason that static stimuli used in previous studies are obviously suitable to separately examine each possible adaptation source. Another disagreement indicated from the review concerned on whether or not sCAE was dependent on retinal-position and scale. We predicted that there may be two parallel adaptation processes with opposite dependency on retinal position for sCAE. In detail, adapting to percept-specified sources may induce retinal-position independent sCAE, while adapting to disparity-specific sources may produce retinal-position dependent sCAE. Another reason why we used dynamic adaptation stimuli is just to verify the prediction.

Chapter 4 describes the details of Experiment 1, aiming to investigate dependency of sCAE on retinal position and scale. Adaptation stimuli were presented with dynamically changed retinal-position, scale or PSI, when test stimuli were always presented at the central position. Result showed that aftereffect magnitude among conditions with different ADI configurations was significantly different and showed a positive correlation with overlapping extent between adaptation and test stimuli, suggesting that sCAE is dependent on retinal position. That means, there should be retinal-position dependent adaptation for sCAE, in addition to retinal-position independent adaptation to percept-specified sources such as shape curvature. Result also indicated that size scaling did not systematically influence adaptation strength, suggesting that sCAE can be independent of scale.

Chapter 5 provide the detailed information about Experiment 2 consisting of three subexperiments, with purpose to investigate adapting mechanism of sCAE. Experiment 2.1 used static adaptation stimuli with different eccentricities in order to examine the influence of

eccentricity on adaptation strength of sCAE. Unlike Experiment 1, test stimuli in Experiment 2.1 were always presented at the same location with adaptation stimuli during each trial. Result showed that the eccentricity imposed due influence on adaptation strength, resulting into retinal-position dependent sCAE to some extent. Experiment 2.2, adopting adaptation stimuli with dynamically-changed size, aimed to verify a hypothesis a hypothesis of adaptation at a higher level of PSI than shape curvature. Result indicated that no statistical difference on aftereffect magnitude was found among condition with different scale ranges for dynamically-changed size, verifying the prediction of PSI adaptation. Experiment 2.3 was conducted in order to test another hypothesis regarding adaptation at a lower level of ADI than shape curvature, by virtual of adaptation stimuli with dynamically-changed PSI. Result showed an aftereffect with magnitude significant larger than zero for adaptation condition with near disparity pedestal, support our prediction of ADI adaptation. It was noted that Adaptation and test stimuli were always presented at the central position in both Experiment 2.2 and Experiment 2.3. Therefore, sCAE can result from adaptation to both disparity-specified ADI and percept-specified PSI - not just widely-supported shape curvature. And it was found that PSI adaptation contributed much more to sCAE than ADI adaptation. Furthermore, the retinal-position dependence of sCAE can be due to ADI adaptation and possible eccentricity effect on adaptation strength, while scale independence of sCAE can result from PSI adaptation.

Chapter 6 summarizes the results of our psychophysical study, which support the prediction of parallel adapting processes for sCAE. One process is independent of retinal position, and the retinal-position independence can be induced by adaptation to percept-specified sources, such as shape curvature and PSI. The other process is dependent on retinal position, and the retinal-position dependence can be caused by adaptation to disparity-specified sources, like ADI. That means, sCAE is due to multi-level adaptation, including not only

adaptation to percept-specified sources but also adaptation to disparity-specified sources. Besides, we clarified the hypothesis under which ADI adaptation was true. That is, during adaptation phase, the lower level of zero-order disparity information can be averaged in space, and the averaged disparity information can be further adapted. Admittedly, it is beyond our knowledge to verify the hypothesis. However, no significant difference on aftereffect magnitude in Experiment 2.2 supported no such averaging process on percept-specified adaptation sources to some extent. In addition, it still keeps uncertain about adaptation to absolute disparity, disparity gradient and shape index. Also, we can not assure whether or not the stimulus edge effect decreased adaptation strength in Experiment 2.1, leaving open the question of how the visual system adapts to static stimuli in peripheral area. However, these unsolved problems do not invalidate any conclusion we drew on dependency and multi-level adaptation of sCAE.

Part II, covering Chapter 7 - 8, details our fMRI study. The study consists of experiments for localizing disparity-related ROIs and one stereoscopic experiment for examining stereo-curvature adaptation using fMRI adaptation (fMRIa) paradigm. For 3D structure data, freesurfer was used to extract brain from skullcap and to compute white matter for each subject, and Brainvoyager QX was used to implement the preprocessing and to create flatten brain mesh.

Chapter 7 provides a detailed review mostly on previous fMRI studies on possible cortical areas, which are selective to disparity and perceived shape. According to the review, Regions of Interest (ROIs) to be examined in our fMRI study should contain 14 areas for each hemisphere. That is, early visual areas (V1, V2v, V2d, V3, VP) ventro-lateral areas (hV4, LO), dorsal areas (V3A, KO/V3B, hMT+/V5, V7) and SFM-related areas (VIPS/V7*, POIPS, DIPS). In fact, we integrated V2v and V2d into V2 as a whole ROI in actual data analysis.

Chapter 8 details our fMRI study on stereo-curvature adaptation. We used event-related fMRIa paradigm to investigate change in BOLD activity in ROIs localized in Appendix B. All stimuli counterphase-flickered to maintain activation strength. Adaptation stimuli were presented stationarily, or with dynamic change in size or PSI. A high-contrast fixation point is either centrally fixed or moving along a Lissajous path in depth. This yielded six distinct adaptation conditions in our study. The test stimuli always kept the same across different adaptation conditions. We used such design to investigate stereo-curvature adaptation based on a fact. That is, if a 3D-shape property is quantitatively the same between adaptation and test stimuli, then adaptation to the property will inhibit cortex response activated by test stimuli. To measure adaptation effects, we subtracted percent signal change between peak value of test stimuli from the value of the time point at which test stimulus onset. Thereafter, the subtraction result was normalized into a value ranged between 0 to 1, with 0 representing for null adaptation and 1 for maximum adaptation. For each ROI, Brainvoyager QX was firstly used to compute and export time course of each functional run. After that, we used Matlab to separate and average time course data for each adaptation condition. Result showed a larger adaptation occurred in higher areas than in early areas. We found disparity adaptation in early areas (V1-V2) and a middle dorsal region (KO/V3B), as well as ADI adaptation in high dorsal area (V7) and IPS areas (VIPS/V7*, POIPS and DIPS), suggesting that high dorsal areas may involve a low-order calculation of disparity averaging compared with early and middle dorsal areas. We also found adaptation to size-variant shape curvature in POIPS region as well as adaptation to size-invariant PSI in early region (VP), ventro-lateral areas (hV4, LO) and IPS regions (VIPS/V7*, DIPS), further support the viewpoint that dorsal visual pathway encodes depth structure metrically while ventral pathway does this categorically. Therefore, multi-level stereo-curvature adaptation indeed occurred.

Chapter 9 concludes for both of our studies. For evidences to multi-level adaptation of sCAE, we conducted two psychophysical studies and one fMRI study. The conclusion we drew from the psychophysical studies is that sCAE is due to parallel adapting processes, of which one is retinal-position dependent owing to disparity-specified adaptation and the other is retinal-position independent resulted from percept-specified adaptation. The fMRI study further provided the neuro evidence to multi-level stereo-curvature adaptation with distinct source distribution in cortical areas between dorsal and ventral visual pathways.

Lastly, Appendix A provided a detailed information on behavioral data acquisition for Experiment 3. Results showed a significant adaptation for different types of adaptation stimuli under pursuit of moving fixation point. it supported the feasibility to use those stimuli to further probe multi-level stereo-curvature adaptation under fMRI environment. Appendix B provides detailed information of ROI localization. Early visual areas was identified on the flattened cortex representations, achieved in each observer with functional data from at least 12 separate runs. The stimuli for the localization was a rotating single- or double-wedge (angle) and an expanding ring (eccentricity). Linear correlation analysis was performed in Brainvoyager QX to identify the border between each two adjacent areas on the flattened mesh. Instead, overlay GLM analysis was performed for the localization of other ROIs. Among dorsal areas, KO/V3B is identified according to the fact that the area is activated much more by kinetic contours than by uniformly moving of random texture pattern. SFM-related areas (VIPS/V7*, POIPS and DIPS) were localized based on the fact that the area is activated much more by 3D structure perceived from rigid motion in depth rather than that perceived from static cue for moving stimuli consisting of nine interconnected lines. Among ventral areas, hMT/V5+ was localized using a moving random dot pattern alternated with its static counterpart, under the reason that the area is activated much more by the former compared to the latter. The stimuli for LOC localization were objects (grayscale images or

line drawings, familiar or novel) and their scrambled version for the reason that the area is activated much more by intact objects than their scrambled counterpart, independent of both whether they appeared in the same or different format and whether they are novel or familiar. Appendix C lists all abbreviations involved in the dissertation and their full forms.

Chapter 2

What sources to be adapted for sCAE?

sCAE has been mostly investigated for depth structure from binocular disparity. After prolonged inspection of stereoscopic surfaces curved in depth, stereo-curvature adaptation gives rise to shifts in perceived curvature for subsequently shown 3D surfaces. Although sCAE may not be perceptible for real objects involving multiple depth cues other than binocular disparity, the adaptation has been confirmed to affect estimation of depth structure from disparity. Thus, it is worth investigating the adapting mechanism of sCAE in order to find out more about how a 3D shape is perceived.

Fig. 2.1 details all possible adaptation sources examined in both the previous studies (Domini, Adams, & Banks, 2001; Berends & Erkelens, 2001a, 2001b; Duke & Wilcox, 2003) and our study for sCAE. These possible sources are considered to be adapted at diverse stages stepping from disparity-specified adaptation, including adaptation to zero- and higher-order disparity as well as average disparity information (ADI), into percept-specified adaptation, including adaptation to shape curvature, primitive shape index (PSI) and shape index (SI).

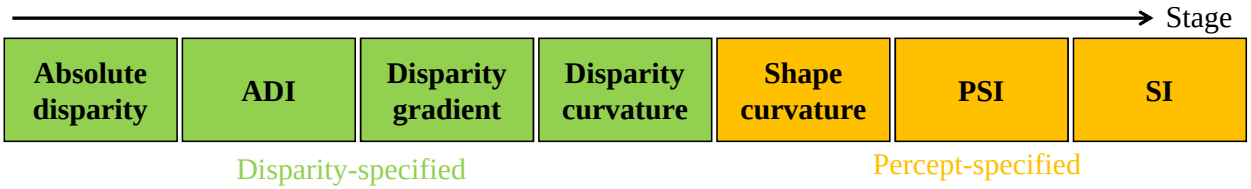

Figure 2.1 List of possible adaptation sources at various stages for sCAE.

Considering the difficulty of isolating disparity adaptation from adaptation to other possible sources, we did not directly investigate disparity information as an adaptation source. Instead, two other properties of stereoscopic 3D shape were originally examined as possible adaptation sources of sCAE, namely, ADI and PSI, when disparity adaptation was smeared by dynamic adaptation stimuli (adaptor) in our study.

2.1 Possible adaptation sources related to disparity

2.1.1 0th-, 1st- and 2nd-order disparity

As shown in Fig. A.1, 0th-order disparities (Point/absolute disparity) are coded to perceive the depth of each location between pairs of retinal images. Absolute disparity is variant of viewing distance and retinal position. 1st-order depth perceived from disparity gradient refers to planar surfaces tilted in depth, and 2nd-order depth perceived from disparity curvature refers to surfaces curved in depth (Orban, 2008). Especially, disparity curvature, as an intrinsic property of stereoscopic 3D shapes, is invariant of viewing distance for real 3D objects.

Possible adaptation to absolute disparity is thought of as occurring at the local level before local disparities are combined to code spatial pattern of disparity including first-order disparities (disparity gradient) and second-order disparities (disparity curvature) (Howard & Rogers, 2012). Previous studies drew inconsistent conclusions on disparity adaptation (Berends & Erkelens, 2001a, 2001b; Duke & Wilcox, 2003; Noest, Van Ee, & Van Den Berg,

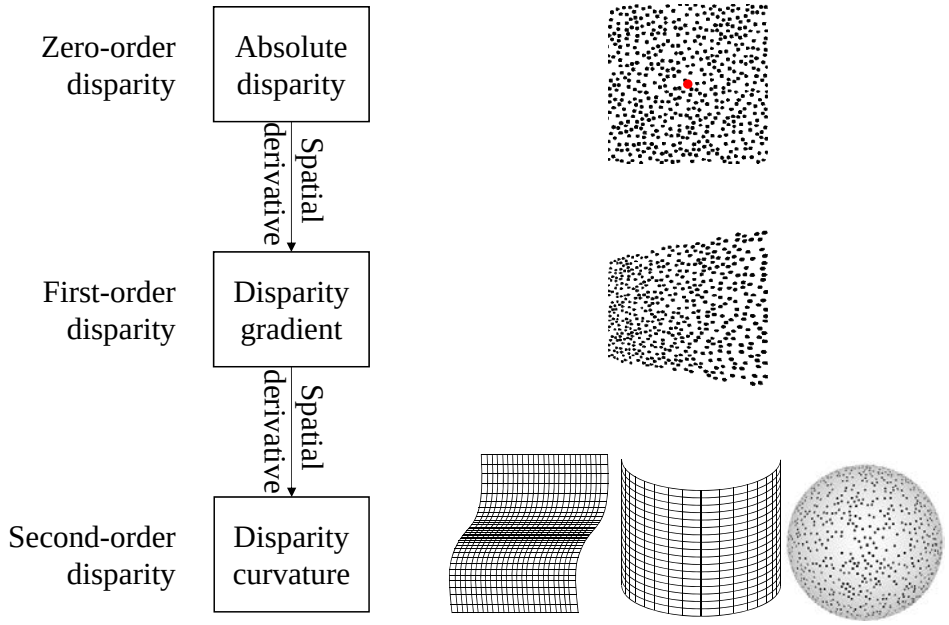

Figure 2.2 Definition of 0th-, 1st- and 2nd-order disparity

2006), because the stimuli used in the studies were not competent to isolate adaptation to shape curvature and disparity information. Possible adaptation to disparity gradient and curvature should be at higher levels than with absolute disparity. In previous studies, disparity curvature was not adapted in the study of Domini et al. (2001), although adaptation to disparity curvature was documented for curvature contrast effect by Te Pas, Rogers, and Ledgeway (1997). In addition, no evidence was found to support whether disparity gradient is adapted or not.

2.1.2 ADI

ADI, the first property we proposed, was generated within visual field subtended by test stimulus (probe) area. There is evidence to support that disparity information can be averaged in space (Anderson, 1992; Rohaly & Wilson, 1994). In this respect, during adaptation time, ADI of each position point P in 2D probe area on screen surface can be calculated

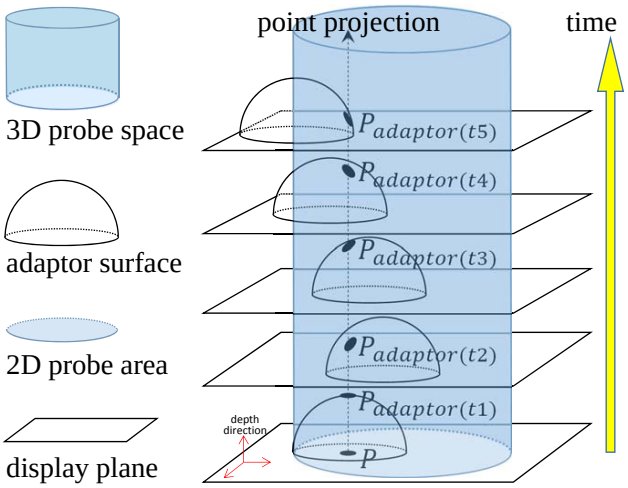

Figure 2.3 ADI calculated in 3D probe space by averaging disparity information of on-adaptor points, which are projected from position points of 2D probe area in depth direction

in 3D probe space as shown in Fig. A.2, and it is measured as the temporally cumulative average on disparity of depth point $P_{adaptor(t)}$, which is projected from P onto adaptor surface in depth direction. Test stimuli always locate at 2D probe area. Obviously, if probe involves changing location, then $P_{adaptor(t)}$ will dynamically alternate in position on the adaptor surface. Equation 2.1 defines ADI in a formulaic form.

$$ADI_P = \fint_0^{adaptation\ time} HD(P_{adaptor(t)})dt, \quad \forall P \in 2D\ probe\ area, \tag{2.1}$$

where HD senses horizontal disparity, P for one position point in probe area, and t for one time point within adaptation time.

In this definition, ADI is still disparity-specified property, suggesting that the possible ADI adaptation should be at a lower level than percept-specified shape curvature. Meanwhile, ADI adaptation should be at a higher level than disparity adaptation and at a lower level than disparity-gradient adaptation, because ADI was a cumulative average of absolute disparities.

2.2 Possible adaptation sources related to percept

2.2.1 Shape curvature and SI

Like disparity curvature, shape curvature is also dependent on radius of curvature, as shown in Equation 2.2.

$$SC \propto \frac{1}{radius\ of\ curvature} \tag{2.2}$$

However, different from disparity curvature, the shape curvature (SC), as a perceived curvature, is variant with viewing distance under fixed disparity information (Rogers & Cagenello, 1989; Domini et al., 2001). In this sense, it is inefficient to specify perceived depth structure only from disparity curvature of viewing-distance invariance, and viewing distance is essential to be taken into consideration as shape curvature does. For this reason, shape curvature should be adapted at a higher level than disparity curvature. Noest et al. (2006) suggested a dominant adaptation to shape curvature compared with absolute disparity as a possible adaptation source. Adaptation to shape curvature was also supported by Domini et al. (2001) and Duke and Wilcox (2003).

Koenderink (1990) proposed the SC classification method, where 3D shapes are defined with qualitative SI, as defined in Equation 2.3, and with quantitative curvedness.

$$SI = -\frac{2}{\pi} \times arctan(\frac{K_{max} + K_{min}}{K_{max} - K_{min}}) \tag{2.3}$$

where K_{max} and K_{min} signifies the principal curvatures maximum and minimum respectively in perpendicular planes.

In this definition, SI adaptation should be at the higher level than shape curvature, because size invariance is true for SI rather than shape curvature. However, no evidence was found to support whether disparity gradient is adapted or not. In our study, SI adaptation was not examined due to the difficulty of isolation between SI and other lower-level sources.

2.2.2 PSI

PSI, the second property we proposed, was defined based on SI definition. In our study, PSI was used to differentiate among 3D shapes with identical SI, as shown in Equation 2.4.

$$PSI = \frac{h}{r} \times SI \tag{2.4}$$

where h symbolizes peak-to-base distance and r size radius. Obviously, PSI can characterize any spherical surface in both qualitative and quantitative manner, considering that the ratio of h to r depicts shape steepness. PSI, different from curvedness, is scale invariant by definition. However, for a specified stimulus size (r), varying the peak-to-base distance (h) alters PSI rather than SI. In other words, the same SI can be shared by shapes with different PSI, but not vice versa. The difference between PSI and curvedness is that PSI is scale invariant whereas curvedness is not. For demonstration, all semi-ellipsoid surfaces including hemispherical surfaces share the same SI, but different semi-ellipsoidal surfaces can be identified by distinct PSIs.

In this respect, possible PSI adaptation should be at a higher level than shape-curvature adaptation, considering that PSI is scale invariant but shape curvature not. Furthermore, PSI adaptation should be at a lower level than SI adaptation, because the SI is invariant of peak-to-base distance of stimuli when curvature direction and stimulus size are constant, but PSI not. Figure 2.4 includes three 3D shapes to illustrate the difference among shape curvature, SI and PSI. The first two shapes differ only in scale, and the third one has larger within-object depth with the same 2D size with the first shape. According to the definitions above, these three shapes have same SI but entirely different shape curvature. Furthermore, the first two shapes share the same PSI and differ from the third one.

To examine adaptation to ADI and PSI, our adaptation stimuli involved dynamic changes in either location, scale or PSI. The dynamic change in scale, referred to as size scaling,

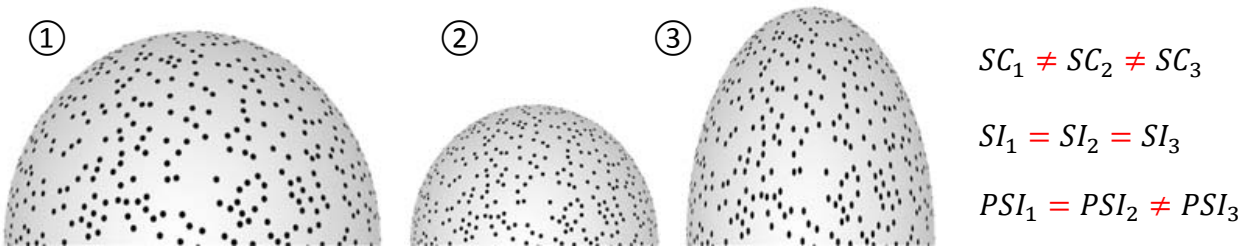

Figure 2.4 Illustration of difference among shape curvature, SI and PSI

smoothly alters stimulus size by periodical expansion-contraction at a constant and high temporal frequency. Although change of stimulus size has been reported to have little effect on shape discrimination performance (Vreven, 2006), it rapidly changes shape curvature, because curvature is mathematically dependent on stimulus size and small objects perceptually appear stretched and large objects squashed along the depth dimension (Champion, Simmons, & Mamassian, 2004). Thus, size scaling can smear adaption to absolute disparity information and shape curvature, and further facilitate examination of adaptation to size-invariant PSI.

The dynamic change in PSI, referred to as PSI scaling, dynamically and smoothly alters PSI by varying peak-to-base distance of size-fixed stimulus at a constant and high temporal frequency. Obviously, PSI scaling smears adaptation to disparity information, shape curvature and PSI of each instantaneously presented adaptation frame, so it can be used to examine ADI adaptation.

Part I

Psychophysical Study

Chapter 3

Introduction

Stereoscopic aftereffects involve binocular disparity as a unique depth cue, and have been generally explained as the consequence of fatigue among neural mechanisms tuned to different patterns of disparity (Köhler & Emery, 1947; Long & Over, 1973; Berends & Erkelens, 2001a, 2001b; Howard & Rogers, 2012) or specific percept (Domini et al., 2001; Duke & Wilcox, 2003). The aftereffects have been generally investigated from aspects of stereo-depth aftereffect (depth ordering aftereffect, sDAE), stereo-slant aftereffect (sSAE) and stereo-curvature aftereffect (sCAE). Specifically, sDAE results from adaptation to surfaces orthogonal to sight line, yielding shifts in perceived depth for subsequently presented fronto-parallel surfaces. sSAE, meanwhile, is due to adaptation to surfaces tilted in depth and involves shifts of perceived slantness for followed spatial plane. For sCAE, after prolonged inspection of binocular surfaces curved in depth, stereo-curvature adaptation gives rise to shifts in perceived curvature for afterwards shown 3D surfaces. There is neural evidence that stereo-curvature adaptation indeed affects estimation of depth structure (Preston, Kourtzi, & Welchman, 2009), so it is worth investigating the adapting mechanism of sCAE in order to further examine how a 3D shape is finally perceived.

3.1 Adapting mechanism of stereo-curvature aftereffects (sCAE)

Since curvature aftereffects in depth direction was first investigated decades ago (Gibson, 1933; Köhler & Emery, 1947), an insufficient number of studies have paid attention to the adapting mechanism of sCAE. Also in previous studies, wherein three types of adaptation stimuli were mostly used with the purpose of separately examining disparity adaptation or shape-curvature adaptation, no consistent answer has been found for sCAE on whether disparity or shape curvature was adapted. The first type of adaptation stimuli is static curved surfaces with static fixation. By manipulating viewing distance, stimuli with different shape curvatures can be obtained under constant disparity information, and stimuli with different disparity information can also be generated under constant shape curvature. Domini et al. (2001) used the method for isolation between disparity adaptation and shape-curvature adaptation for sCAE. Their results reported that significantly different aftereffect magnitudes were found for adaptation stimuli with different shape curvatures and the same disparity information, and that no such difference was found for adaptation stimuli with different disparity information and the same shape curvature. Thus, sCAE was claimed as the result of shape-curvature adaptation. However, Howard and Rogers (2012) suggested that viewing-distance change may influence the adapting mechanism. That is, the same result can be produced by adaptation of disparity detectors followed by distance scaling of the induced disparity signals. If so, the sCAE should be due to disparity adaptation rather than shape-curvature adaptation. But no further experiment has been conducted to confirm this possible explanation for disparity adaptation. Thus, static curved surfaces with static fixation are not suitable for isolating shape-curvature adaptation from disparity adaptation, considering the possible influence of viewing-distance change.

The second type of adaptation stimuli is perceptually fronto-parallel surfaces, which differ in terms of both vertical and horizontal disparity information. To make the stimuli, different depth effects are firstly generated with distinct vertical disparity fields induced by three vertical transformations (vertical scale, vertical shear and vertical quadratic mix), resulting in. Then the different depth effects are nulled by the corresponding horizontal transformations (horizontal scale, horizontal shear and horizontal quadratic scale). These frontal-parallel adaptation stimuli seem to facilitate separate examination of disparity adaptation and shape-curvature adaptation. However, contrary results were obtained in previous studies using the adaptation stimuli. Berends and Erkelens (2001a, 2001b) reported a significant difference of aftereffect magnitude among the stimuli, leading them to claim that stereo-curvature adaptation occurred in a mechanism either sensitive to disparity information, or responsible for modulating the conflicting relationship between vertical disparity and eye position. But Duke and Wilcox (2003) failed to measure the aftereffects of systematic difference among these adaptation stimuli, so they claimed that adaptation to shape (object) curvature governed aftereffect magnitude to a large extent. However, another explanation for their result was also provided by disparity adaptation. That is, the lack of systematic difference in aftereffect magnitude may result from canceling out adaptation to horizontal and vertical disparity of adaptation stimuli. In this respect, the stage at which stereo-curvature adaptation occurs can not be determined using this type of adaptation stimuli.

The last type of adaptation stimuli is static curved surfaces with moving fixation, which was thought to be able to smear possible adaptation to disparity and its gradient. In the study of Noest et al. (2006), spherical or cylindrical surfaces were inspected as adaptation stimuli. The difference of aftereffect magnitude between static fixation and moving fixation was used to examine whether disparity or shape curvature was adapted. Results showed that the difference was small enough, indicating a dominant contribution of shape-curvature

adaptation for sCAE. However, no further evidence was found to confirm or exclude adaptation to disparity and its gradient. Besides, moving fixation involved much eye movements imposing uncertain effects on adaptation.

Accordingly, the previous studies we reviewed were not able to determine the adapting mechanism of sCAE, because of their inappropriate adaptation stimuli to isolate examination of adaptation to disparity and shape-curvature. Only the dominant contribution of shape-curvature adaptation can be determined from the study of Noest et al. (2006).

Here, we predicted that sCAE may be due to multi-level adaptation - not solely to shape-curvature adaptation - based on previous findings of multi-stage adaptation found for sDAE and sSAE. So far, sDAE and sSAE have been shown to result from adaptation at several stages of visual processing from the encoding of binocular disparity (Köhler & Emery, 1947; Blakemore & Julesz, 1971; Long & Over, 1973; Mitchell & Baker, 1973; Howard & Rogers, 2012) to the final depth percept (Balch, Milewski, & Yonas, 1977; Ryan & Gillam, 1993; Berends, Liu, & Schor, 2005; Knapen & Van Ee, 2006). Moreover, the aftereffects have also been ascribed to the recalibration of the mapping between retinal disparity and either perceived depth (Epstein & Morgan, 1970; Mack & Chitayat, 1970; Epstein, 1972) or perceived slant (Adams, Banks, & Van Ee, 2001), suggesting that both sDAE and sSAE can not be explained by adaptation of disparity alone or by adaptation of the percept alone (Poom & Börjesson, 1999). Thus, sCAE may be due to multi-level adaptation. To confirm this prediction, one purpose of our study was to examine both disparity- and percept-specified adaptation sources for sCAE.

For the reason that the stimuli used in previous studies, as listed above, were not suitable for examining adaptation to a single source, especially for the lower-order sources than shape curvature, dynamically-presented spherical surfaces with static fixation were used as adaptation stimuli in our study. It was worth noting that stimulus dynamics here did not

include random change of dot pattern and jitter presentation of stimuli. Furthermore, they were defined only with horizontal disparity rather than with vertical disparity, considering the smaller stimuli adopted in our study compared to previous studies (Berends & Erkelens, 2001a, 2001b; Duke & Wilcox, 2003).

3.2 Dependency of sCAE on retinal-position and scale

Another reason why we used dynamic adaptation stimuli was to investigate dependency of sCAE on retinal-position and scale. So far, the related studies have not drawn definite conclusions on the dependency. Noest et al. (2006) claimed that shape curvature was dominantly coded in a retinotopic frame, for the reason that no significantly different sCAE was found when adaptation and test stimuli were viewed between the same and opposite headcentric hemispheres. The adaptation stimuli were inspected with either static or moving fixation. For static fixation, adaptation and test stimuli completely overlapped in retina no matter whether they were viewed in the same or opposite headcentric hemispheres. Only a small difference of adaptation strength was involved between static and moving fixations, although moving fixation, unlike static fixation, dynamically changed retinal coordinates of adaptation stimuli. This suggested retinal-position independent sCAE. However, the small difference was statistically significant, indicating possible adaptation to retinal-position dependent disparity information in static fixation situation. Furthermore, there may be two parallel adaption processes with opposite dependency on retinal position for sCAE.

Corresponding to our previous prediction about multi-level adaptation for sCAE, adaptation to percept-specified sources, such as shape curvature, can induce retinal-position independent sCAE, and this has been verified by Noest et al. (2006). As another prediction in our study, adaptation to disparity-specified sources, such as disparity information, may produce retinal-position dependent sCAE. Obviously, this prediction can not be confirmed by the study of Noest et al. (2006), because their stimuli can not separately examine the

retinal-position dependency of low-level adaptation. For this reason, the dependency of sCAE on retinal position is not determined to some extent. Furthermore, little attention has been paid to scale dependency of sCAE. Thus, another purpose of our study was to investigate the dependency of sCAE on scale and to verify the prediction that adaptation to disparity-specified sources results in retinal-position dependent sCAE.

In our study, two main experiments were conducted. Experiment 1 aimed to investigate dependency of the sCAE on retinal position and scale. To this end, adaptation stimuli were presented with dynamically changed location or scale, when test stimuli were always presented at the central position. Experiment 2, comprising three sub-experiments, aimed to investigate adapting mechanism of sCAE. Experiment 2.1 used static adaptation stimuli with different eccentricities with the purpose of examining the influence of eccentricity on adaptation strength for sCAE. Unlike Experiment 1, test stimuli in Experiment 2.1 were always presented at the same location with adaptation stimuli during each trial. Experiment 2.2, adopting adaptation stimuli with size scaling, aimed to verify a hypothesis of adaptation at a higher level of PSI than shape curvature. Experiment 2.3 was conducted in order to test another hypothesis regarding adaptation at a lower level of ADI than shape curvature, by virtue of adaptation stimuli with PSI scaling. Adaptation and test stimuli were always presented at the central position in both Experiment 2.2 and Experiment 2.3.

Chapter 4

Experiment 1: Dependency of sCAE on retinal-position and scale

4.1 Question to answer: What sorts of adaptation occur?

Experiment 1 aimed to investigate the dependency of sCAE on scale and to verify the prediction that adaptation to disparity-specified sources results in retinal-position dependent sCAE. To this end, adaptation stimuli were presented with dynamically changed location or scale, when test stimuli were always presented at the central position.

4.2 Methods

4.2.1 Observers

Eight stereo-competent students (aged 21-29 years) from Kochi University of Technology served as observers in Experiment 1. One was an author of the study, whilst the others were paid volunteers and naive to the purpose and ongoing results of the experiment. All had

normal or corrected-to-normal visual acuity with no history of visual disorders, and provided informed consent.

4.2.2 Apparatus

Observers were seated in a dark room with their head supported on a chin rest to prevent head movements, 66 cm in front of a 21 in. (40 × 30 cm) fully flat aperture grill CRT (FlexScan T961, Eizo Nanao Corporation, Japan) at 120 Hz noninterlaced frame rate with 1024 by 768 pixel resolution. At this viewing distance, each pixel subtended 2.04 × 2.04 arcmin. A Minolta CS-100A chroma meter was used to measure luminance and linearize the monitor. All psychophysical experiments were run in Matlab 2007b (Mathworks, Natick, MA) with Psychophysics Toolbox Version 3 (Brainard, 1997; Pelli, 1997; Kleiner, Brainard, & Pelli, 2007). Stimuli were viewed through 120 Hz stereoscopic wireless LCD glasses (NuVision 60GX, MacNaughton, Inc., OR, USA) thus the effective frame rate to each eye was 60 Hz. There was no noticeable flicker at this frame rate. The same apparatus was used in all experiments.

(a) Darkroom (b) CRT display (c) Photometer (d) Chinrest (e) Shutter

Figure 4.1 Apparatus used in psychophysical experiments

4.2.3 Visual Stimuli

For the purpose of avoiding edge contour of stimulus to influence curvature discrimination, all stimuli in our study were spherical surfaces, which were stereoscopically-defined and presented fronto-parallel. Approximately 500 sparse anti- aliased dots were distributed over the surface of a stimulus. White dots (88.5 cd/m^2) were presented on a dark screen (3.88 cd/m^2). As pseudo random-dot stereograms (RDS), all the white dots were nearly uniformly-distributed in a 2D black background covered by stimuli in order to prevent non-uniform dot distribution from affecting stereo-curvature cognition. All stimuli subtended 5.08 - 5.76 deg of visual angle in both horizontal and vertical dimensions within the receptive fields of neurons in higher visual cortex such as area V5 and LOC of primates (Van Der Kooij, Domini, & Te Pas, 2011).

As shown in Fig. 4.2(a) - 4.2(d), all adaptation stimuli used in Experiment 1 were hemispherical surfaces either with random changing of location for both Average_Flat (AF) and Average_Concave (ACC) conditions or with periodical scaling of stimulus size for Dynamic_Size (DS) condition. There was a static hemispherical adaptation surface only in Average_Concave/Fixed_Size (ACV/FS) condition.

Test stimuli, always presented at the central position with a constant size, varied with 11 different spherical curvatures (1/4, 1/8, 1/16, 1/32, 1/64, 0, -1/64, -1/32, -1/16, -1/8 and -1/4), as shown in Fig. 4.2(e). The spherical curvature of test stimuli was specified by the ratio of the signed relative depth of the spherical surface to the size radius of test stimuli. The positive value is for convex surface, negative value for concave surface and 0 for flat plane.

To determine whether or not sCAE is dependent on retinal position, there was different eccentricity configurations among the first adaptation conditions for location change. AF condition involved separation on retinal position between adaptation stimuli and test stimuli

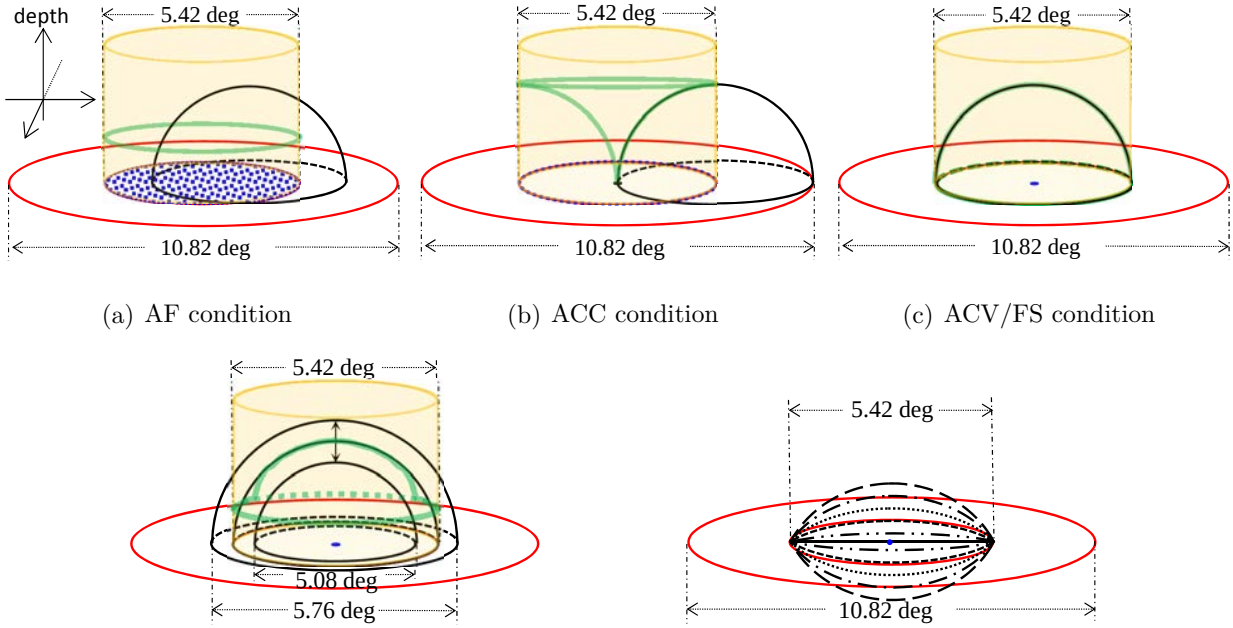

(a) AF condition (b) ACC condition (c) ACV/FS condition

(d) DS condition (e) Test stimuli of 11 curvature levels

Figure 4.2 Schematic illustration of visual stimuli used in Experiment 1. All stimuli were viewed with fixed central vision. Concentric red circles were invisible in actual experiments, and stimulus center located within the blue-dotted texture area for AF condition, along the blue-colored inner circle for ACC condition and at the blue-colored center of concentric circles for the other adaptation conditions. (a) - (b): adaptation stimuli with dynamically changed location at 5 Hz in Experiment 1, where AF was short for Average_Flat, which means that the putative 3D shape from ADI was flat in dark-yellow-colored 3D probe space. Similarly, ACC for Average_-Concave; (c): adaptation stimuli with fixed location and size in Experiment 1, where ACV was short for Average_Convex and FS for Fixed_Size; (d): adaptation stimuli with dynamically changed size at 20 Hz in both Experiment 1, where DS was short for Dynamic_Size; (e): eleven curvature levels of test stimuli. Each dash type corresponded to a pair of test levels with opposite spherical curvatures, and the solid mid-line to flat surface. The green-colored surface across (a) - (c) represented a putative surface encoded by ADI, which is calculated on instantaneous spatial disparity information during adaptation time. Test stimuli were always presented at the central position in Experiment 1, Experiment 2.2 and Experiment 2.3.

ranging from 0 deg to 2.71 deg, yielding a putative flat plane from ADI. For ACC condition, adaptation stimuli with dynamic position always fell on different retinal positions separated by 2.71 deg from the center of test stimuli, resulting in a putative 3D shape with concave curvature from ADI. For ACV/FS condition, the same position was always shared between adaptation and test stimuli in retina, generating a putative 3D shape with convex curvature from ADI. To examine the dependency of sCAE on scale, the unique difference between the last two conditions was whether or not stimulus involved scaling in size. ACV/FS condition presented adaptation stimuli with a fixed size, while DS condition presented adaptation stimuli with size scaling within a range of 5.08 - 5.76 deg. In DS condition, adaptation stimuli with size scaling were always located in the same retinal position as test stimuli, producing a constant PSI with rapidly changed shape curvature.

4.2.4 Procedures

Fig. 4.3 shows the experimental procedure used in the study. For adaptation conditions, each block started with a pre-adaptation phase of 100 s. After an upcoming 0.5 s inter-stimulus interval (ISI) , a top-up adaptation of 10 s followed in order to prevent the aftereffects from decreasing during the key response phase. Subsequent to the top-up adaptation phase was another ISI of 0.5 s. After that, the test stimulus was presented for 0.2 s, which was short enough to minimize adaptation to the test stimulus but long enough to allow for stereo vision. After the test stimulus disappeared, a blank screen was presented for 0.5 s, followed by information about key response in observers' native language. When the observers made a key response, the next trial began after a blank screen was displayed for 0.7 s. A prompt for the number of remaining trials in the current block was given after every 55 trials. Alternation of the top-up adaptation and test continued until the current block was terminated.

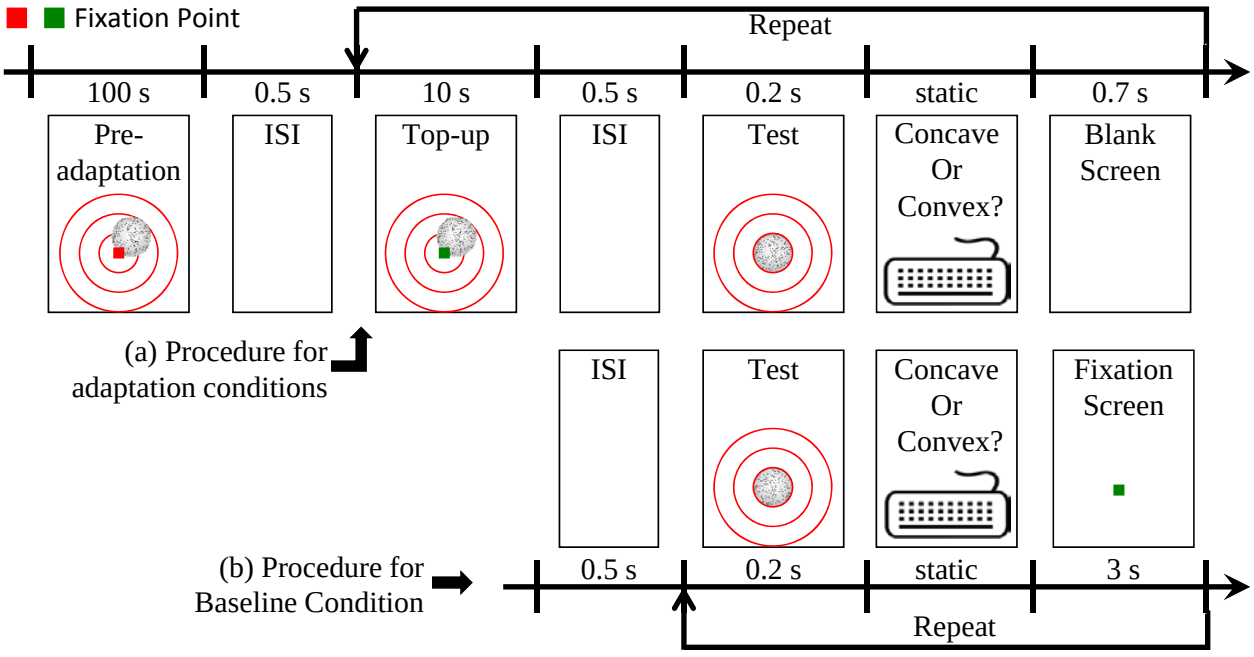

Figure 4.3 Experimental procedures. In actual experiment, random-dot stereograms were adopted without texture and shading effect. And red concentric circles were invisible.

During both pre-adaptation and top-up adaptation phases, the dot pattern on the adaptation surfaces changed randomly at 10 Hz to prevent the formation of afterimages. To constrain eye movements, central squared fixation point (20.3 arcmin) was used with red color during pre-adaptation phase and with green color during top-up phase. With the fixation point, adaptation and subsequent test stimuli necessarily fell on different retinal positions for both ACC condition and AF condition as well as on the same retinal position for both ACV/FS condition and DS condition. The relative disparity between fixation point and stimulus edge was always 3.22 deg larger than maximal relative depth (2.88 deg) of dynamic adaptation stimuli. In other words, the fixation point was always closer to subjects than the stimulus peak. The pedestal disparity ranged from 2.1 arcmin to 4.1 arcmin for DS condition, and fixed with 3.1 arcmin for ACV/FS condition.

For baseline condition, there was no adaptation procedure before test stimulus onset.

Ahead of the next trial, only the fixation point was presented for 3 s in order to concentrate observers' attention and to prevent the afterimage effect of the previous trial. Baseline condition was conducted only when all of adaptation conditions were finished for each subject.

Observers performed a within-object depth discrimination task. On each trial, they were required to judge whether test stimuli appeared concave or convex according to global shape rather than local disparity structure, pressing a designated key to make a corresponding choice of curvature discrimination (CONCAVE or CONVEX). To improve the accuracy of experimental data, another key was available for observers to discard the current trial, in the event that they missed the test stimuli owing to blinking during the onset of test stimuli. The discarded trial would then be shuffled together with the other remaining trials within the current session and excluded from the next trial. Before the experiment proper, each observer first had to see some stereoscopic stimuli to adapt to stereoscopic vision, and then perform a few practice trials ($\sim$5 min) with feedback in order to become familiar with the task. Each observer participated in all the adaptation and base conditions. Only one adaptation condition was involved in each block, and the order of adaptation condition was balanced out. For every adaptation condition, there were 35 repetitions to present each level of test stimuli to each participant. A total of 385 trials were divided into seven 55-trial blocks, the first block of which was a practice block in order to familiarize observers with the corresponding dynamic RDS. Twenty-eight blocks across 4 adaptation conditions were randomly performed for each participant. Before initiating the next different adaptation condition, a sufficiently long break was taken in order to eliminate certain aftereffects of the previous block. The time for each block was around 13 min, and the total time for the adaptation conditions was about 7 hours for each observer. For baseline condition, there were 30 repetitions for each level of test stimuli, and a total of 330 trials were divided into two blocks with each block lasting about 15 min. Thus the total amount of measuring time

per observer was about 7.5 hours regardless of break time.

4.3 Results

The method of constant stimuli was used to determine a psychometric curve. First of all, the data for each condition were sorted into fraction of CONCAVE or CONVEX responses to each test stimulus. The test stimuli were parameterized according to the curvature of the test surfaces. The ratio of CONVEX responses was plotted against the test stimulus, and the resulting psychometric curve was fitted with a sigmoidal function of the form, as depicted in Equation 8.1.

$$f(x) = 1/(1 + e^{-p(1)(x-p(2))}) \tag{4.1}$$

where parameter p(2) gives the test-stimulus parameter corresponding to the point of subjective equality (PSE) , which is 50% point of the psychometric function. And p(1)/4 is the slope at PSE.

Fig. 4.4(a) shows the perceived curvature at PSE under each condition for all eight observers. No aftereffect was involved under baseline condition even though there was a bias of curvature judgment. The negative PSE value in the baseline condition suggested a flat surface was likely to be perceived as a convex surface under no adaptation. We found a significant main effect of condition on PSE ($F_{4,28} = 17.269,\ MSE = 0.014,\ p = 0.00,\ \eta^2 = 0.712$). The subsequent multiple comparison with Bonferroni adjustment revealed that the baseline condition differed significantly from both ACV/FS condition ($p = 0.036$) and DS condition ($p = 0.020$), but not from both AF condition ($p = 0.147$) and ACC condition ($p = 0.586$). Besides, ACV/FS condition was found to be significantly different from both AF condition ($p = 0.004$) and ACC condition ($p = 0.010$). No statistical difference was found between AF condition and ACC condition ($p = 0.069$), neither between ACV/FS condition and DS condition ($p = 1.000$). However, one sample t-test indicated that the PSE value of

AF condition was significantly larger than zero, whilst ACC condition was not. In addition, DS condition differed significantly from both AF condition ($p = 0.008$) and ACC condition ($p = 0.013$).

The magnitudes of the sCAE were calculated from each observer's data by subtracting PSE of the baseline condition from that of each adaptation condition. Repulsive aftereffects show positive values. Fig. 4.4(b) shows the group mean of sCAE averaged from all eight observers. To ascertain whether adaptation to convex surface caused a negative bias in the shape perception of a sequentially viewed surface, a one sample t-test was performed on each adaptation condition. The results indicated that all the adaptation conditions had a significant aftereffect with magnitude larger than zero with exception of ACC condition ($p = 0.057$). Next, to assess whether the effect depended on position and size, one way repeated-measures analysis of variance (ANOVA) was further performed on aftereffect magnitude with the factor of the adaptation condition. The results showed that adaptation condition had a significant main effect on aftereffect magnitude ($F_{3,21} = 24.919,\ MSE = 0.007,\ p = 0.00,\ \eta^2 = 0.781$). Subsequent multiple comparisons between means (Bonferroni adjusted) revealed that ACV/FS condition had significantly larger aftereffect than both AF condition ($p = 0.002$) and ACC condition ($p = 0.006$). Also, the aftereffect magnitude in AF condition was significantly larger than that in ACC condition ($p = 0.044$). Obviously, DS condition differed significantly from both AF condition ($p = 0.008$) and ACC condition ($p = 0.011$). However, no statistical difference was found between ACV/FS condition and DS condition ($p = 1.000$) (all $ps < 0.05$).

4.4 Discussion

The dependency of sCAE on retinal position and scale was examined in Experiment 1. To this end, adaptation stimuli with dynamically changed location and scale were used to smear disparity adaptation and to isolate shape curvature from other possible adaptation sources.

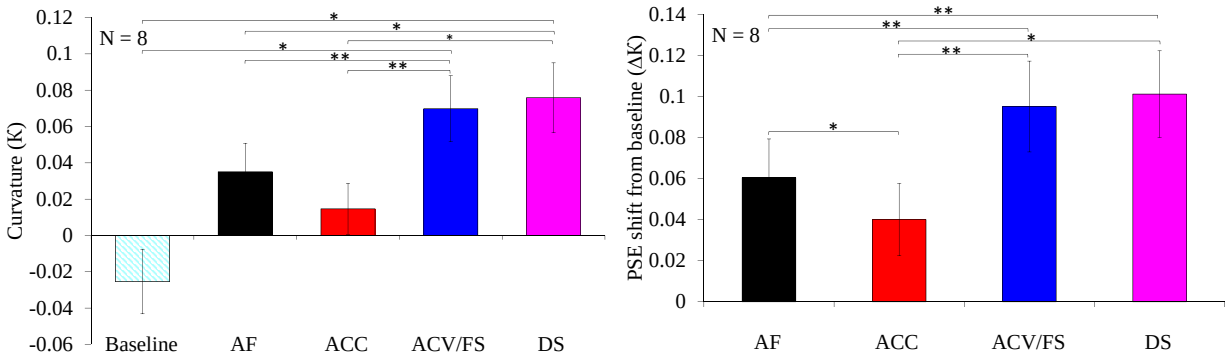

(a) Perceived curvature at PSE across all conditions (b) Group mean of adaptation magnitude

Figure 4.4 Result over all eight observers for Experiment 1. Error bars represent standard errors of means. $*p < 0.05$, $**p < 0.01$

In this way, different ADIs were generated within the visual fields subtended by test stimuli among AF, ACC and ACV/FS conditions. With static fixation during adaptation phase, different retinal positions were mapped onto between adaptation stimuli and test stimuli in both AF condition and ACC condition, as well as the same retinal position in both ACV/FS condition and DS condition.

Previously, stereoscopic aftereffects were assumed to occur only when there was overlap in the neural representation between adaptation and test stimuli. This assumption has been supported by some previous investigations on sSAE (Howard & Rogers, 2012) and sDAE (Köhler & Emery, 1947; Mitchell & Baker, 1973; Smallman & MacLeod, 1997; Long & Over, 1973). In our study, ACV/FS and DS conditions, wherein adaptation stimuli were presented with fixed location, had significantly different PSE-values from baseline condition. But it was not true for AF and ACC conditions, wherein adaptation stimuli were presented with dynamically changed location. This indicated that location overlap between adaptation and test stimuli indeed facilitates stereo-curvature adaptation. Moreover, aftereffect magnitude among AF, ACC and ACV/FS conditions was significantly different and showed a positive correlation with overlapping extent between adaptation and test stimuli, suggesting that

sCAE is dependent on retinal position, supporting the prediction we made for dependency of sCAE on retinal position. That is, there should be retinal-position dependent adaptation for sCAE, in addition to retinal-position independent adaptation to percept-specified sources such as shape curvature.

Besides, the aftereffect with magnitude significantly larger than zero was found in AF condition, wherein the adaptation stimuli were not always at identical location. Thus, sCAE occurred at the non-adapted position. Consistent results have been documented for sDAE and sSAE in previous studies (Van Der Kooij et al., 2011; Taya, Sato, & Nakamizo, 2005), where significant stereoscopic aftereffects were found even when there was no overlap between adaptation and test stimuli. Furthermore, the significant aftereffect in AF condition suggested that it was not essential for stereo-curvature adaptation to continuously stimulate fixed retinal coordinate and constant disparity. This finding is consistent with the finding ofNoest et al. (2006), wherein significant adaptation was found for static adaptation stimuli with moving fixation along Lissajous trajectory. Similar results for sSAE have been found with active eye-movement during adaptation (Bergman & Gibson, 1959; Ryan & Gillam, 1993) or with an oscillating amount of horizontal and vertical disparity in the adaptation stimulus (Berends, Erkelens, & Van Ee, 2000).

Size scaling did not systematically influence adaptation strength, because no statistical difference was found on aftereffect magnitude between ACV/FS condition with fixed size and DS condition with size scaling in Experiment 1. This finding is partly supported by a single-unit study on monkeys (Janssen, Vogels, & Orban, 2000), wherein the 3D shape selectivity was documented as scale invariant for TEs neurons of inferior temporal cortex, which exquisitely code 3D shape from disparity. Thus, sCAE can be independent of scale, which is inconsistent with the finding of Taya et al. (2005) about sSAE, whereby magnitude was found to increase with the ratio of size of the adaptation stimulus to that of test stimulus.

In addition, the scale independence further indicates that the continuous stimulation of constant shape curvature was not essential for stereo-curvature adaptation.

For the retinal-position dependence of sCAE, one possible explanation is adaptation to different ADIs among AF condition, ACC condition and ACV/FS condition, because ADI is disparity-specified and retinal-position dependent. Another alternative explanation for the dependence on retinal position is eccentricity effect on adaptation strength of sCAE. That is, the adaptation strength within the receptive field may be Gaussian-distributed with larger adaptation for detectors closer to the fovea. For the scale independence of sCAE, a possible explanation is adaptation to percept-specified PSI, because PSI is invariant of size changes during size scaling. The ADI adaptation, however, did not contribute to the scale independence in theory, because ADI is size variant and the almost identical ADI was produced with entirely different methods between DS and ACV/FS conditions, with one condition involving size scaling but the other not. The purpose of the subsequent experiment was to verify these explanations regarding dependency of sCAE on retinal position and scale.

Chapter 5

Experiment 2: Adapting mechanism of sCAE

5.1 Question to answer: What to adapt?

In order to investigate the adapting mechanism of sCAE, the possible explanations, provided in Experiment 1, for the dependency of sCAE were examined through three sub-experiments in Experiment 2. Experiment 2.1 examined eccentricity effect on adaptation strength. We predicted that distinct effects should be imposed on aftereffect magnitude by different eccentricities of adaptation stimuli; Experiment 2.2 tested a hypothesis about adaptation to percept-specified PSI. The PSI adaptation was predicted to induce significant aftereffects of no statistical difference across adaptation conditions with distinct configurations of size scaling; Experiment 2.3 tested another hypothesis about adaptation to disparity-specified ADI. The ADI adaptation was predicted to produce significant aftereffects even for dynamic adaptation stimuli with PSI scaling.

As in Experiment 1, all stimuli were random-dot stereograms depicting spherical surfaces, and were presented with static fixation in Experiment 2. However, different adaptation

stimuli were used in the three sub-experiments. Test stimuli used in Experiment 2 were either a subset or all of those used in Experiment 1. The same method was used to measure stereothreshold as in Experiment 1.

The same procedure as Experiment 1 was used in Experiment 2 with exception of different time profile for stimuli presentation. In each of three sub-experiments in Experiment 2, adaptation stimuli were presented for 50 s in the pre-adaptation phase and for 5 s in the top-up phase.

5.2 Experiment 2.1: Eccentricity effect on adaptation strength

5.2.1 Methods

Observers Six stereo-competent observers (aged 27-34 years) participated in Experiment 2.1. All had normal or corrected-to-normal visual acuity. Four of them had participated in Experiment 1. One was an author of the study, whilst the others were paid volunteers and naive to the purpose of the study.

Visual stimuli Static stimuli with different eccentricities were adopted to examine how eccentricity affected adaptation strength. As shown in Fig. 5.1, there were three adaptation conditions with different horizontal eccentricities, including CENTER condition with zero-eccentricity, NEAR condition with 2.71 deg eccentricity and FAR condition with 5.42 deg eccentricity. The central fixation square was red during pre-adaptation phase and green during top-up phase. The constant relative disparity between fixation point and stimulus edge was 3.22 deg larger than the relative depth (2.71 deg) of static adaptation stimuli. The pedestal disparity was 3.1 arcmin for CENTER condition. Because the static adaptation stimuli were presented for a relatively shorter time than in Experiment 1, position jitter

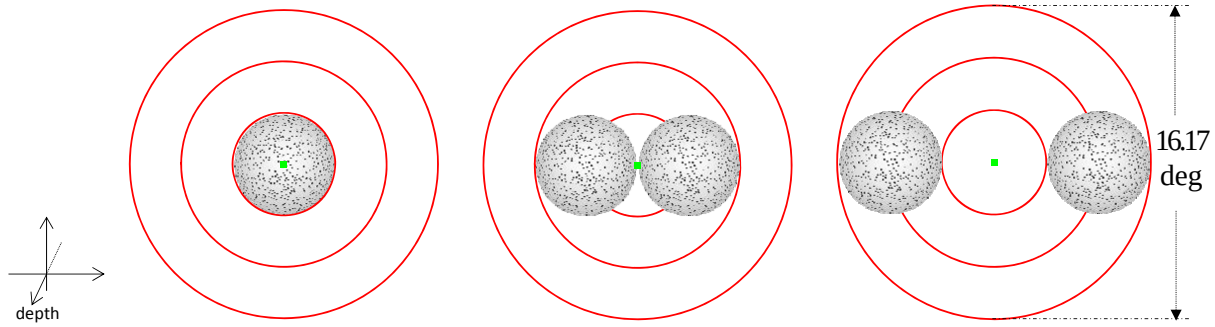

(a) CENTER condition (b) NEAR condition (c) FAR condition

Figure 5.1 Schematic illustration of static adaptation stimuli used in Experiment 2.1. All stimuli were viewed with fixed central vision. Three adaptation conditions were endowed with distinct eccentricity configurations with zero eccentricity for CENTER condition (a), 2.71 deg for NEAR condition (b) and 5.42 deg for FAR condition (c). Adaptation and test stimuli shared the same location during each trial.

instead of dot-pattern change was used to prevent the formation of afterimages. A pilot study suggested that non-uniformness of local distribution on adaptation stimulus surfaces somewhat misled global curvature judgment of test stimuli. In order to circumvent certain influence of the non-uniform dot density, Experiment 2.1 involved uniformly distributed dots on spherical surface of all the stimuli. This was implemented using Recursive Zonal Equal Area Sphere Partitioning Toolbox (Leopardi, 2006). Test stimuli were identical to those used in Experiment 1 and always presented at the same position to the adaptation stimuli. However, test stimuli only varied with seven different spherical curvatures, that is, 1/4, 1/16, 1/64, 0, -1/64, -1/16 and -1/4.

Care was taken to ensure, in the actual experiment, that only binocular disparity cue was available for depth perception, and that the texture and shading effect shown in Fig. 5.1 were invisible. The red concentric circles shown in Fig. 5.1 demonstrate available eccentricity ranges for static adaptation stimuli, and were also invisible in actual experiment.

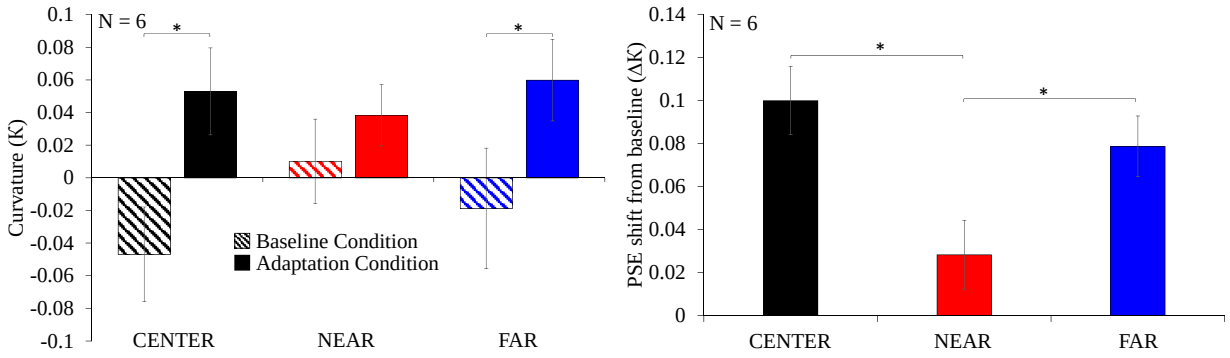

(a) Perceived curvature at PSE across all conditions (b) Group mean of adaptation magnitude

Figure 5.2 Result over all six observers for Experiment 2.1. Error bars represent standard errors of means. $*p < 0.05$

Procedures It is worth emphasizing that both sides of adaptation stimuli, as depicted in Fig. 5.1, were shown during pre-adaptation phase. But for each subsequent trial, only a single side was randomly selected to present during top-up phase, and test stimuli were always presented at identical location to the adaptation stimuli of the top-up phase.

5.2.2 Results

The ANOVA result showed a significant main effect of condition on PSE value ($F_{5,25} = 4.508,\ MSE = 0.011,\ p = 0.005,\ \eta^2 = 0.474$). The multiple comparison with Bonferroni adjustment indicated a significant difference between adaptation condition and its corresponding baseline condition for both CENTER condition ($p = 0.022$) and FAR condition ($p = 0.038$), whereas this was not the case for the NEAR condition ($p = 1.000$) shown in Fig. 5.2(a). There was no statistical difference between every pair of adaptation conditions or test conditions. The main effect of adaptation condition was statistically significant on aftereffect magnitude ($F_{3,10} = 16.039,\ MSE = 0.008,\ p = 0.001,\ \eta^2 = 0.762$). Furthermore, the multiple comparison with Bonferroni adjustment revealed that NEAR condition had a significantly smaller aftereffect than both CENTER ($p = 0.014$) and FAR condition ($p = 0.025$), as shown

in Fig. 5.2(b). However, no significant difference on aftereffect magnitude was found between CENTER and FAR conditions for aftereffect magnitude ($p = 0.41$) (all $ps < 0.05$).

5.3 Experiment 2.2: Adaptation to PSI

5.3.1 Methods

Observers Five stereo-competent observers (aged 27-34 years) participated in Experiment 2.2. All had normal or corrected-to-normal visual acuity. Four of them had participated in Experiment 1. One was an author of the study, whilst the others were paid volunteers and naive to the purpose of the study.

Visual stimuli As shown in Fig. 5.3, dynamic adaptation stimuli with size scaling, similar to those used in the DS condition of Experiment 1, were utilized to smear possible adaptation to both disparity information and shape curvature, and to further examine possible PSI adaptation. Adaptation and test stimuli were always presented at the central position.

The pixel number of size radius of stimuli was used to define the name labels of four adaptation conditions, which included DS_{75-85} condition, DS_{65-95} condition, DS_{50-80} condition and DS_{80-110} condition. For DS_{s1-s2} condition, the radius of the adaptation stimuli was always smoothly and periodically scaling up and down between s1-pixel size and s2-pixel size. Under our experimental settings, the stimulus size was scaled within a range of 5.08 - 5.76 deg for DS_{75-85} condition, 4.40 - 6.44 deg for DS_{65-95} condition, 3.39 - 5.42 deg for DS_{50-80} condition and 5.42 - 7.45 deg for DS_{80-110} condition. The constant relative disparity between fixation point and stimulus edge was 4.07 deg larger than the maximum relative depth (3.73 deg) of adaptation stimuli. The pedestal disparity changed within a range of 7.3 - 9.4 arcmin for DS_{75-85} condition, 5.3 - 11.4 arcmin for DS_{65-95} condition, 8.4 - 14.4 arcmin for DS_{50-80} condition and 2.1 - 8.4 arcmin for DS_{80-110} condition. Considering

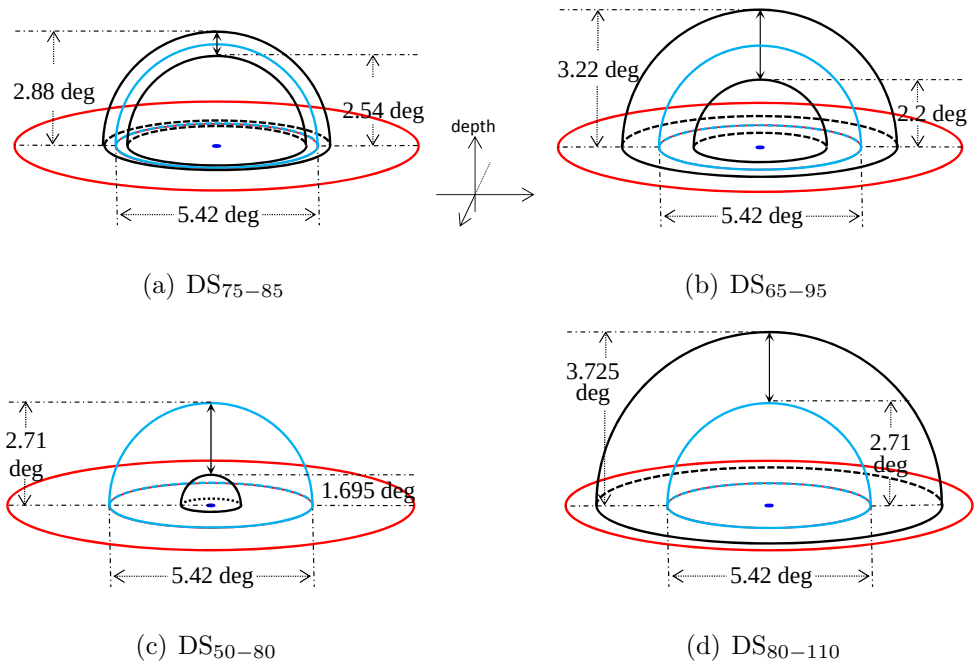

(a) DS_{75-85} (b) DS_{65-95}

(c) DS_{50-80} (d) DS_{80-110}

Figure 5.3 Schematic illustration of dynamic adaptation stimuli used in Experiment 2.2. All stimuli were viewed with fixed central vision. Four adaptation conditions were endowed with distinct scaling range for size change. Adaptation and test stimuli shared the same location during each trial.

that the slight difference of ADIs between DS and ACV/FS conditions in Experiment 1 did not facilitate isolation of the PSI adaptation from ADI adaptation, diverse conditions were configured either with the same ADI (or the same scale mean defined as (s1 + s2) / 2) but different relative scaling ranges ($\Delta s = |s1 - s2|$), or with different ADIs but the relative same scaling range in Experiment 2.2. Specifically, the same ADI was shared only between DS_{75-85} condition and DS_{65-95} condition, while there was the same relative scaling range among conditions DS_{65-95}, DS_{50-80} and DS_{80-110}. The different ADIs here can provide observers with perceptual difference for size scaling. To prevent the formation of afterimages, dot pattern on the adaptation stimuli was changed randomly at 10 Hz, as applied in Experiment 1. The same test stimuli were adopted as in Experiment 2.1.

For each adaptation condition, the initial and the last frame of the scaled adaptation

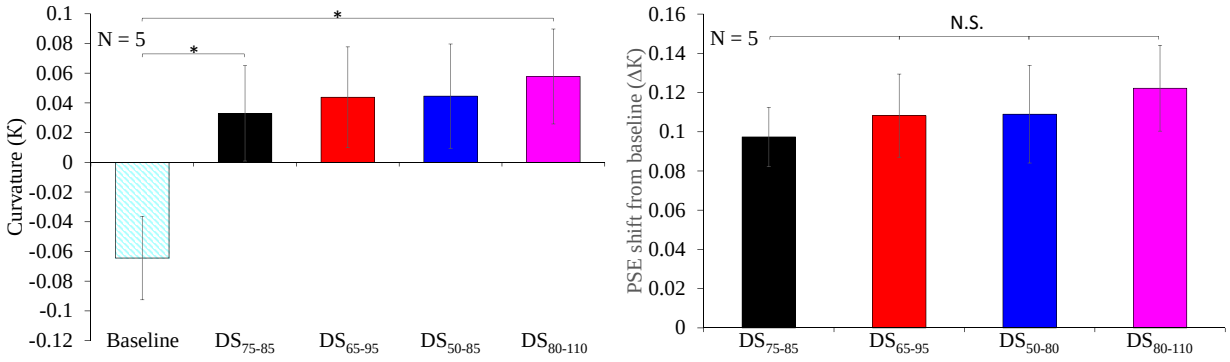

(a) Perceived curvature at PSE across all conditions (b) Group mean of adaptation magnitude

Figure 5.4 Result over all five observers for Experiment 2.2. Error bars represent standard errors of means. $*p < 0.05$.

stimuli shared the same stimulus size (5.42 deg) with test stimuli for each trial. That is, the opposite initial scaling direction was determinedly involved between DS_{50-80} condition and DS_{80-110} condition, whereas there was the randomized initial direction for both DS_{75-85} condition and DS_{65-95} condition.

Procedures Under the current settings, the size scaling of adaptation stimuli was cycled only ten times for pre-adaptation phase and one time for top-up phase.

5.3.2 Results

The ANOVA result showed a significant main effect of condition on PSE ($F_{4,16} = 20.283$, $MSE = 0.012$, $p = 0.00$, $\eta^2 = 0.835$). The subsequent multiple comparison with Bonferroni adjustment revealed that baseline condition had a significant smaller aftereffect than DS_{75-85} condition ($p = 0.029$) and DS_{80-110} condition ($p = 0.050$), as shown in Fig. 5.4(a). No other significant effect was found for PSE curvature among any of the conditions. For aftereffect magnitude shown in Fig. 5.4(b), all the adaptation conditions had aftereffects significantly larger than zero in one sample t-test. However, no significant main effect of adaptation

condition was found on aftereffect magnitude ($F_{3,12} = 1.901,\ MSE = 0.001,\ p = 0.183$) (all $ps < 0.05$).

5.4 Experiment 2.3: Adaptation to ADI

5.4.1 Methods

Observers The same observers participated in Experiment 2.3.

Visual stimuli As shown in Fig. 5.5, dynamic adaptation stimuli with PSI scaling were used to eliminate possible adaptation to disparity information, shape curvature and PSI, and to further examine possible ADI adaptation. Adaptation and test stimuli were always presented at the central position.

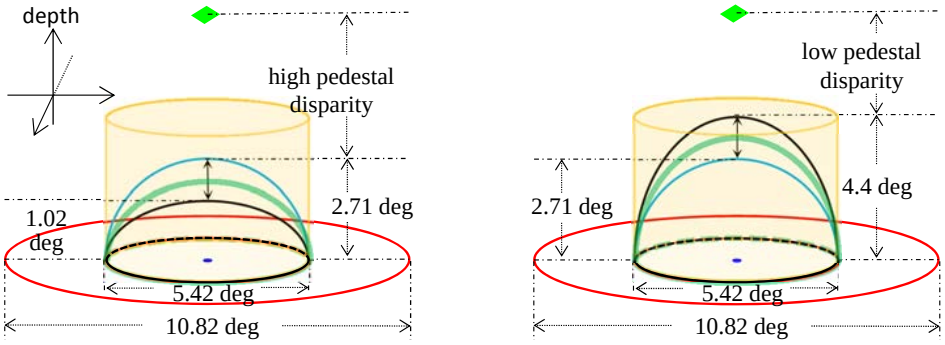

(a) DPSI_{30-80} (b) DPSI_{80-130}

Figure 5.5 Schematic illustration of dynamic adaptation stimuli used in Experiment 2.3. DPSI was short for Dynamic_PSI , which means that adaptation stimuli dynamically changed PSI at 20 Hz. All stimuli were viewed with fixed central vision. Two adaptation conditions were endowed with distinct scaling range for PSI change, producing different green-colored ADIs. Adaptation and test stimuli shared the same location during each trial.

Unlike Experiment 2.2, all the adaptation stimuli kept a constant size of 5.42 deg in Experiment 2.3, and their peak-to-base distance altered rapidly. In this sense, the adaptation stimuli were not hemispherical but mostly semi-ellipsoidal surfaces. However, the PSI scaling

of the adaptation stimuli were perceived very smoothly, because these stimuli mathematically shared a unified ellipsoid formula. Because PSI scaling is relatively difficult to perceive compared with size scaling if only binocular disparity cue is available for depth perception, Experiment 2.3 adopted a larger range for PSI scaling than that for size scaling in Experiment 2.2 in order to perceive a significant PSI scaling. For the same reason, dots of identical depth were distributed uniformly on stimulus surfaces. This was implemented using Recursive Zonal Equal Area Sphere Partitioning Toolbox (Leopardi, 2006). Position jitter was used to prevent the formation of afterimages. The current study involved two adaptation conditions including DPSI_{30-80} condition and DPSI_{80-130} condition. The same rule as Experiment 2.2 was applied to name condition label except the pixels number representing the metrics of peak-to-base distance of dynamic adaptation stimuli. That is, $\mathrm{DPSI}_{\mathrm{h1-h2}}$ denoted that the peak-to-base distance of adaptation stimuli was always smoothly and periodically scaling up and down between h1-pixel height and h2-pixel height. Obviously, there was the same relative range (Δh = |h1 - h2|) but different scale means ((h1 + h2) / 2) for the PSI scaling between these two adaptation conditions. The constant relative disparity between fixation point and stimulus edge was 4.74 deg larger than the maximum relative depth (4.4 deg) of dynamic adaptation stimuli. The pedestal disparity changed within a range of 12.7 - 22.6 arcmin for DPSI_{30-80} condition and 2.2 - 12.7 arcmin for DPSI_{80-130} condition. Also, owing to the difficulty of perceiving the PSI scaling, Experiment 2.3 adopted the same test stimuli as Experiment 1. That is, eleven different test levels were involved instead of seven as in Experiment 2.2.

Procedures During each trial for all adaptation conditions, the same PSI with the peak-to-base distance of 80 pixels distant was shared by both the initial and the last frame of the scaled adaptation stimuli. The PSI scaling of adaptation stimuli was cycled only ten times for pre-adaptation phase and one time for top-up phase.

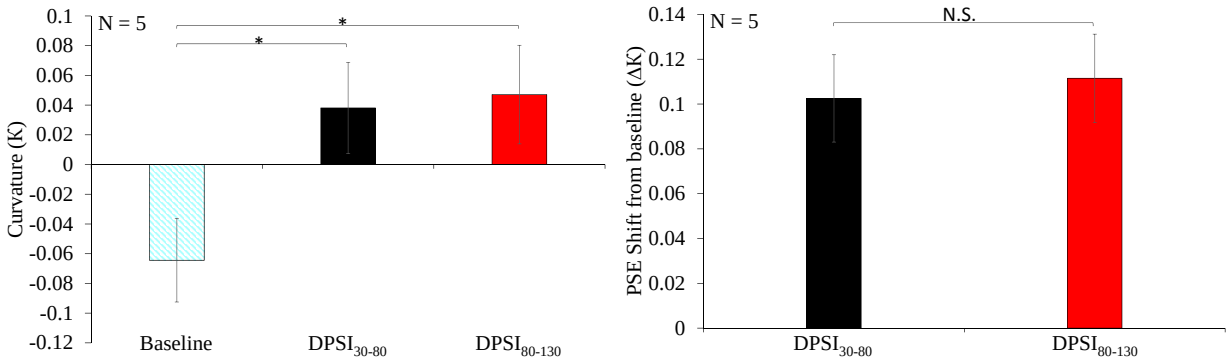

(a) Perceived curvature at PSE across all conditions (b) Group mean of adaptation magnitude

Figure 5.6 Result over all five observers for Experiment 2.3. Error bars represent standard errors of means. $*p < 0.05$.

5.4.2 Results

The ANOVA result showed a significant main effect of condition on PSE ($F_{2,8} = 28.458,\ MSE = 0.019,\ p = 0.00,\ \eta^2 = 0.877$). The subsequent multiple comparison with Bonferroni adjustment indicated the baseline condition differed significantly from both DPSI_{30-80} condition ($p = 0.019$) and DPSI_{80-130} condition ($p = 0.014$), as shown in Fig. 5.6(a). No statistical difference was found between these two adaptation conditions ($p = 0.701$). For adaptation strength shown in Fig. 5.6(b), there was also no significant main effect of adaptation condition on aftereffect magnitude ($F_{1,4} = 1.964,\ MSE = 0.000,\ p = 0.234$). However, the aftereffect magnitude of both adaptation conditions was significantly larger than zero-value in one sample t-test (all $ps < 0.05$).

5.5 Discussion

5.5.1 Eccentricity effect on adaptation strength

In Experiment 2.1, no significant difference in PSE-value was found among three baseline conditions, suggesting that individual difference was large for curvature discrimination task

under different eccentricity configurations. However, the individual difference became much smaller for adaptation magnitude. Also, a significant difference of PSE-value between baseline and adaptation situation was found for CENTER condition but not for NEAR condition. Accordingly, a significantly larger aftereffect was obtained for CENTER condition than for NEAR condition, the eccentricity (2.71 deg) of which was the upper limit of eccentricity of dynamic adaptation stimuli with changing location in Experiment 1. In this respect, the eccentricity effect on adaptation strength can be used to some extent to explain the retinal-position dependence in Experiment 1.

However, as discussed byNoest et al. (2006), extraction of depth structure can be error prone at a large slant in strips along object contour. The NEAR condition in Experiment 2.1 just involved a large slant ($\pi/2$) in stimulus edges, which always located at the central position. Thus the insignificant aftereffect in NEAR condition may be from the stimulus edge effect. Plus because there was no significant difference on aftereffect magnitude between CENTER and FAR conditions, there could be no eccentricity effects on adaption strength, if the stimulus edge effect can decrease adaptation strength. For this reason, eccentricity effect on adaptation strength can induce the retinal-position dependent of sCAE only when stimulus edge on fovea is not considered to decline adaptation strength.

5.5.2 Adaptation to PSI

The hypothesis tested in Experiment 2.2 concerned adaptation at a higher level of PSI than shape curvature for sCAE. To validate this hypothesis, adaptation stimuli with size scaling was adopted in order to smear both possible disparity adaptation and certain shape-curvature adaptation. A comparison was made among four adaptation conditions with two distinct relative size ranges, of which 10 pixels for DS_{75-85} condition as well as 30 pixels for DS_{65-95}, DS_{50-80} and DS_{80-110} conditions. The same ADI was only involved between DS_{75-85} and

DS_{65-95} conditions. The results agreed with the hypothesis on PSI adaptation, because significant aftereffects were found for all adaptation conditions with perceptually different size-scaling settings, which involved either the same ADI and different relative scaling ranges or the same relative scaling range and different ADIs. Furthermore, no statistical difference on aftereffect magnitude was found among these conditions. Accordingly, there should be an adaptation to size-invariant PSI. Also, PSI adaptation contributed much more to sCAE than other adaptations such as possible ADI adaptation. Thus, PSI condition can be used to explain the scale independence of sCAE in Experiment 1.

5.5.3 Adaptation to ADI

The hypothesis tested in Experiment 2.3 is related to stereo-curvature adaptation at a lower level of ADI than shape curvature. The hypothesis can not be definitely rejected, although no significant difference was found on aftereffect magnitude even for adaptation conditions with different ADIs in Experiment 2.2. One possible explanation for the lack of any significant difference is a much larger contribution of PSI adaptation to sCAE compared with ADI adaptation. To validate this hypothesis, Experiment 2.3 adopted the adaptation stimuli with PSI scaling in order to circumvent possible disparity adaptation as well as certain adaptation to both shape curvature and PSI. The result showed significant aftereffects even for adaptation conditions with the periodical PSI scaling, suggesting that continuous stimulation of constant PSI was not essential for stereo-curvature adaptation.

No statistical difference on aftereffect magnitude was found between $DPSI_{30-80}$ and $DPSI_{80-130}$ conditions, although there was rather smaller ADI for $DPSI_{30-80}$ condition than $DPSI_{80-130}$ condition. However, the lack of any significant difference did not contradict the hypothesis of ADI adaptation, considering a large difficulty of perceiving PSI change in DPSI30-80 because of a high pedestal disparity. It can be thought of as within-

shape discrimination task to perceive PSI scaling in Experiment 2.3. Vreven (2006) reported that within-shape discrimination was increasingly difficult with increasing pedestal disparity. Thus, the large pedestal disparity involved in $DPSI_{30-80}$ condition made observers fail to perceive the PSI change of dynamic adaptation stimuli. This is in agreement with observers' subjective feedback. After each block corresponding to $DPSI_{30-80}$ condition, all of five observers reported no change on the adaptation stimulus, but they can perceived the adaptation stimulus as convex. Admittedly, it is beyond our knowledge to examine how pedestal disparity influences stereo-curvature adaptation. But there is a possible explanation for the significant aftereffect in $DPSI_{30-80}$ condition, which involved a high pedestal disparity. That is, a perceptually constant convex 3D shape can resulted from the high difficulty of perceiving the PSI range in $DPSI_{30-80}$ condition. Moreover, there is a possible adaptation to shape curvature of the constant 3D shape. Thus, $DPSI_{30-80}$ condition had an aftereffect with no significantly smaller magnitude than DPSI80-130 condition, in that shape-curvature adaptation dominantly contributes to sCAE.

Actually, ADI adaptation can be completely determined only from the significant aftereffect in $DPSI_{80-130}$, which involved significantly smaller pedestal disparity. It can be considered that there is no pedestal effect on adaptation strength, promoting observers to perceive the dynamic PSI change of adaptation stimuli to a large extent. The perceived PSI change can smear adaptation to both shape curvature and PSI. Also, considering the same relative scaling range used in all adaptation conditions of Experiment 2.3, we conducted a secondary experiment in order to examine influence of end curvature and relative scaling range on adaptation strength in PSI scaling situation. Four adaptation conditions involved either the same relative scaling range but distinct curvatures for end (or starting) frame or the same end curvature but distinct relative scaling ranges. The results showed no significant difference on adaptation strength among these conditions, indicating no significant

effect of both end curvature and relative scaling range on aftereffect magnitude. In these regards, the significant aftereffect in DPSI80-130 certainly resulted from the ADI adaptation, in accordance with our hypothesis about ADI adaptation.

In summary, sCAE can result from adaptation to both disparity-specified ADI and percept-specified PSI. And PSI adaptation contributes much more to sCAE than ADI adaptation, as shown in Experiment 2.1. Furthermore, the retinal-position dependence of sCAE, found in Experiment 1, can be due to ADI adaptation and possible eccentricity effect on adaptation strength, while scale independence of sCAE can result from PSI adaptation.

Chapter 6

General discussion for psychophysical study

In our study, retinal-position dependent sCAE was found, supporting that there should be two parallel adapting processes for sCAE. One process is independent of retinal position, and the retinal-position independence can be induced by adaptation to percept-specified sources, such as shape curvature and PSI. The other process is dependent on retinal position, and the retinal-position dependence can be caused by adaptation to disparity-specified sources, like ADI. Thus, our result also support the prediction we made for adapting mechanism of sCAE. That is, sCAE is due to multi-level adaptation, including not only adaptation to percept-specified sources but also adaption to disparity-specified sources.

Among these possible adaptation sources listed in Fig. 6.1, disparity curvature was not adapted in the study of Domini et al. (2001), although adaptation to disparity curvature was documented for curvature contrast effect by Te Pas et al. (1997). Shape curvature was determined to be dominantly adapted in the study of Noest et al. (2006). Our study further supports the dominant contribution of shape-curvature adaptation for sCAE, as all

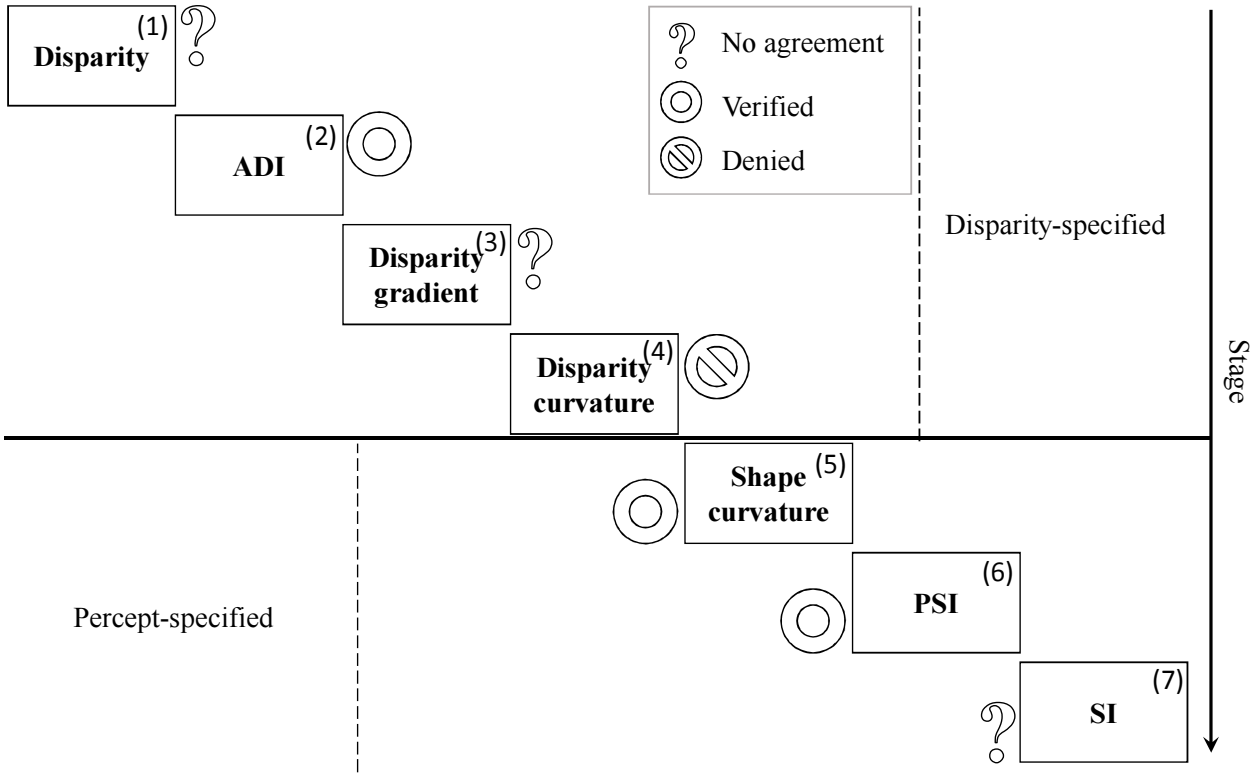

Figure 6.1 Results of deciding adaptation sources for sCAE. (1) had been discussed under no agreement by Berends & Erkelens (2001a, 2001b), Duke & Wilcox (2003) and Noest et al. (2006); (5) had been verified by Domini et al. (2001) and Duke & Wilcox (2003); (4) had been denied by Domini et al. (2001); (2) and (6) were verified in our study; (3) and (7) need to be further confirmed.

adaptation conditions had positive PSE-values even for ACC condition in Experiment 1. In addition to shape curvature, our study confirms that there are other adaptation sources including disparity-specified ADI and percept-specified PSI, and shows that PSI adaptation contributes much more to sCAE than ADI adaptation.

Here, a conclusion about ADI adaptation was drawn under a hypothesis. That is, during adaptation phase, the lower level of zero-order disparity information can be averaged in space, and the averaged disparity information can be adapted, but it is more difficult for higher-level adaptation sources to be averaged. We did not consider the averaging process for other higher-level adaptation sources including shape curvature, PSI and SI, because these sources

are at percept-specified stages and at a much higher level than absolute disparity. A similar hypothesis has been proposed in Howard and Rogers (2012), who suggested that adaptation to zero-order disparity rather than higher-order sources could be scaled by viewing distance, when explaining the experiment results of Domini et al. (2001).

We did not consider the averaging process on percept-specified adaptation sources including shape curvature and PSI based on two reasons. First, there is no related study to support that percept-specified sources can be averaged according to our knowledge. Second, high levels of percept-specified sources were assumed to be more difficult to be averaged. This assumption makes sense at least for shape curvature. Supposing a substantive contribution of averaged shape curvature on adaptation strength, there would be significantly different aftereffects among four adaptation conditions in Experiment 2.2, in which no significant difference was actually obtained on aftereffect magnitude.

Inconsistent conclusions were drawn on disparity adaptation in previous studies (Berends & Erkelens, 2001a, 2001b; Duke & Wilcox, 2003; Noest et al., 2006), because of incompetent stimuli used to isolate adaptation to shape curvature and disparity information. In our study, the adaptation to absolute disparity is still not determined, considering that disparity information is rapidly altered for our dynamic adaptation stimuli. Thus, disparity adaptation remains largely uncharted. A similar situation can be found for adaptation to disparity gradient. Also, we could not determine possible adaptation to SI at a higher level than PSI, considering that SI is independent of size and PSI. However, adaptation to ADI and PSI is determined in our study, suggesting that multi-level adaptation occurs for sCAE. Specifically, the stereo-curvature adaptation can occur at not only percept-specified stage but also disparity-specified stage.

In addition, if the stimulus edge effect does not decrease adaptation strength in NEAR condition of Experiment 2.1, it was beyond our knowledge to explain the strong adaptation

for FAR condition, wherein static adaptation stimuli were presented in peripheral visual area. This leaves open the question of how the visual system adapts to static stimuli in peripheral area. However, it does not invalidate any conclusion we drew on dependency and multi-level adaptation of sCAE.

Part II

fMRI Study

Chapter 7

Introduction

Up to now, no enough previous fMRI studies have provided evidences to support multi-level stereo-curvature adaptation, which covers adapting to both disparity- and percept-related sources, as found in our psychophysical studies. However, there are many human fMRI studies showing brain cortices selective to disparity or for disparity-defined 3D shapes, as shown in Table 7.1.

7.1 Possible cortical areas sensitive to disparity

There is an undeniable fact that disparity-selective neurons broadly distribute in most visual areas in terms of human functional MRI studies. The selectivity to disparity exists along multiple levels of the visual hierarchy, starting from as early as striate cortex (also known as primary visual cortex or V1) and further encompassing extra-striate and higher-order areas, such as posterior parietal and the inferior temporal cortices (Chandrasekaran, Canon, Dahmen, Kourtzi, & Welchman, 2007), in both the dorsal and ventral visual streams as shown in the fMRI study of Durand, Peeters, Norman, Todd, and Orban (2009) and the fMRI-informed EEG source-imaging study of Cottereau, Ales, and Norcia (2014). However, disparity-selective responses in extra-striate areas are more likely linked to the perception of

stereoscopic depth than their counterpart in striate area V1. Besides, distinct responses to disparity between dorsal and ventral visual pathway were found in terms of onset time and selectivity. Specially, brain activities of perceptual relevance in dorsal stream earlier emerge than those in ventral stream. Furthermore, dorsal areas showed selective responses tuned to disparity content, while ventral areas encode binocular disparity with the identical sign in a categorical manner (Preston, Li, Kourtzi, & Welchman, 2008). In addition, single-/multi-unit recordings showed several differences for macaque on the representation of stereoscopic depth within single area such as V1 (Prince, Cumming, & Parker, 2002), MT/V5 (DeAngelis & Uka, 2003) and V4 (Tanabe, Doi, Umeda, & Fujita, 2005).

Stereoscopic depth sensitivity has been found in human early visual areas including V1, V2, V3 and VP (ventral posterior cortex) . Smith and Wall (2008) found strong selectivity for near and far depth planes in all early visual areas. Moreover, Preston et al. (2008) indicated similar selectivity for both correlated and anticorrelated stimuli in V1, which is conventionally thought to be only involved in absolute disparity processing. No orientation-specific adaptation effects in primary visual cortex (V1), but increasing effects along the hierarchy of visual areas (V2, V3 and hV4) (Boynton & Finney, 2003). However, Neri, Bridge, and Heeger (2004) reported a small adaptation effect to both absolute and relative disparity in early visual areas.

Disparity-selective responds have been found in dorsal areas, such as V3A region (Preston et al., 2008). Cottereau, McKee, Ales, and Norcia (2012) in their fMRI-informed EEG source-imaging study, reported that V3A region were sensitive to relative disparity other than to absolute disparity. However, Neri et al. (2004) found more adaptation to absolute disparity than that to relative disparity in dorsal areas (V3A, hMT+/V5, V7).

Among ventro-lateral areas, hV4 region provides an early contribution to disparity discrimination (Cottereau et al., 2014). Neri et al. (2004) reported neurons with responses

Table 7.1 Review on selectivity of ROIs

Cortical Area		Selective To
early	V1	absolute disparity for anticorrelated/correlated RDS
	V2	absolute/relative disparity, 3D shape coherence (V2v)
	V3	absolute disparity
	VP	absolute disparity, 3D shape
ventro-lateral	hV4	absolute/relative disparity
	LO	relative disparity, 3D shape
dorsal	V3A	absolute/relative disparity, 3D shape
	KO/V3B	3D shape
	hMT+/V5	relative disparity, 3D shape
	V7	3D shape
IPS	VIPS/V7*	3D shape, position in depth
	POIPS	3D shape
	DIPS	3D shape

selective to relative disparity rather than to absolute disparity in the region. And They found that ventral areas (hV4, V8/V4α) involved an equal adaptation to absolute and relative disparity.

7.2 Possible cortical areas sensitive for disparity-defined 3D shape

Brain activity in both dorsal and ventral visual areas varies in correspondence with an observer's perception of shape defined by disparity (Chandrasekaran et al., 2007; Durand

et al., 2009). Dorsal areas (visual and parietal) shows preferential disparity selectivity for correlated stimuli, suggesting a metrical representation in these areas for depth structure of disparity-defined 3D stimuli. In contrast, ventro-lateral areas, such as LO (lateral occipital cortex) region, do so categorically (Preston et al., 2008). As shown in Table 7.1, IPS regions and most dorsal areas were more selective to disparity-defined 3D shape than early visual areas and ventro-lateral areas in human brain.

It has been reported, in human early visual areas, that extraction and processing of 3D shape from disparity were performed in V2v region (Georgieva, Peeters, Kolster, Todd, & Orban, 2009). And significant relationships between shape coherence and fMRI response were found in VP area (Chandrasekaran et al., 2007).

Stronger activation in ventro-lateral regions, such as LO region, than that in earlier retinotopic regions for disparity-defined shape, suggesting that these regions are involved in the processing of depth information (Mendola, Dale, Fischl, Liu, & Tootell, 1999). The region represents depth position in a categorical manner (Preston et al., 2008). Responses in the region were found to be diagnostic of stimulus symmetry (Chandrasekaran et al., 2007). However, the region showed no selectivity for 3D shape defined by contours or monocular depth cues (Kourtzi & Kanwisher, 2000).

Human dorsal areas also showed response selectivity for disparity-defined 3D shape. Georgieva et al. (2009) reported that extraction and processing of 3D shape from stereo were performed in V3A complex. Besides V3A, other dorsal regions, including KO/V3B and V7 were found to involve for processing of disparity-defined depth (Preston et al., 2009). The posterior part of the hMT+/V5 region also showed selectivity for depth structure (Durand et al., 2009). Similar to LO, fMRI responses in KO/V3B and hMT+/V5 are diagnostic of shape coherence (Chandrasekaran et al., 2007). Preston et al. (2009) reported a important role KO/V3B and V7 in 3D shape estimation. Using ambiguous probe stimulus with zero

disparity, they showed the essence of adaptive context to extract 3D shape from disparity, and claimed a neural adaptation representation of perceptual aftereffect at percept stage other than at disparity stage.

Many studies reported estimation of depth structure from stereo in IPS regions including VIPS/V7* (ventral intraparietal sulcus) , POIPS (parieto-occipital intraparietal sulcus) and DIPS (dorsal intraparietal sulcus) (Georgieva et al., 2009; Durand et al., 2009; Preston et al., 2009). In these region, stronger selectivity for disparity-defined 3D shape was found compared with other regions, as shown in Table 7.1.

Besides, there are other areas in human brain involving extraction and processing of 3D shape from stereo, at least including an inferior temporal region (posterior ITG) and two premotor regions (dPrCS and vPrCS) (Georgieva et al., 2009).

7.3 fMRI adaptation paradigm & adaptation quantification

There is a limited spatial resolution in conventional mapping methods used for fMRI studies, which measure overall neural activation within a voxel possibly housing a mixture of neuronal populations, each of which tuned to an exclusive property. However, fMRI adaptation (fMRIa) can overcome the spatial resolution limitation, and enable to tag subpopulations of neurons within an imaging voxel. Thus it provides a powerful tool for assessing the functional properties of cortical neurons.

As a robust experience-related cortical dynamics, repeated presentation of a stimulus induces a stimulus-specific adaptation (also known as repetition suppression), which depends critically on the sameness of two successive stimuli. Obviously, the adaptation will inhibit brain activity, when the same subpopulation within one voxel is stimulated by these two stimuli (Kourtzi & Kanwisher, 2001). Thus, the adaptation provides a technique to infer

nature of representations across different stages of a processing stream. If responses to a identical-stimulus pairs are reduced compared to their nonidentical counterpart, then the response decline is usually interpreted as evidence of neuronal selectivity for the stimulus feature in question (Larsson & Smith, 2012).

Adaptation has been reported at multiple spatial and temporal scales (see in review of Weiner, Sayres, Vinberg, and Grill-Spector (2010)). It exists two distinct types of design for fMRIa studies. One is blocked design, which measures repetition suppression induced by multiple repetitions of the same stimulus without intervening items. The other is event-related design, which measure repetition suppression after a single presentation with either no or many intervening items. Actually, there is another increasingly popular mixed design, which integrates advantages of both blocked and event-related design. As reviewed by Grill-Spector, Henson, and Martin (2006) and Larsson and Smith (2012), fMRIa paradigm has been widely used with multiple purposes from to examine selectivity of low-level visual information through to probe high-level conceptual representation and further to identify neurons with more abstract response properties.

Depending on different experimental purposes and design, distinct methods are used to quantify adaptation effects in fMRIa paradigms. For a block-designed fMRIa paradigm, adaptation aftereffects are measured as a ratio, usually referred to as adaptation ratio, between the activation, measured as percent signal change, in a condition and averaged activation in the non-adapted epoch (Grill-Spector & Malach, 2001).

For event-related-designed fMRIa paradigm, pairwise stimuli are presented as adaptor and probe within one stimulus trial. Adaptation effects are usually measured as amplitude difference of response between adapted and unadapted probe for each voxel. There are two distinct methods available to determine the response for unadapted probe stimulus. In one method, nonrepeated stimulus or object was used to differ between adaptor and probe.

Thereafter, adaptation effects are measured as amplitude difference between repeated and nonrepeated response (Grill-Spector et al., 1999; Grill-Spector & Malach, 2001; Sayres & Grill-Spector, 2006; Smith & Wall, 2008; Andresen, Vinberg, & Grill-Spector, 2009; Weiner et al., 2010; Freud, Ganel, & Avidan, 2013). The other method for unadapted probe is to use blank stimulus for adator as baseline condition. The adaptation effects were usually defined as the ratio of response amount from adaptation condition to that from baseline condition (Neri et al., 2004; Preston et al., 2009).

In our psychophysical study, two novel properties of disparity-defined 3D shapes, ADI and PSI, were investigated to show multi-level adaptation for sCAE. We found stereo-curvature adaptation occurred to both disparity- and percept-related sources. Many cortices involve disparity-selective responses, and shows percept-related selectivity for disparity-defined 3D shape. However, there is response difference on selectivity to absolute and relative disparity among cortices along dorsal and ventral visual pathways. And distinction also exists in cortices with percept-level selectivity. Specially, some region showed size invariance for 2D/3D shape, while the other not. Therefore, the previous findings of selectivity to disparity and perceived shape are not enough to support the multi-level stereo-curvature adaptation found in our psychophysical study. To this end, an fMRIa experiment was conducted to probe multi-level adaptation across cortical regions involving selectivity to disparity and perceived shape in our study. Another purpose of the fMRI study is to determine size-invariant cortical regions and coarse distribution of source adapted in human brain.

To investigate multi-level adaptation using an fMRIa paradigm, we isolated distinct adaptation sources across different experimental condition. Like in our psychophysical study, stimulus dynamics, including dynamically changed size and PSI of adaptation stimuli, was used in order to separately examine PSI and ADI. However, unlike in our psychophysical study, we did not used dynamic location for adaptation stimuli to quantitatively charac-

terize ADI in the fMRI study. Instead, ADI adaptation was eliminated by moving fixation along Lissajous path in a random invisible planar, which is orthogonal to fronto-parallel planes. Before the fMRIa experiment, we used independent functional scans for localization of ROIs involving selectivity to disparity and perceived shape. The ROIs including early visual regions (V1, V2d, V2v, V3, VP), ventro-lateral regions (hV4, LO), dorsal regions (V3A, KO/V3B, hMT+/V5, V7) and SFM-related regions (VIPS/V7*, POIPS, DIPS), as shown in Appendix B. Besides, adaptation effects were also examined at a coarser spatial level, when we performed data analysis on an inseparable ROI containing all subregions in early, ventro-later or dorsal areas.

Chapter 8

Experiment 3: fMRIa examination of multi-level adaptation

8.1 Question to answer: What and where to adapt in human brain?

For the purpose of neuro evidences to further verify multi-level stereo-curvature adaptation, which was drawn as conclusion of our psychophysical experiments, a human fMRIa experiment was conducted to test for disparity-defined 3D shapes onto fMRI adaptation selectivities of ROIs along the path of either ventral or dorsal stream from early visual areas. To this end, we designed adaptation conditions for isolation of adaptation to specified kinds of adaptation sources, including both disparity-related (absolute disparity and ADI) and percept-related sources (shape curvature and PSI).

8.2 Methods

8.2.1 Observers

A total of four subjects (aged from 25 to 41 yr; 3 male and 1 female; YP, SH, WY, MY) took part in the fMRIa experiment reported here, including both authors. YP and WY participated in the previous psychophysical experiments. All had normal or corrected-to-normal vision including good stereoacuity. And all of them participated in the experiment on behavioral data acquisition as shown in Appendix A. When screening the participants, some volunteers were rejected due to excessive head movement in trial fMRI scans or poor ability to see the stereo-defined RDS. The experiment was conducted in accordance with procedures, approved by Kochi University of Technology, and written informed consent was obtained. Standard MRI scanning procedures were followed for all participants, and volunteers were paid for their time.

8.2.2 Data acquisition

Acquisition and processing of 3D structural data Each subject underwent a high-resolution T1-weighted anatomical scan of the whole brain at 3T (Magnetom Verio with I-class; Siemens, Erlangen, Germany) using a 32-channel head coil at Research Center for Brain Communication in Kochi University of Technology in order to localize ROIs (Regions of Interest) and visualize the functional data. The structural magnetic resonance imaging was performed using a three-dimensional magnetization-prepared-rapidacquisition-gradient-echo (3D MPRAGE) sequence lasting 8 min and 34 sec (TR (time to repeat) = 2250 msec, 192 slices, 1 mm isotropic voxels, single-shot multi-slice mode, interleaved series, FA (flip angle) = 9°, TE (time to echo) = 3.08 msec, FOV (field of view) = 256 × 256 mm^2, bandwidth = 230 Hz/pixel).

Acquisition and processing of 2D functional data The same scanner were used to acquire functional data. But we used different array head coils with 32-channel in ROI localization experiments and 12-channel in depth experiment. The stimulus image signal was generated by a personal computer at a frame of 60 Hz. The image was back-projected from gamma-corrected video projectors (DLA-X70R, 60 Hz, 1024 × 768 resolution; JVC, Yokohama, Japan) onto a translucent screen located at the end of the scanner bore (at the side of the subject's head). Participants lay supine in the scanner, looked up into an angled mirror to the rear of the bore. Soft wedges were used to stabilize head position and minimize head movement during scanning.

To measure the blood oxygenation level-dependent (BOLD) signal as a function of time, the T2*-weighted magnetic resonance images were acquired during visual stimulation using a two-dimensional, gradient-recalled echo-planar (GR-EPI) pulse sequence. In depth experiment, to achieve stereoscopic presentation, we used a pair of video projectors (JVC DLA-X70R) that contained separate spectral interference filters (fMRI Projector System; Kiyohara Optics Inc., Tokyo, Japan). The images from the two projectors were optically combined using a beam-splitter before being passed through a wave guide into the scanner room. The interference filters produce negligible overlap between the emission spectra for each projector with the result that there is extremely little cross talk. Stimuli were back-projected onto a screen inside the bore of the magnet. Observers viewed stereoscopic stimuli via a mirror above their heads, through polarizing goggle (Screen Box; Kiyohara Optics Inc., Tokyo, Japan) with prism lenses to adjust the viewing angle of each image of each eye and make fusion comfortable. The viewing distance was 71 cm as shown in Fig. 8.1(a).

Also in depth experiment, scanning took place over at most two sessions on different day for each participant. Each session ended with an anatomical (2D, T2-weighted) scan. fMRI data were recorded with an echo-planar imaging sequence using standard parameters

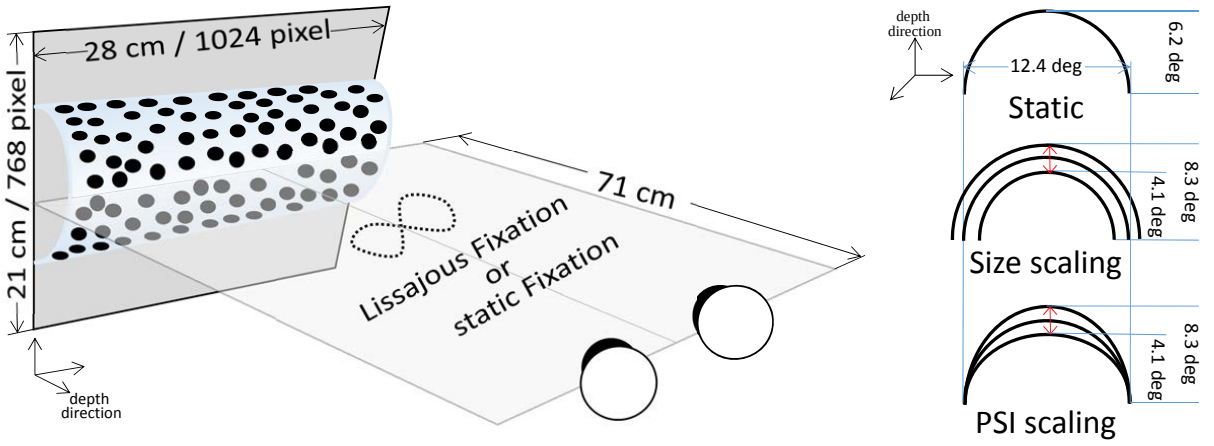

(a) Experiment environment (b) Sagittal stimulus

Figure 8.1 Schematic illustration of experimental set-up in Experiment 3.

(TR = 2000 ms, 30 contiguous axial slices, interleaved acquisition order, 3 mm isotropic voxels, base resolution of 64 × 64 voxels, FOV = 192 × 192 mm, FA = 80°, TE = 30 ms, bandwidth = 2368 Hz/pixel). We acquired 12 - 18 functional runs, each consisting of 156 images, for every subject. The first three volumes were discarded to allow for magnetization equilibration. Within each session, in order to facilitate 3D motion correction of the fMRI data and subsequent co-registration of the fMRI data to the anatomical scan, a T2-weighted scan was performed with the same slice specifications as the functional series (TR = 6000 ms, 30 contiguous axial slices, interleaved multi-slice mode, descending series, 3 mm isotropic voxels, base resolution of 256 × 256 voxels, FOV = 192 × 192 mm, FA = 160°, TE = 58 ms, bandwidth = 181 Hz/pixel).

In ROI localization experiments, only one projector was used. One session mostly include different ROI localizers with distinct TR parameters, like 3000-ms TR for localizers of hMT+/V5, KO/V3B and SFM-related ROIs as well as 2000-ms TR for LOC localizer and retinotopic mapping experiment, so one T2-weighted scan was performed with the same slice specifications as the functional series of each TR setting.

8.2.3 Visual stimuli

All stimuli in our fMRI study were generated by Matlab 2012a (Mathworks, Natick, MA), using Psychophysics Toolbox Version 3 (Brainard, 1997; Pelli, 1997; Kleiner et al., 2007). The stimuli, defined by crossed (convex) disparities, were horizontal hemi-cylinders. Stimuli consisted in black and white dots (1.2 arcmin size, anti-aliased for sub-pixel resolution, 44% density for static situation) on a 50% gray background. Hemi-cylinders were symmetric to both the horizontal and the vertical midline. The horizontal width of the hemicylinderical surface subtended a fixed visual angle of 22.3 deg so that participants can not perceive horizontal circular edges of the hemicylinder. The maximal stimulus height was 16.6 deg and the minimum size 8.2 deg. They were counter-phase flickered at 6.7 Hz. As shown in Fig. 8.1(b), there were three kinds of stimuli: static stimulus, size-scaling stimulus and PSI-scaling stimulus.

Subjects passively viewed the stimulus while maintaining fixation at a black rectangle (2.6 arcmin), which was superimposed on the stimulus and was either fixed at center or moving along Lissajous path in depth. The initial and final fixation distance were always 61 cm during each adaptation phase, no matter whether fixation path was static or Lissajous. Obviously, three stimulus types were combined with two fixation types, yielding six different adaptation conditions including StaticFixStaticStim condition, MoveFixStaticStim condition, StaticFixDynamicScale condition, MoveFixDynamicScale condition, StaticFixDynamicPSI condition and MoveFixDynamicPSI condition, as shown in Table. 8.1.

Adapting to adaptation sources of distinct types was eliminated in each stimulus. To this end, moving fixation along Lissajous path was used to eliminate adaptation to disparity-related sources of retinal dependence, size scaling to eliminate adaptation to retinal-dependent disparity and retinal-independent shape curvature, as well as PSI scaling to eliminate adaptation to all examined sources except ADI under static fixation. However, PSI scaling was

Table 8.1 Design intention of six adaptor stimuli. Each adaptor type was designed to eliminate specific kinds of adaptation sources. Each cell element answers whether row adaptor eliminates column source, where Y stands for a positive answer and N for negative answer. SFSS stands for StaticFixStaticStim condition , MFSS for MoveFixStaticStim condition , SFDS for StaticFixDynamicScale condition , MFDS for MoveFixDynamicScale condition , SFDP for StaticFixDynamicPSI condition and MFDP for MoveFixDynamicPSI condition .

			Elimination of adaptation to ?			
Stimulus Type	Fixation Type	Adaptation Condition	retinal-dependent & disparity-related		retinal-independent & percept-related	
			disparity	**ADI**	**shape curvature**	**PSI**
static	static	**SFSS**	N			
	moving	**MFSS**	Y		N	
dynamic scale	static	**SFDS**	Y	N	Y	N
	moving	**MFDS**	Y		Y	N
dynamic PSI	static	**SFDP**	Y	N	Y	
	moving	**MFDP**	Y		?	

perceptually invisible under moving fixation, so there is no significant perceptual difference between MoveFixStaticStim and MoveFixDynamicPSI condition, in accordance with subject feedbacks.

8.2.4 Behavioral data

As mentioned above, three types of adaptation stimuli were examined under either static fixation or pursuit of moving fixation point. For the static fixation, these stimuli were confirmed to induce a significant stereo-curvature adaptation in Experiment 1 and Experiment 2.

For the situation of pursuing fixation point moving along a Lissajous orbit, we conducted additional psychophysical experiment detailed in Appendix A. Result showed a significant adaptation for each type of adaptation stimulus, corresponding to a significant difference on PSE between baseline condition and each adaptation condition in Fig. A.2(a). Moreover, we did not find any statistical significance on comparison of adaptation amount among adaptation conditions, as shown in Fig. A.2(b).

Therefore, all of conditions, examined in the fMRIa experiment, indeed induced significant adaptation. Based on the fact, we can continue to use hemodynamic method to verify our hypothesis of multi-level stere-curvature adaptation.

8.2.5 fMRIa paradigm and protocol

Each scanning session comprised 6-12 runs, each of which lasted 5 min 12 sec. The experiment used an event-related adaptation paradigm, as depicted in Fig. 8.2. The event-related scans consisted of one 18-trial experimental epoch and two 16-sec fixation epochs, one at the beginning and one at the end of the scan during which only the fixation cross was presented. The experimental epoch consisted of 3 blocks, each of which included six trials for six different adaptation conditions presented in a randomized oder. In each trial, stimuli were presented in pairs including an adaptation stimulus (adaptor) and a test stimulus (probe). Adaptor was presented for 6.6 sec, followed by a ISI of 0.4 sec and finally by probe for 1 sec. The 6.6-s adaptation period used in our study and the repulsive aftereffects we observed are most consistent with a gain change interpretation of fMRI adaptation. The ISI provides a degree of separation of the response to adaptor and probe without losing the effects of adaptation (Smith & Wall, 2008). A fixed inter-trial interval (ITI) of 8 sec then followed before the start of the next trial. Each subject performed 12 - 18 runs for a total of 36 - 54 trial per adaptation condition. The test stimuli were always the same across different trials.

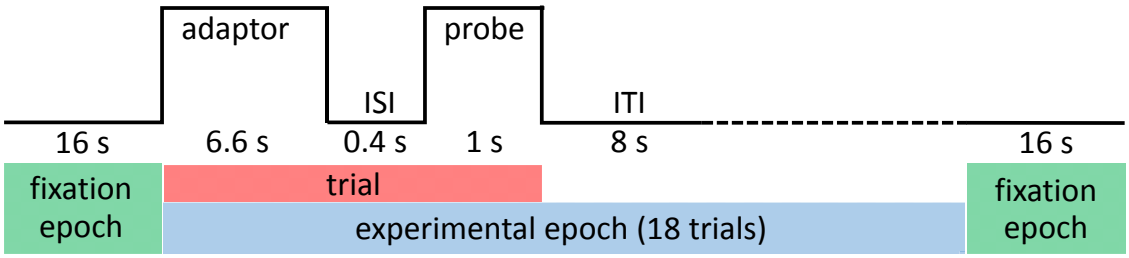

Figure 8.2 Experimental protocol for single functional series

The attention task during the adaptation phase required observers to attend to the pedestal distance-change.

8.2.6 fMRI data analysis

For each individual observer, T1-weighted 3D anatomical data were transformed into Talairach space and inflated and flattened surfaces of both hemispheres were rendered using BrianVoyager QX. The Freesurfer software package (http://surfer.nmr.mgh.harvard.edu/) was used to segment contiguous volume regions of the scalp, outer skull, inner skull and to convert these MRI volumes into inner skull, outer skull, and scalp surface. The brain was extracted from skull and other tissues. Subsequently, the extracted brain were transformed into Talairach space using Brainvoyager QX software (version 2.8, Brain Innovation, Maastricht, The Netherlands). Before segmentation of white matter (WM) and gray matter (GM), the computed WM from Freesurfer was used as a mask to yield a significantly distinct intensity between these two tissues. Lastly, the reconstruction of the cortical sheet was implemented by inflating the segmented flatted-GM and flattening surfaces of each hemisphere for each subject so as to facilitate the visualization of functional maps.

T2*-weighted 2D functional data, for both ROI localization and the depth experiment, were preprocessed only with 3D motion correction. The fMRI data were aligned to the subject's corresponding anatomical scan and transformed into Talairach space. Automated

alignment procedures were followed by careful visual inspection and manual fine-tuning at each stage of alignment to correct for misalignment error. Rigid-body transformations were done onto co-registration of 2D functional data to the within-session 3D anatomical scan, and then any residual misalignment between fMRI scans collected across different sessions appeared very small (less than 1 mm). After across-session alignment, the 4D functional data underwent Talairach transformation followed by a series of preprocessing including linear trend removal, spatial smoothing with 4 mm Gaussian kernel (FWHM) , and temporal high-pass filtering (3 cycles per run cut-off). It should be noted that no slice scan time correction was applied in the whole preprocessing of fMRI data. For each participant, T2-weighted anatomical data for each TR setting was used as a reference, using which the functional images with the same slice parameters were co-registered into T1-weighted anatomical data before transformed into Talairach space.

The Brainvoyager QX was used for all stages of the analysis, including preprocessing, multiple linear regression, reconstruction of the cortical sheet, and visualization of functional maps. BOLD time series were analyzed separately for each hemisphere. For ROI localizer of each subject, the voxel-wise statistical analyses of BOLD signal change were based on the application of the fixed-effects general linear model (GLM) with a boxcar waveform (ON/OFF) convolved with a two-gamma hemodynamic response function with default parameters. The data from each subject were z-normalized before the GLM computation. Activation clusters had to meet a threshold of at least $p < 0.05$ (corrected for multiple comparison using the false discovery rate method, FDR).

Localization of ROIs Retinotopic data were analyzed in accordance with known anatomical structures, by fitting a model to the time course obtained with the rotating wedges and expanding concentric rings as shown in Fig. B.1. This consist of a rectangular wave of appropriate duty cycle reflecting when the stimulus entered a particular portion of the visual

field, convolved with the hemodynamic impulse response function. The phase of the fitted response was taken as an index of visual field location in terms of polar angle. Reversal of the direction of phase change across the cortical surface were taken as boundaries of visual areas (Sereno et al., 1995). ROIs (visual areas V1-V4) were drawn by eye based on these boundaries viewed on flattened version of each participant's reference anatomy, transformed into Talairach space. The functional data from the fMRIa experiment were also transformed into Talairach space in order that time-course data could be extracted from the V1-V4 ROIs.

Visual cortical area V7 was defined as a region anterior and dorsal to V3A, while KO/V3B was defined as the set of contiguous voxels that were located anterior to V3A, inferior to V7 and posterior to the hMT+/V5 and that responded significantly higher to kinetic boundaries than uniform motion of RTP stimuli as shown in Fig. B.3. hMT+/V5 was defined as the set of voxels in the temporal cortex that responded significantly higher to a coherently moving array of dots than to a static array of dots as shown in Fig. B.4. SFM-related areas were defined as the set of voxels within or surrounding intraparietal sulcus that responded significantly higher to 3D shape from depth rotation than 3D shape from static cues of inter-connected line stimuli as shown in Fig. B.5. The LOC area, with subregions LO and pFs, was defined as the set of voxels in lateral occipital-temporal cortex that responded significantly higher to intact than scrambled images of objects as shown in Fig. B.2.

Analysis of fMRI time course signals For each cortical ROI (early areas, V3A, KO/V3B, V4, hMT+/V5, V7, LOC and SFM-related areas), we extract the time courses from each voxel and normalized to percentage signal change by dividing by the mean signal intensity of baseline. We then determined the mean response for each region by averaging the fMRI reponse across a set of voxels (n = 50) that responded most strongly to stimulus presentation relative to fixation across all condition. We computed responses for individual trials for 20 time points, of which the first time points of rest (fixation only) prior to each

stimulation period served as its baseline. Then the time course for individual trials was normalized to zero baseline by subtracting the mean of the four time points before stimulus onset. These four time points correspond to the response to the fixation phase that was similar across conditions. We determined the peak of the fMRI time course in each ROI based on maximum likelihood estimate (MLE) fits to the data using two Gamma functions (one for the initial response and one for the undershoot) and a baseline. This showed that peak responses occurred 10 - 12 s after the beginning of each trial (4 - 6 s after probe stimulus onset) for all conditions and across ROIs, consistent with the hemodynamic lag properties. To calculate the amplitude of the response for each trial, we averaged the response of the three time points centered on the peak of the fMRI time course for each subject and ROI. Finally, we normalized the BOLD response for each session by dividing the response for each trial by the maximum mean response for all trials in a session. This procedure allowed us to control for variability of the fMRI response across scanning session.

Event-related averages were computed for each trial type and mean response were extracted for each ROI showing the mean response over one whole trial period, including 8-s post-trial interval.

Quantization of adaptation effects In our study, no baseline condition was set due to the same probe stimulus used across different adaptation conditions. That means, we did not care about the absolute adaptation amount in each adaptation condition but paid more attention on the difference of adaptation effects across different adaptation conditions. Therefore, we firstly calculated adaptation effects (AE) as the decline of averaged fMRI activation amplitude in unit of percent signal change (PSC) of time windows of 2 sec after probe stimulus onset relative to response at the last time point before probe stimulus onset,

as shown in Equation 8.1.

$$AE = PSC_{adaptor} - PSC_{probe} \tag{8.1}$$

where $PSC_{adaptor}$ denotes the response amplitude at the last time point before probe stimulus onset, when the response was evoked only by adaptor stimulus. And PSC_{probe} signifies the response amplitude averaged over the the 2-sec time windows after probe stimulus onset. Within the time window, the response peak for probe stimulus always occurred across adaptation conditions in our study. A normalization operation is then performed on the calculated AE, yielding a normalized adaptation effect (nAE) ranged from 0 to 1, as shown in Equation 8.2,

$$nAE = \frac{AE - AE_{min}}{AE_{max} - AE_{min}} \tag{8.2}$$

where AE_{max} and AE_{min} were decided empirically after the AE calculation of all adaptation conditions across all ROIs. Obviously, a nAE closer to 0 stands for a smaller adaptation, while a nAE closer to 1 for a larger adaptation.

8.3 Results: Combined-subject analysis

The purpose of the study was to test what levels of adaptation sources were adapted for sCAE in neurons, primarily in high dorsal and ventral ROIs but also in other early visual areas, that were thought to be selectively responsive to lower- and higher-order disparities processing, using the adaptation procedure discribed in the Methods section.

8.3.1 Time courses

Early visual areas For all four subjects, acceptable results for ROIs were obtained for early visual areas (V1, V2, V3 and VP) in both hemispheres. As described in Methods section, these areas were identified using the traveling wave methods with single- or double-

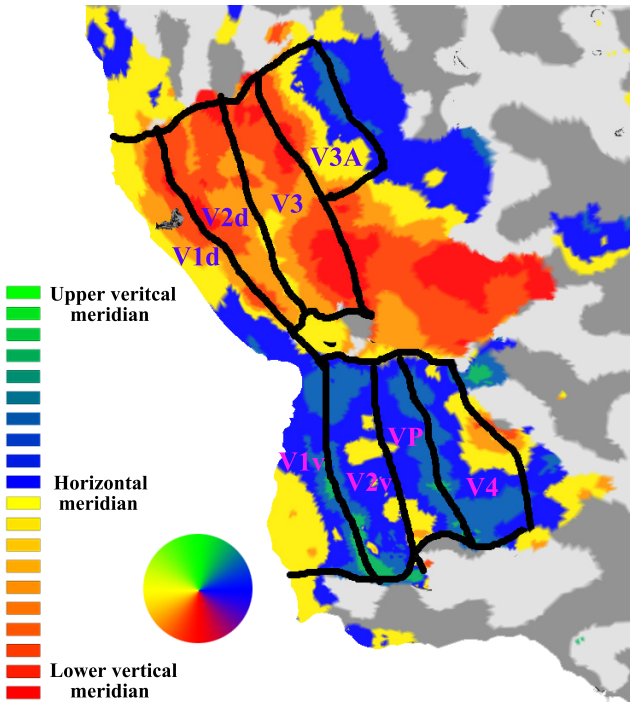

(a) Retinotopic mapping for early visual areas, V3A and V4

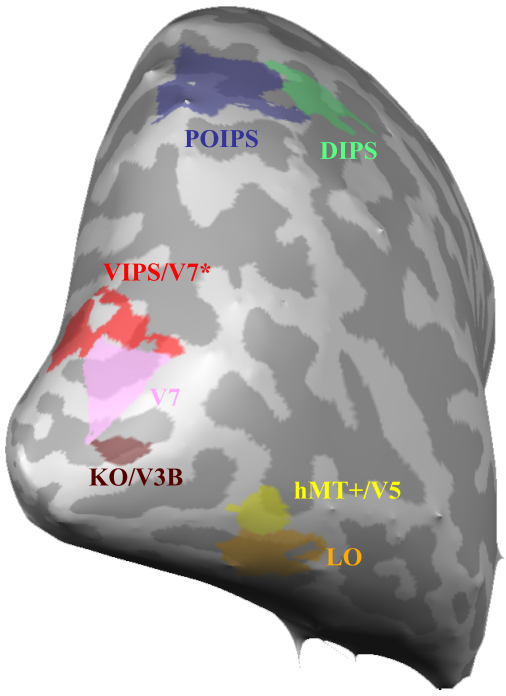

(b) Locations of dorsal, ventro-lateral and SFM-related areas

Figure 8.3 Regions of interest from one representative participant. (a): flatmap from the right hemisphere showing early areas V1 - V3 as well as V3A and V4; (b): inflated representation showing the locations of high dorsal and ventral areas.

angle stimuli as shown in Fig. B.1. Fig. 8.3(a) shows a representative result of retinotopic mapping on flattened mesh of right hemisphere.

Fig. 8.4 shows mean time courses extracted from the ROIs in early visual areas. Each trace represents the response to one trial of a given adaptation condition, averaged over 12 (or 18 only for subject YP) repetitions per subject and across 8 hemispheres from all 4 subjects. Time zero represents the onset of adaptor stimulus and shades bars indicate the presence of the adaptor and probe stimuli. Prior to adaptor stimulus onset, response are falling from the previous trial, of which the influence is counterbalanced. The response to adaptor stimulus mostly begins to build about 1-sec after the onset of adaptor stimulus,

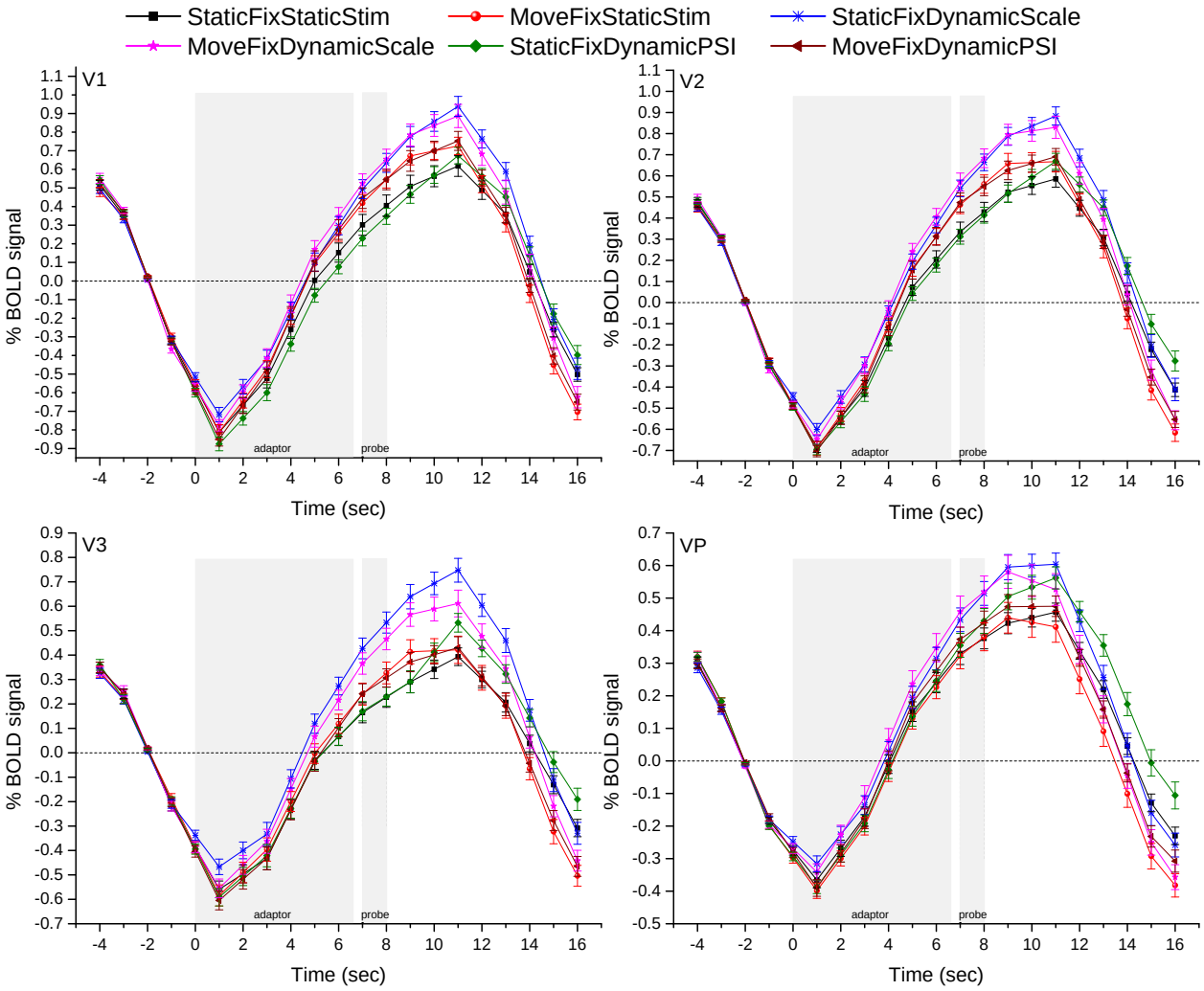

Figure 8.4 Mean time course of early visual areas across subjects, hemispheres and runs

different from 2-sec in the study of (Smith & Wall, 2008). Until the onset of probe stimulus, six trial types yield distinct time courses, as adaptor stimulus is different across adaptation conditions. Thereafter, they diverge based on the same reason, although probe stimulus is always the same across trials. Before starting to fall, the responses in all adaptation conditions peak about 2-3 secs after the onset of probe stimulus.

The results for the areas are similar in all respects. In all areas, a larger responses to probe stimulus were obtained for the dynamic-scaled adaptor than both stationary and PSI-scaled

adaptors, largest in StaticFixDynamicScale condition with static fixation and then in MoveFixDynamicScale condition with moving fixation. Also in most areas except VP, the smallest responses were shown in StaticFixStaticStim condition, and almost the same responses were shared between MoveFixStaticStim and MoveFixDynamicPSI conditions. Besides, we found a deceleration of response increment within the 2-sec time window before peak achievement in StaticFixStaticStim condition across all regions of early visual areas, with the overall larger deceleration in V1 and V2 regions than that in V3 and VP regions.

However, for StaticFixDynamicPSI condition within the time window, an accelerated increment of responses to probe stimulus was only observed in V3 region among early visual areas, while we found no significant acceleration in V1-V3 regions. Different from the other three regions, VP region showed a slight deceleration of response increment in StaticFixDynamicPSI condition and a significant decrement of responses to probe stimulus in MoveFixDynamicScale condition.

Ventro-lateral areas For ventro-lateral areas, V4 region was defined as an entire hemifield anatomically located adjacent to VP according retinotopy results, as shown in Fig. 8.3(a). We identified LO region, using stimuli shown in Fig. B.2, based on an independent localizer scan (3 runs) using both functional and anatomical cues. That is, LO was defined as a region that responses more strongly to objects and was located along the lateral extent of the occipital lobe. In our study, we did not include the result of pFs region as another object-selective region in LOC, because it was difficult to be identified for some subjects.

The time courses for the areas are shown in Fig. 8.5. Similar to early visual areas, StaticFixDynamicScale condition showed the largest responses to probe stimulus, and a smaller responses to probe stimulus were found in StaticFixStaticStim, MoveFixStaticStim and MoveFixDynamicPSI conditions than that in other three conditions. Also, there was a significant sooner increment of responses within the 2-s time window before peak arrival in

StaticFixDynamicPSI condition across both regions of dorsal areas.

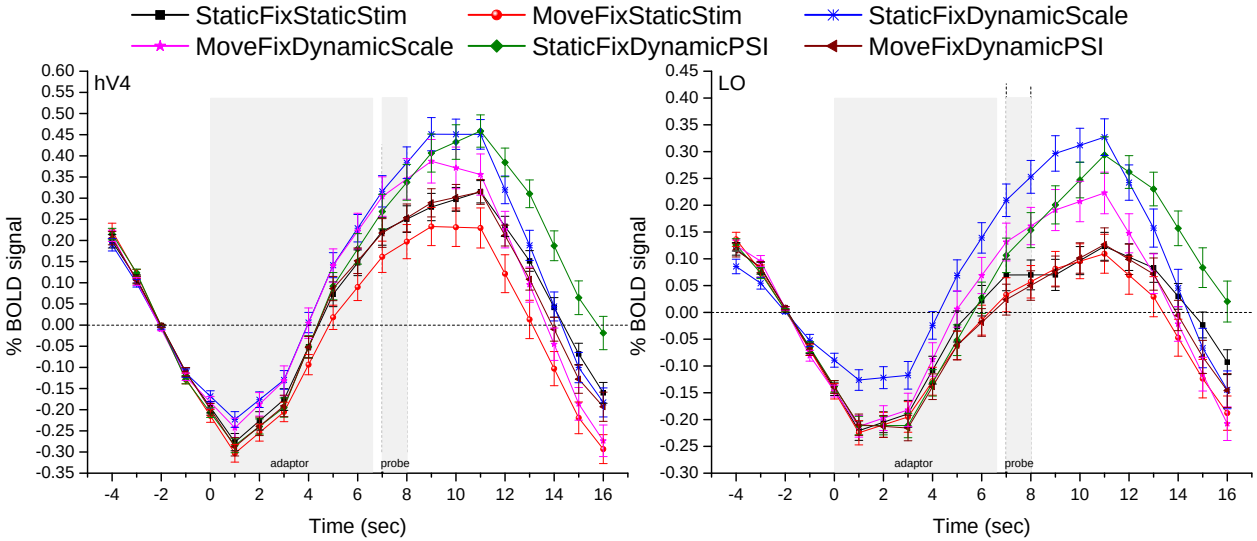

Figure 8.5 Mean time courses for ventral-lateral areas across subjects, hemispheres and runs

However, different from early visual areas, the responses to probe stimulus got larger in StaticFixDynamicPSI condition and was smaller only than that in StaticFixDynamicScale condition. Besides, the time course of StaticFixDynamicScale condition, with much larger responses for both adaptor and probe stimuli, significantly diverged from other conditions in LO region.

Dorsal areas The result for localization of dorsal ROIs were shown in Fig. 8.3(b). Among dorsal areas, KO/V3B and hMT+/V5 were identified using independent localizer scans, while V3A and V7 were defined by hand.

KO/V3B was identified using dynamic RTP stimuli with kinetic edges, as shown in Fig. B.3. Using extraction-and-contraction RDS shown in Fig. B.4, hMT+/V5 region was defined as a cluster of activated voxels near the ascending limb of the inferior temporal sulcus (ITS). V3A was manually defined as an entire hemifield region located adjacent to V3, and was distinguished from KO/V3B according to the fact that KO/V3B locates the ventral portion

of V3A. V7 region was identified by hand in terms of the anatomical position of V3A and VIPS/V7*, and was defined as a region anterior and dorsal to V3A as well as inferior to VIPS/V7*.

Fig. 8.6 shows us the time courses of dorsal areas. All areas shows an acceleration of response increment within the 2-s time window before peak arrival to different extent in StaticFixDynamicPSI condition. And the smallest responses were found in StaticFixStat-

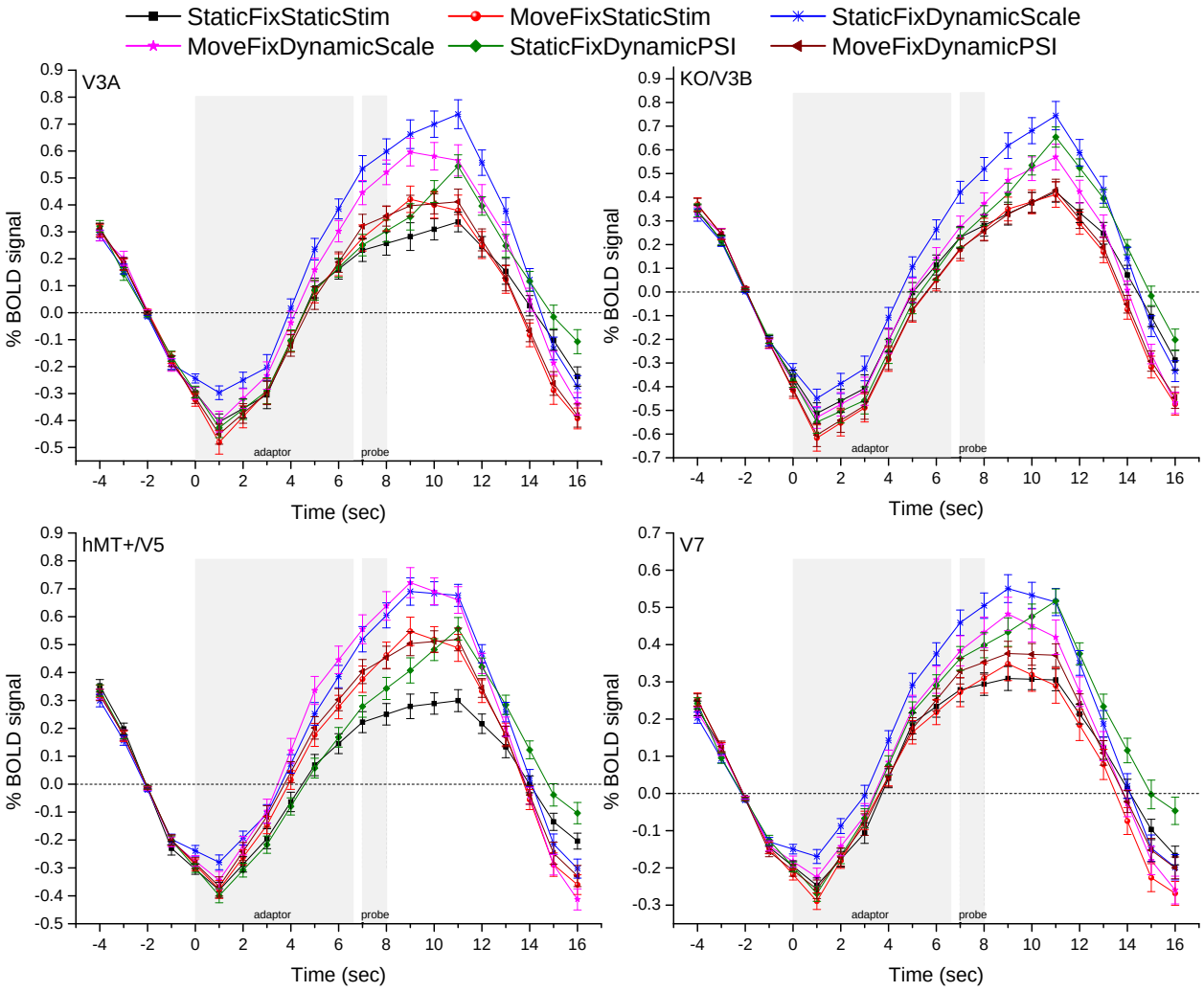

Figure 8.6 Mean time courses for dorsal areas across subjects, hemispheres and runs

icStim condition, and then in MoveFixStaticStim and MoveFixDynamicPSI conditions. In hMT+/V5, MoveFixDynamicScale condition has no smaller responses than StaticFixDynamicScale condition. Apart from hMT+/V5 region, other dorsal areas shows the largest responses to probe stimulus in StaticFixDynamicScale condition. Except V7 region, the second smallest responses in MoveFixStaticStim and MoveFixDynamicPSI conditions involves no significant difference in amplitude.

SFM-related areas The result of localization of SFM-related ROIs were shown in Fig. 8.3(b). Separate subregions of SFM-related areas were identified based on an independent localizer scan (3 runs) using the RLP stimuli as shown in Fig. B.5. Acceptable results of localization were obtained for all the subregions with exception of DIPS region, which was not clear only for subject SH. Here, we did not differentiate DIPS into subregions DIPSA and DISPM, considering unclear borders we obtained to delineate between them for most subjects.

The time courses across SFM-related areas was shown in Fig. 8.7. They are somewhat different from those in other ROIs. Firstly, although the largest responses to probe stimulus was found for dynamic-scaled adaptor across all SFM-related areas, not in static fixation but in moving fixation. Secondly, StaticFixDynamicPSI condition involved a higher delay to achieve the peak responses to probe stimulus than other adaptation conditions. Thirdly, for both POIPS and DIPS, a deceleration in response increment was found within the 2-s time window before peak arrival in StaticFixDynamicPSI condition.

However, like in dorsal areas, StaticFixStaticStim condition involved the smallest responses to probe stimulus across all SFM-related areas.

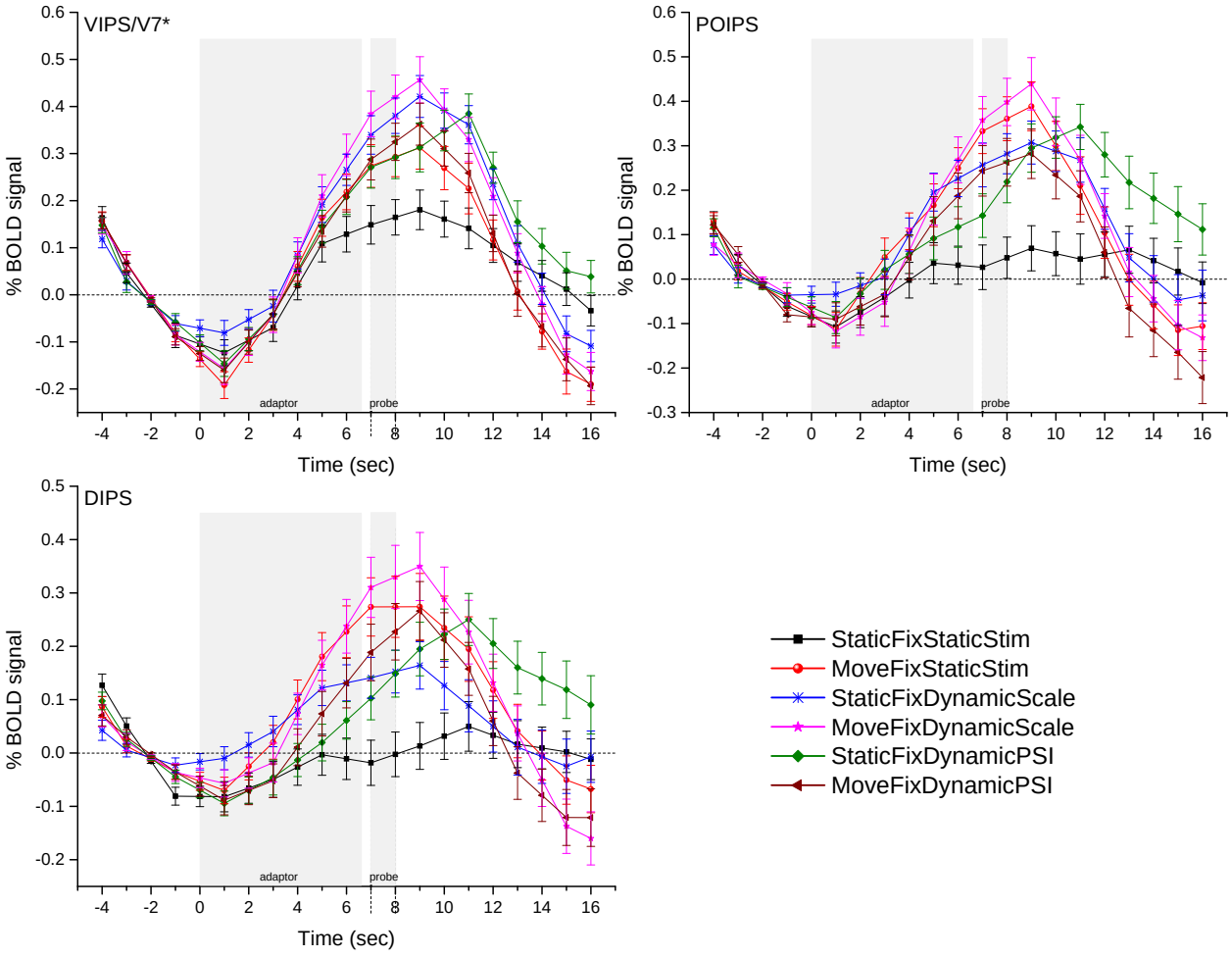

Figure 8.7 Mean time courses for SFM-related areas across subjects, hemispheres and runs

8.3.2 Measuring for adaptation effects

To quantify the adaptation effects, a normalized adaptation effects, referred to as nAE, was calculated as described in Methods section. For each condition, the mean AE in each ROI was firstly obtained by averaging AE over all voxels on 3 trials within each run. The mean AE corresponding to each run was then normalized into a value ranged between 0 to 1. Thereafter, all resulted nAEs for each condition were averaged across subjects, hemishpheres

and runs in each ROI as shown in Fig. 8.8.

Individual and inter-hemisphere difference of adaptation effects To assess between-subject and inter-hemisphere differences on nAE, we made a Three-Way repeated-measures ANOVA (4 SUBJECT $\times$ 2 HEMISPHERE $\times$ 6 CONDITION) in each ROI with exception of DIPS region involving 3 subjects, as shown in Table 8.2. Especially for subject YP, we only used the first 12 runs of his 18 runs in total. All multiple comparisons involved Boferroni adjustment in the following statistical analysis.

In early-areas ROI, SUBJECT ($F(3, 33) = 3.792$, $p = 0.019$, $\eta^2 = 0.256$) imposed significant main effects on nAE. Multiple comparison showed a significant difference of AE between subject YP and subject WY. CONDITION also imposed a significant main effect on nAE in early-areas ROI ($F(5, 55) = 2.506$, $p = 0.041$, $\eta^2 = 0.186$), although no significant difference was found between either pair of conditions.

For ROIs (V1 - V3 and VP) with finer partition in early visual areas, a significant main effect of SUBJECT on nAE was found in V1 ($F(3, 33) = 7.267$, $p = 0.001$, $\eta^2 = 0.398$) and VP ($F(3, 33) = 14.235$, $p = 0.000$, $\eta^2 = 0.564$) but not in V2 and V3. Multiple comparison showed indicated that subject WY had significantly smaller nAE from subjects YP (V1&VP: $p = 0.000$) and SH (V1: $p = 0.001$, VP: $p = 0.005$) as well as from subject MY only in VP region ($p = 0.001$). HEMISPHERE had a significant main effect on nAE in V2 region ($F(1, 11) = 18.163$, $p = 0.001$, $\eta^2 = 0.623$), and left hemisphere involved a significantly larger nAE than right hemisphere ($p = 0.001$) in terms of multiple comparison. Besides, there was a nAE difference of close to significance ($p = 0.058$) between left and right hemispheres in VP region, although no significant main effect of HEMISPHERE on nAE was found. No any other statistical significance on nAE was found in early-area ROI and its subregions.

In ventro-lateral-areas ROI, a significant main effect of SUBJECT ($F(3, 33) = 11.463$, $p = 0.000$, $\eta^2 = 0.510$) on nAE was found. Multiple comparison showed a significantly

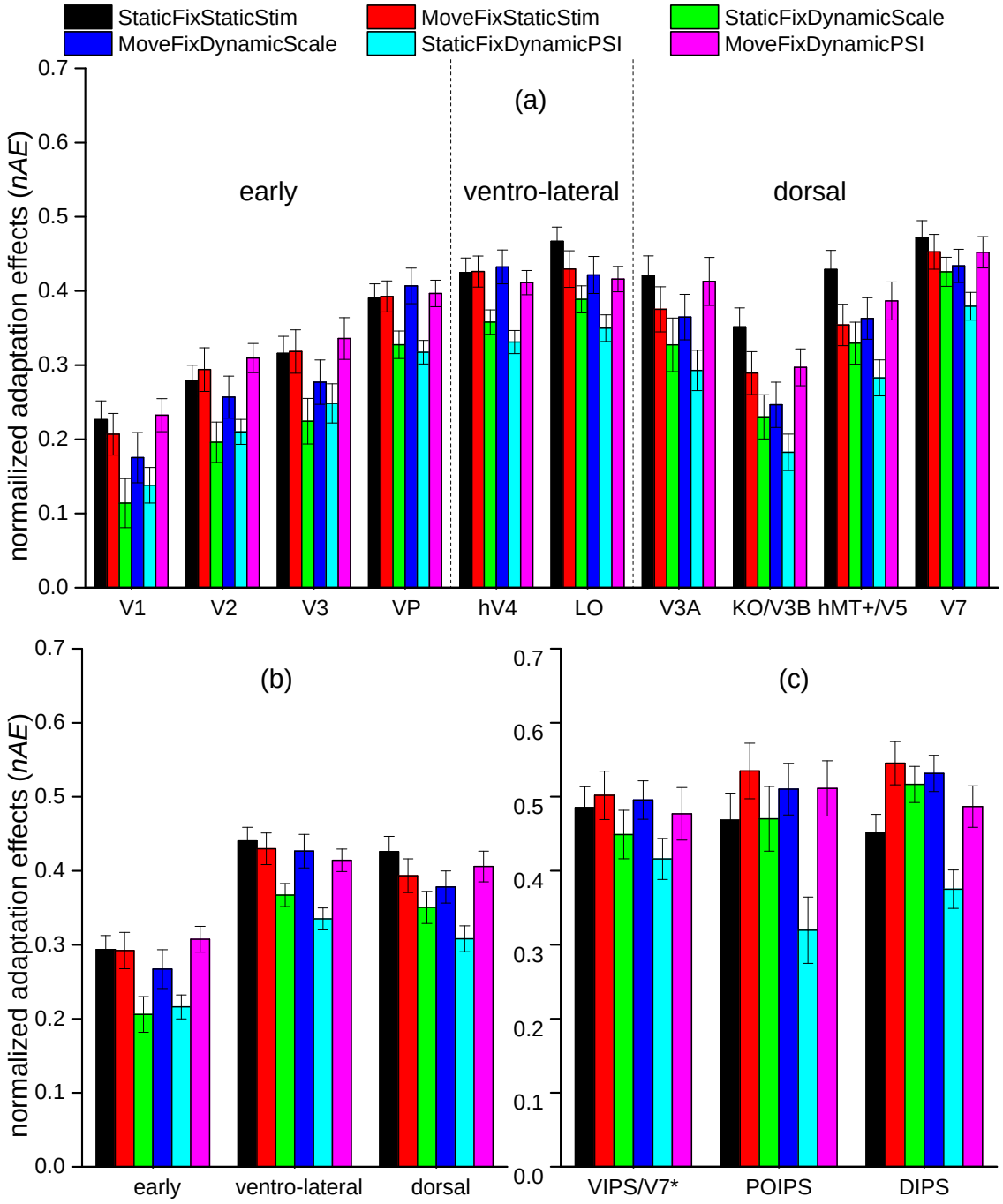

Figure 8.8 *nAE* statistics for each condition in ROIs. (a) normalized mean *AE* for individual areas to 4 adaptation conditions. (b). normalized mean *AE* averaged for early, ventro-lateral and dorsal regions. (c). normalized mean *AE* for SFM-related regions VIPS/V7*, POIPS and DIPS. Error bars indicate the SEM of *AE* across subjects, hemispheres and runs.

Table 8.2 Statistical significance of Three-Way (4 SUBJECT × 2 HEMISPHERE × 6 CONDITION) ANOVA on nAE in ROIs. Prepositive stars represent the statistical significance of main effects of factors, with $\tilde{*}p<0.06$, $*p < 0.05$, $**p < 0.01$ and $***p < 0.001$. Each inequality represents for a significant partial order in multiple comparison with Boferroni adjustment. LH stands for left hemisphere and RH for right hemisphere. SFSS stands for StaticFixStaticStim condition, MFSS for MoveFixStaticStim condition, SFDS for StaticFixDynamicScale condition, MFDS for MoveFixDynamicScale condition, SFDP for StaticFixDynamicPSI condition and MFDP for MoveFixDynamicPSI condition.

Cortical Area	SUBJECT	HEMISPHERE	CONDITION
early visual areas	* WY < YP		*
V1	** WY < YP&SH		
V2		** LH > RH	
V3	**		*
VP	*** WY < YP&SH&MY	$\tilde{*}$	*
ventro-lateral areas	*** WY < YP&SH&MY		*
hV4	*** WY < YP&SH&MY		*
LO	*** WY < SH&MY	* LH < RH	*
dorsal areas	*	* LH < RH	* SFSS > SFDS
V3A	*	* LH < RH	$\tilde{*}$ MFDS > SFDP
KO/V3B	*** YP < WY&SH&MY	* LH < RH	** SFSS > SFDS &MFDS&SFDP
hMT+/V5	** WY < MY		* MFSS > SFDP
V7			
VIPS/V7*	**		MFDS > SFDP
POIPS	*** YP < SH	$\tilde{*}$	* MFSS > SFDP
DIPS	* YP < WY	*** LH > RH	** MFSS > SFDP

different nAE of subject WY from either of other subjects including MY ($p = 0.004$), YP ($p = 0.049$) and SH ($p = 0.000$). CONDITION also imposed a significant main effect on nAE in ventro-lateral-areas ROI ($F(5, 55) = 3.180$, $p = 0.014$, $\eta^2 = 0.224$), although no significant difference was found between either pair of conditions.

For ROIs (hV4 and LO) with finer partition in ventro-lateral areas, a significant main effect of SUBJECT on nAE was found in hV4 region ($F(3, 33) = 11.407$, $p = 0.000$, $\eta^2 = 0.509$) and LO region ($F(3, 33) = 8.567$, $p = 0.000$, $\eta^2 = 0.438$). Subject WY had significantly different nAE from subjects MY (hV4: $p = 0.004$, LO: $p = 0.012$) and SH (hV4: $p = 0.009$, LO: $p = 0.003$) as well as from subject YP ($p = 0.008$) only in hV4 region. HEMISPHERE had a significant main effect on nAE in LO region ($F(1, 11) = 8.204$, $p = 0.015$, $\eta^2 = 0.427$), and right hemisphere showed a significantly larger nAE than left hemisphere ($p = 0.015$). No any other significance was found in ventro-lateral-areas ROI and its subregions.

In dorsal-areas ROI, a significant main effect on nAE was found for either of factor: SUBJECT ($F(3, 33) = 3.704$, $p = 0.021$, $\eta^2 = 0.252$), HEMISPHERE ($F(1, 11) = 7.096$, $p = 0.022$, $\eta^2 = 0.392$) and CONDITION ($F(5, 55) = 2.966$, $p = 0.019$, $\eta^2 = 0.212$). Multiple comparison showed a significant difference on nAE between left and right hemispheres ($p = 0.022$). StaticFixStaticStim condition involved a significantly larger nAE than StaticFix-DynamicPSI condition ($p = 0.043$). No significant difference was found between any pair of subjects.

For ROIs (V3A, KO/V3B, hMT+/V5 and V7) with finer partition in dorsal areas, a significant main effect of SUBJECT on nAE was found in KO/V3B ($F(3, 33) = 19.743$, $p = 0.000$, $\eta^2 = 0.642$) and hMT+/V5 ($F(3, 33) = 4.931$, $p = 0.006$, $\eta^2 = 0.310$). Multiple comparison showed that subject YP had a significantly different nAE from either of other subjects: MY ($p = 0.001$), WY (0.004) and SH ($p = 0.001$) in KO/V3B. In hMT+/V5 region, a significant difference of nAE was found between subjects MY and WY ($p = 0.015$).

We also found a significant main effect of SUBJECT on nAE in V3A ($F(3, 33) = 3.574$, $p = 0.024$, $\eta^2 = 0.245$), although no significant difference on nAE was found among subjects in multiple comparison. HEMISPHERE imposed a significant main effect on nAE in V3A ($F(1, 11) = 7.528$, $p = 0.019$, $\eta^2 = 0.406$) and KO/V3B ($F(1, 11) = 7.679$, $p = 0.018$, $\eta^2 = 0.411$). According to multiple comparison, right hemisphere showed a significantly larger nAE than left hemisphere (V3A: $p = 0.019$, KO/V3B: $p = 0.018$). CONDITION imposed a significant main effect on nAE in KO/V3B ($F(5, 55) = 4.925$, $p = 0.001$, $\eta^2 = 0.309$) and hMT+/V5 ($F(5, 55) = 3.026$, $p = 0.017$, $\eta^2 = 0.216$), as well as imposed a main effect of close to significance on nAE in V3A ($F(5, 55) = 2.295$, $p = 0.058$, $\eta^2 = 0.173$). Multiple comparison showed, MoveFixDynamicScale condition showed a significantly larger nAE than StaticFixDynamicPSI condition in V3A region ($p = 0.025$). StaticFixStaticStim condition had significant larger nAE than StaticFixDynamicScale ($p = 0.023$), MoveFixDynamicScale ($p = 0.045$) and StaticFixDynamicPSI ($p = 0.002$) in KO/V3B region. MoveFixStatic-Stim condition showed a significantly larger nAE than StaticFixDynamicPSI condition in hMT+/V5 region ($p = 0.036$). No any other significance was found in dorsal-areas ROI and its subregions.

For SFM-related ROIs, SUBJECT imposed significant main effect on nAE in VIPS/V7* region ($F(3, 33) = 5.475$, $p = 0.004$, $\eta^2 = 0.332$), POIPS region ($F(3, 33) = 8.487$, $p = 0.000$, $\eta^2 = 0.436$) and DIPS region ($F(3, 33) = 5.113$, $p = 0.015$, $\eta^2 = 0.317$). Multiple comparison showed that subject YP involved a significantly smaller nAE than subject SH in POIPS region ($p = 0.022$) and than subject WY in DIPS region ($p = 0.026$). However, we found no significant difference of nAE between any pair of subjects in VIPS/V7* region. A significant main effect of CONDITION on nAE was found in POIPS ($F(5, 55) = 3.329$, $p = 0.011$, $\eta^2 = 0.232$) and DIPS ($F(5, 55) = 4.024$, $p = 0.003$, $\eta^2 = 0.268$). Multiple comparison showed that MoveFixStaticStim condition had a significantly larger nAE than

StaticFixDynamicPSI condition in POIPS region ($p = 0.006$) and DIPS region ($p = 0.044$). Besides, we found a significantly larger nAE in MoveFixDynamicScale condition than that in StaticFixDynamicPSI condition in VIPS/V7* region ($p = 0.047$), although CONDITION factor imposed no significant main effect on nAE in the ROI. HEMISPHERE imposed a significant main effect on nAE only in DIPS region ($F(1, 11) = 36.472$, $p = 0.000$, $\eta^2 = 0.768$) and a significant difference of nAE was found between both of hemispheres ($p = 0.000$) in multiple comparison.

fMRI selective adaptation within ROIs StaticFixStaticStim condition showed an obviously larger nAE than other two conditions with static fixation within ROIs except SFM-related areas, as shown in Fig. 8.8. To examine adaptation magnitude across different conditions, a one-way repeated-measures ANOVA with the factor CONDITION was performed on nAE averaged across 8 hemispheres from all subjects in each ROI except DIPS region, in which YP data were not available, as shown in Table 8.3. All multiple comparisons in the following statistical processing involved Boferroni adjustment.

In early-areas ROI, CONDITION imposed a significant main effect on nAE ($F(5, 35) = 7.531$, $p = 0.000$, $\eta^2 = 0.518$). Multiple comparison showed a significantly smaller nAE for StaticFixDynamicScale condition than StaticFixStaticStim condition ($p = 0.006$), MoveFixStaticStim condition ($p = 0.038$) and MoveFixDynamicPSI condition ($p = 0.005$). Besides, StaticFixDynamicPSI condition had a significantly smaller nAE than MoveFixDynamicPSI ($p = 0.000$).

For ROIs with finer partition in early visual areas, CONDITION imposed a significant main effect on nAE in V1 ($F(5, 35) = 5.271$, $p = 0.001$, $\eta^2 = 0.430$), V2 ($F(5, 35) = 5.619$, $p = 0.001$, $\eta^2 = 0.445$), V3 ($F(5, 35) = 8.197$, $p = 0.000$, $\eta^2 = 0.539$) and VP ($F(5, 35) = 7.330$, $p = 0.000$, $\eta^2 = 0.512$). Multiple comparison showed, StaticFixDynamicScale condition had a significantly smaller nAE than StaticFixStaticStim condition in V1 ($p =$

Table 8.3 Statistical significance of One-Way ANOVA with factor CONDITION on nAE in ROIs. Prepositive stars in cells represent for the significance level of larger nAE row condition than that for column condition, with $^{*}p < 0.05$, $^{**}p < 0.01$ and $^{***}p < 0.001$. ROIs in cells involved the pairwise comparison with the statistical significance. SFSS stands for StaticFixStaticStim condition, MFSS for MoveFixStaticStim condition, SFDS for StaticFixDynamicScale condition, MFDS for MoveFixDynamicScale condition, SFDP for StaticFixDynamicPSI condition and MFDP for MoveFixDynamicPSI condition.

stimulus:	static		size-scaled		PSI-scaled	
fixation:	static	moving	static	moving	static	moving
>	**SFSS**	**MFSS**	**SFDS**	**MFDS**	**SFDP**	**MFDP**
SFSS			**early, **V1 *V2, *dorsal **KO/V3B		**VP, **ventro-lateral **hV4, **LO, *V3A ***dorsal, **hMT+/V5 ***KO/V3B, **V7	
MFSS			*early, *V2 *V3		**ventro-lateral **hV4, **dorsal *VIPS/V7*, **DIPS	
SFDS						
MFDS			*hV4		***ventro-lateral *dorsal, **hV4, **LO *VIPS/V7*, *DIPS	
SFDP						
MFDP			**early, *V2 **V3, *VP		***early, *dorsal, *V1 **V2, **V3, *VP	

0.008) and V2 ($p = 0.045$), than MoveFixStaticStim condition in V2 ($p = 0.027$) and V3 ($p = 0.049$), as well as than MoveFixDynamicPSI condition in V2 ($p = 0.026$), V3 ($p = 0.002$) and VP ($p = 0.012$). Besides, adaptor with dynamic PSI had a significantly larger nAE under moving fixation than under static fixation in V1 ($p = 0.017$), V2 ($p = 0.008$), V3 ($p = 0.001$) and VP ($p = 0.012$). In VP, StaticFixStaticStim condition had a significantly larger nAE than StaticFixDynamicPSI condition ($p = 0.008$). No any other significance was found in early-areas ROI and its subregions.

In ventro-lateral-areas ROI, CONDITION imposed a significant main effect on nAE ($F(5, 35) = 12.265$, $p = 0.000$, $\eta^2 = 0.637$). Multiple comparison showed a significantly smaller nAE for StaticFixDynamicPSI condition than that for StaticFixStaticStim condition ($p = 0.001$), MoveFixStaticStim condition ($p = 0.003$) and MoveFixDynamicScale condition ($p = 0.000$).

For ROIs with finer partition in ventro-lateral areas, CONDITION imposed a significant main effect on nAE in V4 ($F(5, 35) = 9.695$, $p = 0.000$, $\eta^2 = 0.581$) and LO ($F(5, 35) = 6.870$, $p = 0.000$, $\eta^2 = 0.495$). Multiple comparison showed, StaticFixDynamicPSI had a significantly smaller nAE than StaticFixStaticStim condition (hV4: $p = 0.002$, LO: $p = 0.007$) and MoveFixDynamicScale condition (hV4: $p = 0.006$, LO: $p = 0.011$) in two subregions of ventro-lateral areas. In V4 region, we also found a significantly smaller nAE for StaticFixDynamicPSI condition than that for MoveFixStaticStim condition ($p = 0.007$) as well as for StaticFixDynamicScale condition than that for MoveFixDynamicScale condition ($p = 0.029$). No any other significance was found in ventro-lateral-areas ROI and its subregions.

In dorsal-areas ROI, CONDITION imposed a significant main effect on nAE ($F(5, 35) = 13.624$, $p = 0.000$, $\eta^2 = 0.661$). Multiple comparison showed that StaticFixDynamicPSI condition had a significantly smaller nAE than StaticFixStaticStim condition ($p = 0.000$), MoveFixStaticStim condition ($p = 0.007$), MoveFixDynamicScale condition ($p = 0.033$) and

MoveFixDynamicPSI condition ($p = 0.027$). Besides, a significantly smaller nAE was found in StaticFixDynamicScale condition than in StaticFixStaticStim condition ($p = 0.035$).

For ROIs with finer partition in dorsal areas, CONDITION imposed a significant main effect on nAE in V3A ($F(5, 35) = 6.889$, $p = 0.000$, $\eta^2 = 0.496$), KO/V3B ($F(5, 35) = 8.937$, $p = 0.000$, $\eta^2 = 0.561$), hMT+/V5 ($F(5, 35) = 3.868$, $p = 0.007$, $\eta^2 = 0.356$) and V7 ($F(5, 35) = 4.823$, $p = 0.002$, $\eta^2 = 0.408$). Multiple comparison showed, StaticFixDynamicPSI condition had a significantly smaller nAE than StaticFixStaticStim condition in V3A ($p = 0.018$), KO/V3B ($p = 0.000$), hMT+/V5 ($p = 0.004$) and V7 ($p = 0.002$). StaticFixDynamicScale condition had a significantly smaller nAE than StaticFixStaticStim condition in KO/V3B ($p = 0.008$). No any other significance was found in dorsal-areas ROI and its subregions.

For SFM-related ROIs in IPS areas, CONDITION imposed a significant main effect on nAE in VIPS/V7* ($F(5, 35) = 2.650$, $p = 0.039$, $\eta^2 = 0.275$), POIPS ($F(5, 35) = 4.242$, $p = 0.004$, $\eta^2 = 0.377$) and DIPS ($F(5, 25) = 5.490$, $p = 0.002$, $\eta^2 = 0.523$). Multiple comparison showed that StaticFixDynamicPSI condition had a significantly smaller nAE than MoveFixStaticStim condition (VIPS/V7*: $p = 0.043$, DIPS: $p = 0.003$) and MoveFixDynamicScale condition (VIPS/V7*: $p = 0.040$, DIPS: $p = 0.036$) in both VIPS and DIPS. No any other significance was found in SFM-related ROIs.

8.3.3 Spatial distribution of adaptation effects

Each condition showed a similar overall trend across ROIs. Consistent with previous studies, an increasingly large adaptation was found along paths from striate towards extra-striate cortices. Especially, the measured mean nAE monotonically increased from V1 through V2 and V3 to VP in early visual areas as shown in Fig. 8.8(a). The trend was also observed from KO/V3B through hMT+/V5 into V7 in dorsal areas. Furthermore, as shown in Fig. 8.8(b),

the overall nAE averaged over early visual areas was smaller than that averaged over both ventro-lateral and dorsal areas, although no significant difference was found between hV4 and LO within ventro-lateral areas, and a minima was found in KO/V3B along the dorsal stream. Moreover, as shown in Fig. 8.8(c), the largest nAE was achieved in SFM-related areas more dorsal than V7.

Just in mean level, StaticFixDynamicScale condition showed a significantly larger nAE than StaticFixDynamicPSI in ventro-lateral, dorsal and SFM-related areas rather than in early areas. And StaticFixStaicStim condition showed a significant larger nAE than MoveFixStaticStim condition only in LO and dorsal areas but not in early visual areas and SFM-related areas.

To examine nAE of each condition across ROIs, we performed a One-Way ANOVA with repeated-measures design of ROI factor for each adaptation condition, as shown in Table. 8.4. A significant main effect of factor ROI on nAE was found for all conditions, with StaticFixStaticStim condition ($F(15, 105) = 9.003$, $p = 0.000$, $\eta^2 = 0.563$), MoveFixStaticStim condition ($F(15, 105) = 10.853$, $p = 0.000$, $\eta^2 = 0.608$), StaticFixDynamicScale condition ($F(15, 105) = 16.129$, $p = 0.000$, $\eta^2 = 0.697$), MoveFixDynamicScale condition ($F(15, 105) = 11.800$, $p = 0.000$, $\eta^2 = 0.628$), StaticFixDynamicPSI condition ($F(15, 105) = 5.794$, $p = 0.000$, $\eta^2 = 0.453$) and MoveFixDynamicPSI condition ($F(15, 105) = 9.853$, $p = 0.000$, $\eta^2 = 0.585$). In the subsequent statistical processing, all multiple comparisons involved Boferroni adjustment. Along either dorsal or ventral processing stream, no significantly enhanced nAE was found for each adaptation condition in one ROI compared with any of other higher ROIs. And we found significant differences of nAE among some ROIs for adaptation conditions except both StaticFixStaticStim and MoveFixDynamicPSI conditions.

For MoveFixStaticStim (MFSS) condition, compared with V1 of early visual areas, a significantly larger nAE was found in hV4 ($p = 0.009$) of ventro-lateral areas, V7 ($p = 0.021$)

Table 8.4 Repeated-measures ANOVA with one factor ROI on *nAE* for each adaptation condition. Cell elements represent adaptation conditions with a significantly larger *nAE* in row ROI than in column ROI, where each condition is highlighted with distinct colors, and SFSS stands for StaticFixStaticStim condition, MFSS for MoveFixStaticStim condition, SFDS for StaticFixDynamicScale condition, MFDS for MoveFixDynamicScale condition, SFDP for StaticFixDynamicPSI condition and MFDP for MoveFixDynamicPSI condition.

>	early	V1	V2	V3	VP	ventral	hV4	LO	dorsal	V3A	KO/V3B	hMT+/V5	V7	VIPS/V7*	POIPS	DIPS
early																
V1																
V2																
V3																
VP		MFDS	MFDS													
ventral	MFSS SFDS MFDS	MFSS SFDS MFDS	MFDS													
hV4	MFSS SFDS MFDS	MFSS MFDS	MFDS													
LO	SFDS SFDS	SFDS MFDS														
dorsal	SFDS															
V3A																
KO/V3B																
hMT+/V5																
V7	MFSS SFDS MFDS SFDP	MFSS SFDS MFDS	SFDS MFDS SFDP									SFDP				
VIPS/V7*	SFDS MFDS	SFDS MFDS	SFDS MFDS	SFDS					SFDS MFDS SFDP	MFDS SFDP						
POIPS	MFSS SFDS	 SFDS	MFSS SFDS	 SFDS					 SFDS	 SFDS						
DIPS	MFSS SFDS MFDS	MFSS SFDS MFDS	MFSS SFDS MFDS	 SFDS	 SFDS	 SFDS	 SFDS		 SFDS	 SFDS		 SFDS				

of dorsal areas and DIPS ($p = 0.046$) of SFM-related areas. Also, ROIs including POIPS ($p = 0.012$) and DIPS ($p = 0.016$) of SFM-related areas showed a statistical significance on a larger nAE than V2 of early visual areas.

For StaticFixDynamicScale (SFDS) condition, a significantly larger nAE was found in LO region of ventro-lateral areas ($p = 0.035$) than V1 of early visual areas, yielding a significantly larger overall nAE in ventro-later areas than in early visual areas ($p = p = 0.048$). hV4 region in ventro-lateral areas also showed a significantly larger nAE than early-visual-areas ROI ($p = 0.030$) but not separated V1. A significantly larger nAE was found in only V7 region of dorsal areas than both V1 ($p = 0.020$) and V2 ($p = 0.006$) of early visual areas, yielding a significantly larger overall nAE in dorsal areas than in early visual areas ($p = 0.032$). All ROIs of SFM-related areas showed a significantly larger nAE than V1 (DIPS: $p = 0.035$, POIPS: $p = 0.035$, DIPS: $p = 0.014$), V2 (DIPS: $p = 0.025$, POIPS: $p = 0.016$, DIPS: $p = 0.002$), V3 (DIPS: $p = 0.021$, POIPS: $p = 0.006$, DIPS: $p = 0.012$) of early visual areas. Only POIPS and DIPS showed a significantly larger nAE than V3A of dorsal areas (POIPS: $p = 0.007$, DIPS: $p = 0.010$). Only DIPS region showed a significantly larger nAE than V3 ($p = 0.012$) and VP ($p = 0.013$) of early visual areas as well as hV4 ($p = 0.013$) of ventro-lateral areas. As results, the nAE in all ROIs of SFM-related areas was significantly larger than the overall nAE averaged over both early visual areas (VIPS/V7*: $p = 0.008$, POIPS: $p = 0.006$, DIPS: $p = 0.001$) and dorsal areas (VIPS/V7*: $p = 0.031$, POIPS: $p = 0.010$, DIPS: $p = 0.002$). But there was no significantly larger nAE found in VIPS/V7* region than that in either of separated ROIs in dorsal areas. Besides, a significantly larger nAE was found in only DIPS region than the overall nAE over ventro-lateral areas ($p = 0.021$).

For MoveFixDynamicScale (MFDS) condition, compared with both V1 and V2 of early visual areas, a significantly larger nAE was found in VP (V1: $p = 0.050$, V2: $p = 0.019$) of early visual areas, hV4 (V1: $p = 0.006$, V2: $p = 0.000$) of ventro-lateral areas, V7 (V1: p

= 0.007, V2: $p = 0.026$) of dorsal areas, as well as both VIPS/V7* (V1: $p = 0.014$, V2: $p = 0.018$) and DIPS (V1: $p = 0.016$, V2: $p = 0.005$) of SFM-related areas. We also found a significantly larger nAE in LO of ventro-lateral areas than in V1 region ($p = 0.047$). As results, the nAE averaged over ventral-lateral areas ($p = 0.004$) rather than dorsal areas was significantly smaller than that averaged over early areas. Compared with early areas treated as a whole ROI, a larger nAE of statistical significance was also found in both VIPS/V7* ($p = 0.019$) and DIPS ($p = 0.018$) but not in POIPS, which was significantly different from neither of other ROIs. Besides, VIPS/V7* showed a significantly larger nAE than V3A region ($p = 0.040$) in dorsal areas but not than either of ROIs in ventro-lateral areas, resulting into a larger nAE of statistical significance in VIPS/V7* than the dorsal-areas ROI ($p = 0.044$).

For StaticFixDynamicPSI (SFDP) condition, with dorsal areas, V7 region involved a significantly larger nAE than hMT+/V5 region ($p = 0.029$). Also a significantly larger nAE was found in V7 region than that in V2 of early visual areas ($p = 0.018$), yielding a statistical significance on larger nAE in V7 than early-visual-areas ROI, which treated early visual areas as a whole ROI. Besides, VIPS/V7* of SFM-related areas showed a significantly larger nAE than V3A of dorsal areas, although no significant difference of nAE was found between VIPS/V7* and dorsal-areas ROI.

8.4 Discussion

As shown in Fig. 8.8, our result further support the widely accepted viewpoint that higher areas in the visual processing stream might adapt more easily than lower areas.

As shown in Table. 8.1, moving fixation or stimulus dynamics were used to eliminate adaptation to specified kinds of adaptation sources among adaptation conditions. As results, each condition involved distinct combination of possible adaptation sources. Here, a simplification of description is applied on six adaptation conditions and their possible adaptation sources as follows,

1) SFSS[DA|SP]: StaticFixStaticStim (SFSS) condition possibly adapts brain cortices with both disparity-related (disparity [D] & ADI [A]) sources, which are put on left side of "|", and percept-related (shape curvature [S] & PSI [P]) sources put rightside;

2) MFSS[-|SP]: MoveFixStaticStim (MFSS) condition possibly adapts brain cortices with only percept-related (shape curvature [S] & PSI [P]);

3) SFDS[A|P]: StaticFixDynamicScale (SFDS) condition possibly adapts brain cortices with disparity-related ADI [A] and percept-related PSI [P];

4) MFDS[-|P]: MoveFixDynamicScale (MFDS) condition possibly adapts brain cortices with only percept-related PSI [P];

5) SFDP[A|-]: StaticFixDynamicPSI (SFDP) condition possibly adapts brain cortices with only disparity-related ADI [A];

6) MFDP[-|?]: MoveFixDynamicPSI (MFDP) condition keeps unclear on whether or not involving percept-related adaptation, because of the difficulty to perceive PSI scaling under moving fixation).

8.4.1 Disparity adaptation in V1-V2 and KO/V3B regions

In human brain, disparity-related activity have been found to be distributed broadly, such as in V3A and hMT+/V5 of dorsal areas as well as hV4 and LOC of ventro-lateral areas. However, a definite adaptation to disparity was observed only in V1-V2 and KO/V3B.

Only SFSS[DA|SP] possibly involved disparity adaptation. In One-Way ANOVA of Table 8.3, the condition showed a significantly larger nAE than SFDS[A|P] in early areas (V1, V2) and dorsal areas (KO/V3B), as well as than SFDP[A|-] in early areas (VP), ventro-lateral

areas (hV4, LO) and dorsal areas (V3A, KO/V3B, hMT+/V5, V7). This suggested that adaptation indeed occurred in SFSS[DA|SP].

V1-V2 regions In Table 8.4, two conditions, MFSS[-|SP] and MFDS[-|P], only with possible percept-related adaptation induced a significantly smaller nAE in V1-V2 of early areas than in higher areas, especially for ventro-lateral and SFM-related areas. However, SFSS[DA|SP] showed no significant difference on nAE was among all ROIs. Thus, disparity adaptation in SFSS[DA|SP] indeed occurred in V1-V2 regions at least. This can be further supported by the fact that these two regions involved a significantly larger nAE of SFSS[DA|SP] than that of SFDS[A|P], as shown in One-Way ANOVA of Table 8.3.

This result supports the findings of previous studies. Early visual areas have been documented to show strong disparity selectivity in monkey single-unit recording (Poggio, González, & Krause, 1988) and human fMRI studies (Smith & Wall, 2008; Preston et al., 2008).

KO/V3B region Three-Way ANOVA in Table 8.2 indicated, SFSS[DA|SP] was significant larger than SFDS[A|P], SFDP[A|-] and MFDS[-|P] in KO/V3B region, in which no significant difference was found among SFDS[A|P], SFDP[A|-] and MFDS[-|P]. This suggests that adaptation to disparity or shape curvature much likely occurs in KO/V3B. However, adaptation to shape curvature can be denied in KO/V3B, because there is no significant nAE difference between KO/V3B and V1-V2, while percept-involved-only conditions (MFSS[-|SP] and MFDS[-|P]) always induced a significantly smaller nAE in V1-V2 regions than in higher areas. Thus, disparity adaptation can also occur in KO/V3B to large extent.

Many previous studies showed an important role in 3D shape perception. Tyler, Likova, Kontsevich, and Wade (2006) treated KO region as an areas functionally distinct from V3B, and found the region contain information to extract depth structure. Using an ambiguous

probe stimulus with zero disparity, Preston et al. (2009) claimed neural representation in V3B/KO region related to perceived 3D shape instead of simply disparity, in term of a correspondence between fMRI rebound and behavioral repulsion effect in the region. However, other studies provided with evidences to support disparity processing in KO/V3B region. Preston et al. (2008) found that high dorsal areas, including KO/V3B, contained information of high diagnostics for perceiving disparity-defined depth. Ban, Preston, Meeson, and Welchman (2012) found that V3B/KO integrated two congruent depth cues (disparity and motion) to improve performance of depth estimation. The ADI adaptation in KO/V3B, found in our result, provides a further support for disparity processing in the region.

As mentioned above, other ROIs in addition to KO/V3B also showed a significantly larger nAE for SFSS[DA|SP] than that for SFDP[A|-]. These ROIs contain VP of early areas and all of ventro-lateral and dorsal regions except KO/V3B, but neither of SFM-related regions. Neurons in the ROIs are possibly adapted with disparity, shape curvature or PSI, which are determined with the contrast of SFSS[DA|SP] minus SFDP[A|-].

8.4.2 ADI adaptation in V7 and SFM-related regions

In accordance with the viewpoint of Howard and Ian on disparity selectivity (Howard & Rogers, 2012). Unlike luminance-selective neurons, disparity-selective neuron are exclusively selective for absolute disparity, so the response to a disparity-defined stimulus in a specific ROI results from an integration of responses from different disparity-selective neurons within the ROI. Accordingly, a spatio-temporal averaging on disparity information can occur for RDSs with dynamic disparity. Obviously, ADI involves a low-order calculation of averaging on disparity. Beside SFSS[DA|SP], both SFDS[A|P] and SFDP[A|-] may produce ADI adaptation, as shown in Table 8.1. However, ADI is unique possible adaptation sources for SFDP[A|-] but not for SFDS[A|P], which also possibly induces shape-curvature curvature.

Adaptation to ADI was found in V7 and all of SFM-related regions. Moreover, ADI was adapted with increasing amount along the path from VIPS/V7* through POIPS into DIPS, in accordance with the trend of increasing nAE induced by SFDS[A|P] across the SFM-related regions, as shown in Table 8.4.

V7 region In Table 8.4, V7 region showed a significantly larger nAE than V2 of early areas and hMT+/V5 region for SFDP[A|-] condition, which only induced ADI adaptation. This suggests that V7 region indeed involved adaptation to ADI. And there should be no ADI adaptation occurred in V2 region, considering ADI resulted from a low-order calculation.

SFM-related regions A direct evidence was found to support ADI adaptation in VIPS/V7* region. The region showed a significantly larger nAE induced by SFDP[A|-] than V3A, as shown in Table 8.4.

There are indirect evidences to support ADI adaptation in POIPS region, although SFDP[A|-] did not induced a significant difference on nAE between POIPS and any other ROI, as shown in Table 8.4. A significantly larger nAE was found for both MFSS[-|SP] and SFDS[A|P] in POIPS region than that in V2 region. However, many more regions (V1, V3, V3A) were found to be significantly different on nAE from POIPS region for SFDS[A|P] than that for MFSS[-|SP]. In the following analysis, POIPS prefers to be adapted with shape curvature rather than with PSI. Thus, in POIPS region, the different adaptation patterns between MFSS[-|SP] and SFDS[A|P] resulted from ADI adaptation to large extent.

In Table 8.4, similarly to POIPS, DIPS did not showed significant different nAE for SFDP[A|-] from any other ROI. However, the region is claimed to be adapted with ADI in our study. In the following analysis, PSI adaptation is confirmed in DIPS, yielding a significantly larger nAE in the region than only V1-V2 for both MFSS[-|SP] and MFDS[-|P]. But many more regions (V3-VP, hV4, LO, V3A, hMT+/V5) were found to be significantly different on

nAE from DIPS region for SFDS[A|P] than that for either MFSS[-|SP] or MFDS[-|P]. Thus, we thought that the pattern difference of adaptation amount results from ADI adaptation occurred in DIPS region.

ADI adaptation in dorsal areas (V7 & SFM-related areas) is consistent with the claim of Preston et al. (2008), who found a selectivity for the specific disparity content in dorsal areas. That means, under static fixation, different disparity content was responded exclusively in dorsal areas. Meanwhile, the distinct responses were averaged in real time.

8.4.3 Shape-curvature adaptation in POIPS region

Table 8.1 indicates, adaptation to shape curvature may be induced by not only SFSS[DA|SP] but also MFSS[-|SP] condition. In addition, MFDP[-|?] may involve shape-curvature adaptation due to its perceptual indifference with MFSS[-|SP] condition.

POIPS region Table 8.2 shows, in POIPS region, MFSS[-|SP] induced a significantly larger *nAE* than SFDP[A|-], although no significant difference of *nAE* was induced by SFDP[A|-] between POIPS and any other ROI in Table 8.4. We did not observe the statistical significance between MFDS[-|P] and SFDP[A|-] in POIPS region, as shown in Table 8.2 & 8.3. Meanwhile, Table 8.4 showed no significant difference on *nAE* induced by MFDS[-|P] between POIPS and any other ROI, suggesting a significant adaptation to shape curvature in POIPS region.

8.4.4 PSI adaptation in VP, hV4, LO, V7, VIPS/V7* and DIPS regions

As shown in Table 8.1, PSI adaptation may be induced in all conditions except SFDP[A|-], in which PSI scaling was used in order to eliminate adaptation to PSI. Especially, MFDS[-|P]

possibly induces unique adaptation to PSI. Besides, MFDP[-|?] may involve PSI adaptation due to its perceptual indifference with MFSS[-|SP] condition.

Adaptation to PSI was found in VP, ventro-lateral areas, V7, VIPS/V7* and DIPS. Considering PSI is invariant of size, so these regions involve size-invariant responses for disparity-defined 3D shapes to large extent. Murray, Boyaci, and Kersten (2005) published an abstract showing that size invariance was evident as early as V3 in dorsal areas but not apparent until LO region in ventral areas. Pribram (1991) claimed that V3, VP and V4 involved to extract invariance of size, color and shape. In contrast, (Cadieu et al., 2007) showed an object-related response of dependence on size and viewpoint in V4, V3A, MT, and V7 at intermediate processing stages. In the study of Sawamura, Georgieva, Vogels, Vanduffel, and Orban (2005), VIPS/V7* and DIPS showed a less size invariance than ventral shape-selective regions including LOS, post ITG and mid FG, suggesting no strong size invariance in human IPS areas.

VP region Compared with both V1 and V2, VP region showed a significantly larger nAE for MFDS[-|P] but not for any of other conditions, as shown in Table 8.4. Thus, VP should only involve adaptation to percept-related PSI. Mendola et al. (1999) showed size invariance for 2D contour-defined shape in the region. Our result extends the size invariance into disparity-defined 3D shapes.

Ventro-lateral regions Ventral visual pathway is usually thought to mediated object recognition in primate brain. hV4 region, positioned within ventral pathway, has been documented to show position invariance (Cadieu et al., 2007). However, Konen and Kastner (2008) showed object-related responses of size variance for different types (2D, 3D and line drawings) of object stimuli in hV4. In contrast, the region showed size invariance in our study. As shown in Table 8.4, we found a significant difference on nAE between hV4 and V1

for both MFSS[-|SP] and MFDS[-|P] as well as between hV4 and V2 for MFDS[-|P], so hV4 should involve adaptation to percept-related sources, especially for PSI. This result was further supported by the factor that MFDS[-|P] induced a significantly larger nAE than both SFDS[A|P] and SFDP[A|-] in hV4 region, as shown in Table 8.3. Also in hV4, MFSS[-|SP] induced a significantly larger nAE than SFDP[A|-]. However, further evidences were need to support adaptation to shape curvature in hV4 region.

Table 8.4 showed a significantly different nAE for MFDS[-|P] and SFDS[A|P] rather than for MFSS[-|SP] between LO and V1, so LO, another region positioned within ventral pathway, should also involve adaptation to PSI rather than both shape curvature and ADI, with further support that MFDS[-|P] induced a significantly larger nAE than SFDP[A|-] in LO region, as shown in Table 8.3. Furthermore, the result showed a size invariance of 3D object (shape) recognition in LO region, which has been linked into the functionality of object processing among human brain cortices. In primate brain, size invariance has been described across object-responsive human LOC and macaque IT cortex (Sawamura et al., 2005; Cadieu et al., 2007; Eger, Ashburner, Haynes, Dolan, & Rees, 2008), further verifying PSI adaptation in LO region.

V7 region Similar V4 region in ventro-lateral areas, V7 of high dorsal areas had a significantly larger nAE than early regions (V1, V2) for MFSS[-|SP], SFDS[A|P] and MFDS[-|P] conditions, as shown in Table 8.4. This suggests that adaptation to not only ADI but also percept-related sources occurred in V7 region. Here, the adaptation to PSI in V7 is inconsistent of the finding in Konen and Kastner (2008), who claimed that object-responsive activation in the region was dependent on object size.

VIPS/V7* region VIPS/V7* region has been confirmed to involve ADI adaptation induced by SFDP[A|-]. In Table 8.2 & 8.3, MFDS[-|P] induced a significantly larger nAE

than SFDP[A|-] in the region. Meanwhile, Table 8.4 shows no significant difference on nAE produced by MFSS[-|SP] between VIPS/V7* and any other region, suggesting the region involved adaptation to PSI. This result received a further secondary support that the region involved a significantly larger nAE for MFSS[-|SP] than that for SFDP[A|-], as shown in Table 8.3.

DIPS region As shown in Table 8.4, DIPS region involved a significantly larger nAE induced by MFDS[-|P] than V1-V2, suggesting a significant PSI adaptation in DIPS. For PSI adaptation in DIPS region, there are two additional evidences: 1) MFDS[-|P] induced a significantly larger nAE than SFDP[A|-] in the region, as shown in Table 8.3; and 2) MFSS[-|SP] and MFDS[-|P] induced a significantly larger nAE than only V1-V2. Accordingly, there is indeed PSI adaptation in DIPS region, where less likely involved shape curvature.

8.4.5 ROIs with undetermined adaptation mechanism

Considering that the absence of adaptation cannot simply be taken to mean that the underlying neuronal population are not selective for the chosen stimulus when to interpret null results, undetermined adaptation mechanism involved in many ROIs.

Adaptation to ADI in V3A & hMT+/V5 regions ADI adaptation has not been determined yet in V3A and hMT+/V5 regions. In Table 8.2, SFDP[A|-] induced a significantly or close to significantly smaller nAE than MFDS[-|P] in V3A region and than MFSS[-|SP] in hMT+/V5 region. However, these two regions still keep uncharted on what sources to be adapted under three considerations: 1) no significant difference of nAE was found between either of them and any of the other ROIs, as shown in Table 8.4; 2) Table 8.3 showed, in both V3A and hMT+/V5 region, no significant difference of nAE for all pairwise comparisons except that between SFSS[DA|SP] and SFDP[A|-]; 3) SFDP[A|-], involving unique adapta-

tion to ADI, induced a significant difference on nAE only between V7 and V3A as well as between VIPS/V7* and hMT/V5+, as shown in Table 8.4, so V3A and hMT+/V5 may not involve ADI adaptation at all. Therefore, the adaptation mechanism of V3A and hMT+/V5 remains open.

Adaptation to PSI in POIPS region POIPS region has been confirmed to involve adaptation to shape curvature, but it is still uncharted for whether the region is adapted with PSI. Table 8.4 showed that POIPS involved a significantly larger nAE than V2 for MFSS[-|SP], which induced a significantly larger nAE than SFDP[A|-] in the region, as shown in Table 8.2. However, there was no significant difference on nAE induced by MFDS[-|P] between POIPS and any other ROI, so it is difficult to decide whether PSI was adapted in POIPS. In Table 8.4, POIPS showed a significant larger nAE induced by SFDS[A|P] than V1-V3 and V3A, but it still fail to decide PSI adaptation in POIPS, considering uncertain ADI adaptation in the region.

Adaptation to shape curvature in VIPS, DIPS and dorsal regions Shape-curvature adaptation is also undetermined in DIPS. MFSS[-|SP] induced a significantly larger nAE than SFDP[A|-], as shown in Table 8.2 & 8.3. Unfortunately, MFDS[-|P] also induced a significantly larger nAE than SFDP[A|-], as shown in Table 8.3. Obviously, it is difficult to infer whether shape curvature is adapted in DIPS only from the current result. Based on similar reasons, VIPS also keep uncertain for shape-curvature adaptation.

Adaptation to shape curvature was found only in POIPS. However, there is no adequate evidence to support whether shape curvature is adapted in dorsal areas. All of dorsal regions showed a significantly larger nAE for SFSS[DA|SP] than that for SFDP[A|-], as shown in Table 8.3. In hMT+/V5 region, MFSS[-|SP] induced a significantly larger nAE than SFDP[A|-], as shown in Table 8.2. Also, MFSS[-|SP] induced a significantly larger nAE

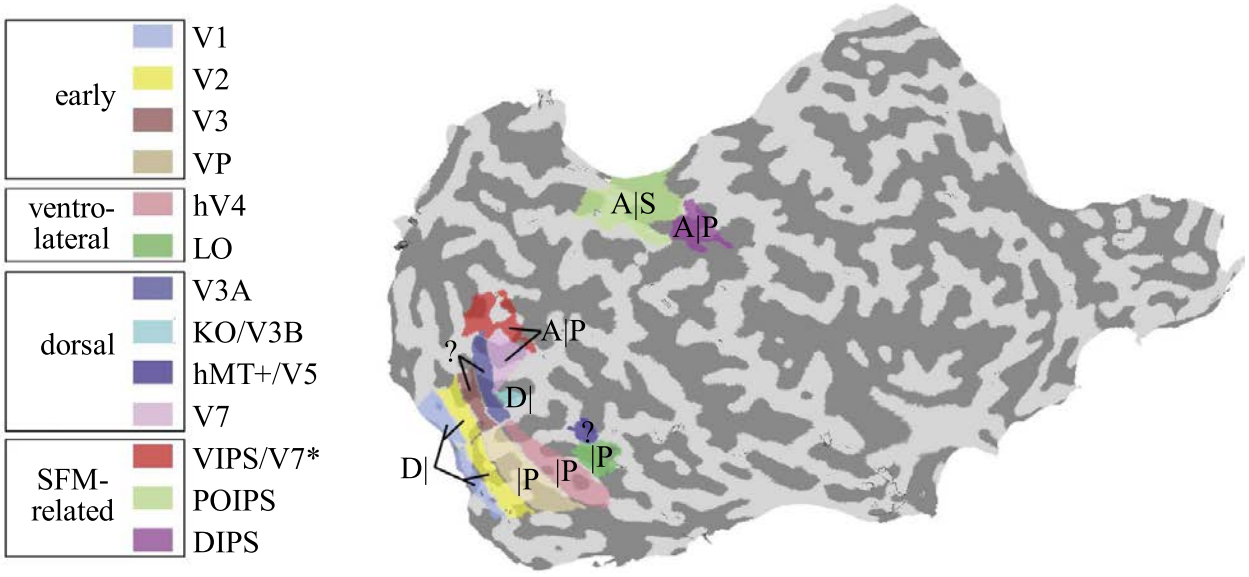

Figure 8.9 Spatial distribution of adaptation sources among ROIs. D represents for disparity adaptation, A for ADI adaptation, S for shape-curvature adaptation and P for PSI adaptation. The question mark in some ROIs means an uncharted adapting mechanism. Placed before "|", D and A belong to disparity-related sources. S and P, placed after "|", belong to percept-related sources.

in V7 region than that in V1 region, as shown in Table 8.4. Thus, we can not exclude shape-curvature adaptation in dorsal areas.

8.4.6 How adaptation sources distribute along visual pathways?

As shown in Fig. 8.9, early visual areas (V1-V2) and KO/V3B region showed adaptation to zero-order disparity. ADI also related to disparity rather percept, but it involved a low-order calculation of averaging on disparity. Thus, we did not observe a significant ADI adaptation in both early and ventral-lateral cortices but in a high dorsal V7 and all of SFM-related region (VIPS/V7*, POIPS and DIPS). Shape curvature and PSI belong to percept-related adaptation sources, which are adapted at much higher levels than disparity and ADI, as shown in Fig. 2.1. Shape curvature is size invariant, and is thought as a metrical property for 3D shapes. Adaptation to shape curvature was found only in a SFM-related POIPS

region. As a categorical property of 3D shapes, PSI is invariant of size, and adapted in ventro-lateral areas (hV4 and LO) and SFM-related areas (VIPS/V7* and DIPS).

The adaptation to PSI in VP, high dorsal areas and SFM-related areas provides a distinct understanding for object identification, which was conventionally thought to be performed in ventral (What) pathway rather than in dorsal (Where / How) pathway.

Chapter 9

Conclusion

To summarize, the dependency and the adapting mechanism of sCAE were investigated in terms of dynamic adaptation stimuli with changing location, size or PSI. Many conclusions can be drawn in our study.

Firstly, sCAE is indeed due to multi-level adaptation at both disparity-related and percept-related stages. In addition to shape curvature, the adaptation sources of sCAE at least include disparity-specified ADI and percept-specified PSI, both of which were originally investigated in our study. ADI was defined as a cumulatively averaged disparity information of each adaptation frame within test stimulus area. The ADI adaptation was obviously at a lower level than shape-curvature adaptation. PSI was defined based on SI, and invariant of size changes. Different from SI, PSI is dependent of peak-to-base distance of spherical surfaces with fixed size, suggesting that PSI is adapted at a higher level than scale-variant shape curvature. Our study showed that PSI adaptation contributed much more to sCAE than ADI adaptation. Therefore, the sCAE is to some extent the consequence of interaction between diverse levels of adaptation, like other kinds of stereoscopic aftereffects (Epstein & Morgan, 1970; Mack & Chitayat, 1970; Epstein, 1972; Adams et al., 2001).

Secondly, two parallel adapting processes coexist with different dependency on reti-

nal position for sCAE. That is, adaptation to retinal-position dependent sources, such as disparity-specified ADI, can induce retinal-position dependent sCAE, while adaptation to retinal-position independent sources, such as percept-specified shape curvature, can produce retinal-position independent sCAE shown in the study of Noest et al. (2006). Also, adaptation to size invariant PSI can produce scale independent sCAE. Besides, eccentricity effect on adaptation strength can induce the retinal-position dependent sCAE to some extent.

Thirdly, dorsal visual pathway more likely encodes depth structure metrically while ventral pathway does this categorically, in terms of the finding of PSI adaptation in ventrolateral areas and shape-curvature adaptation in SFM-related areas. Actually, there are more previous evidences to support the conclusion (Chandrasekaran et al., 2007; Preston et al., 2008). However, we also found PSI adaptation in SFM-related areas, suggesting that the size-invariant processing of identifying 3D object is not only involved in ventral areas but also in these areas.

Lastly, high dorsal areas may involve a low-order calculation of disparity averaging compared with early and middle dorsal areas, considering ADI adaptation involved in V7 and higher dorsal areas (VIPS/V7*, POIPS and DIPS).

Appendix A

Behavioral data acquisition for Experiment 3

Under static fixation, as shown in both Experiment 1 and Experiment 2, a significant stereo-curvature adaptation was found for adaptation stimuli with different types including static, size scaling and PSI scaling. However, it is not clear about whether it is true for those stimuli under pursuit, as used in Experiment 3. To this end, we conducted the psychophysical experiment, where fixation point, pursued by observers, involved a movement along a Lissajous orbit in depth.

A.1 Observers

A total of six subjects (aged from 25 to 41 yr; 3 male; ZJ, WL, YP, SH, WY, MY), including both authors, took part in the psychophysical experiment with purpose to acquire behavioral data for Experiment 3. YP, WL and WY participated in the previous psychophysical experiments including both Experiment 1 and Experiment 2. All had normal or corrected-to-normal vision including good stereoacuity. The written informed consent was obtained for all observers, who were paid for their time.

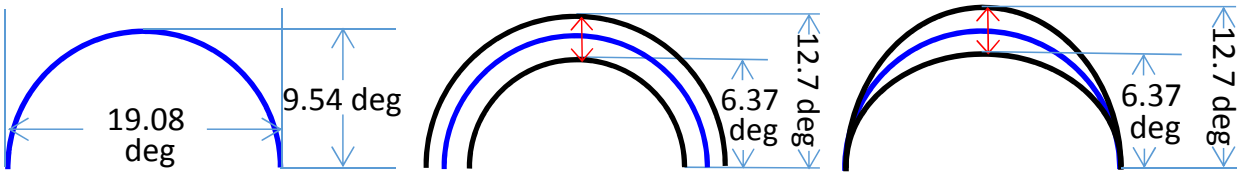

(a) MFSS condition (b) MFDS condition (c) MFDP condition

Figure A.1 Adaptation stimuli for behavioral data acquisition of Experiment 3.

A.2 Methods

A.2.1 Visual stimuli

As mentioned above, pursuit was involved in all of adaptation conditions. That means, the specific eye movement was occurred, corresponding to a in-depth Lissajous orbit along which fixation point was moving, as shown in Fig. 8.1(a). Corresponding to three stimulus types in Experiment 3, three adaptation conditions were involved in the experiment, including MFSS, MFDS and MFDP, as shown in Fig. A.1. Similar to adaptation stimuli, test stimuli were semi-cylindrical surfaces. Seven curvature levels were used as in Experiment 2.1 and Experiment 2.2. The same to our previous psychophysical experiments, the viewing distance was 66 cm.

For baseline condition, no adaptation stimuli were involved during adaptation phase, but there was still pursuit of moving fixation point along Lissajous orbit, in order to eliminate effect of the specific eye movement caused by the pursuit.

A.2.2 Procedure & adaptation measurement

The same experimental procedure was used as in Experiment 2. Here, as used in our previous psychophysical experiments, adaptation was measured as PSE difference between adaptation and baseline conditions.

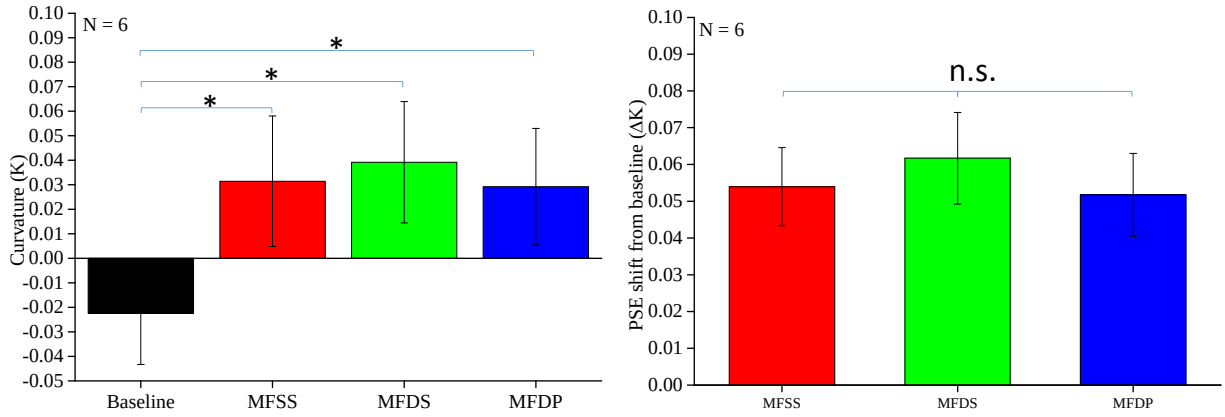

(a) Perceived curvature at PSE across all conditions

(b) Group mean of adaptation magnitude

Figure A.2 Result over all six observers for behavioral data acquisition of Experiment 3. Error bars represent standard errors of means. $*p < 0.05$

A.3 Results

The One-Way repeated measures ANOVA showed a significant main effect of condition on PSE ($F_{3,15} = 16.700,\ MSE = 0.005,\ p = 0.00,\ \eta^2 = 0.770$). As shown in Fig. A.2(a), the subsequent multiple comparison with Bonferroni adjustment showed that baseline condition was significantly smaller on PSE than MFSS condition ($p = 0.023$), MFDS condition ($p = 0.026$) and MFDP condition ($p = 0.035$). However, we did not find any statistical significance on comparison among adaptation conditions on PSE. (all $ps < 0.05$).

As shown in Fig. A.2(b), there was no significant main effect of condition on adaptation amount ($F_{2,10} = 0.927,\ MSE = 0.000,\ p = 0.427,\ \eta^2 = 0.156$).

Appendix B

Visul stimuli for mapping regions of interest

B.1 Retinotopy for early visual areas

For the early visual areas in each hemisphere, retinotopic organization with respect to the angular dimension was measured using clock-wise rotating single-wedge (width = 60 deg in polar angle width) or double-wedge (45 deg in polar angle width each). Retinotopic organization with respect to eccentricity was measured using a thin expanding ring (width = 1/6 of the maximum stimulus radius). A fixation point was shown at the center of the screen. When measured in the 3T system the maximum stimulus radius subtended 20 deg visual angle.

These stimuli produce a traveling wave of activity in retinotopically-organized areas, and the phase of activity at a given location in cortex uniquely identifies the location in space it represents. Both stimuli consisted of a contrast reversing (6 Hz for single-wedge and 8 Hz for double-wedge) black and white checkerboard structure. During each experimental scan, the single-wedges and rings passed through 10 cycles with one full stimulus cycle of 24 sec

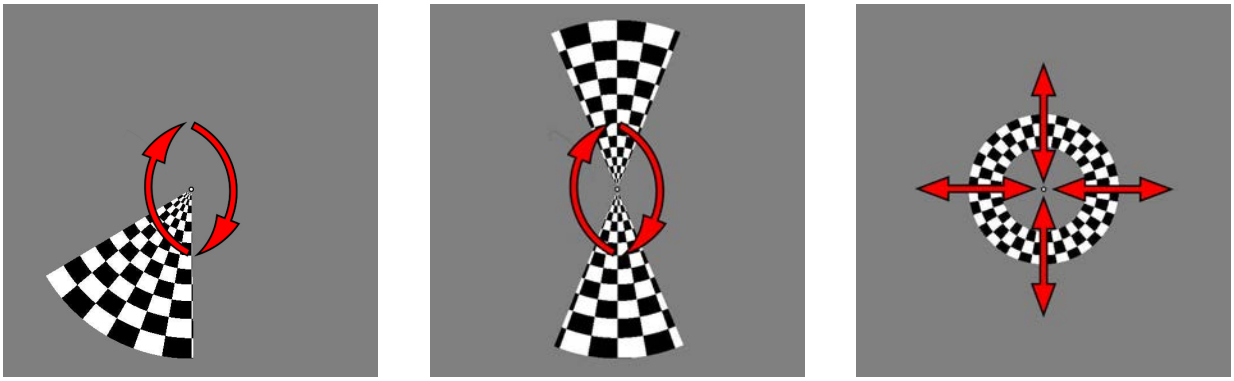

(a) SingleWedge (b) DoubleWedge (c) Eccentricity

Figure B.1 Stimuli for retinotopic mapping of early visual areas

each, while the double-wedges and rings passed through 8 cycles with one full stimulus cycle of 32 sec each. The single-wedge of polar angle was scanned in 8 separate functional runs, the double-wedge of polar angle in 10 runs, and the ring of eccentricity in 5 - 8 runs.

B.2 Localization of ROIs in ventro-lateral areas

To localize LOC areas , we used object images of 300 × 300 pixels as stimuli, which were exactly the same as used in the study of Kourtzi and Kanwisher (2000) with except of image content. There were four types of image sets of which half sets consisting of intact objects and the other half the scrambled versions of the same objects. For either half, the images of each set were either grayscale (GS) photographs or line drawing (LD) of objects. Within each image set of the same type, the images can be familiar (FM) or novel (NV) to subjects with the same possibility. The line drawings were generated by tracing the external outline and their internal contours of the objects depicted in grayscale photographs. The scrambled images were created firstly by dividing the intact images in a 20 × 20 square grid and then by scrambling the positions of each of the resulting squares. The grid lines presented both in the intact and in the scrambled images.

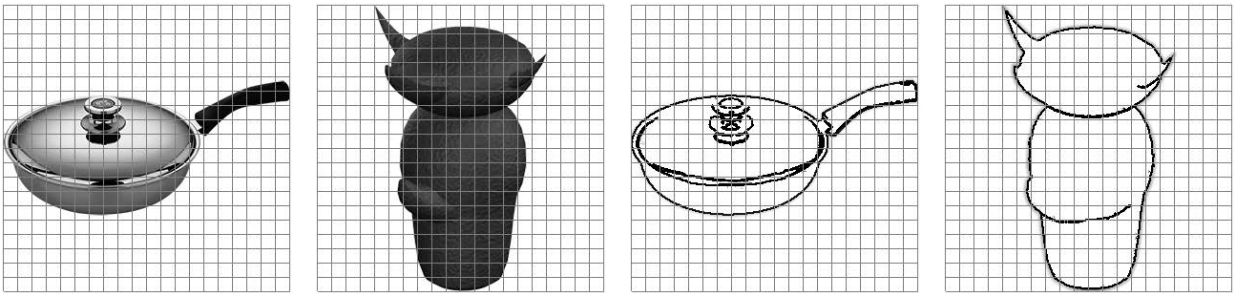

(a) GS_FM_Itact (b) GS_NV_Intact (c) LD_FM_Intact (d) LD_NV_Intact

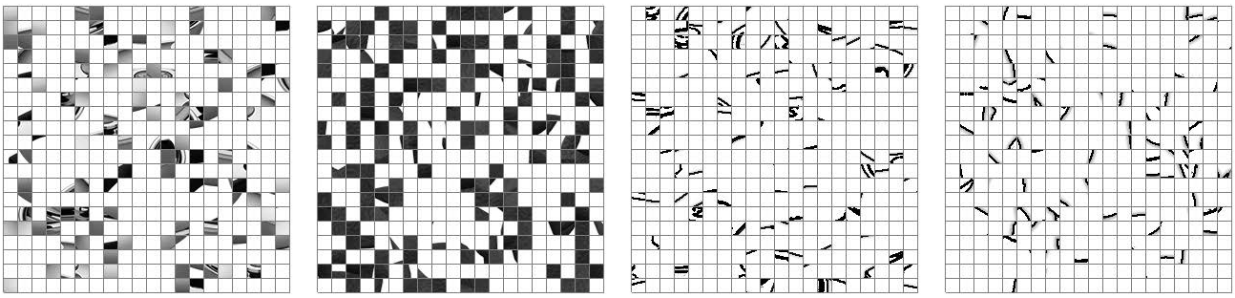

(e) GS_FM_Scramble (f) GS_NV_Scramble (g) LD_FM_Scramble (h) LD_NV_Scramble

Figure B.2 Schematic illustration of visual stimuli for LOC Localizer

A block presentation design was used. Each scan consisted of sixteen 16-sec stimulus epochs with fixation periods interleaved. Twenty different images of the same type were presented in each stimulus epoch. The observers viewed blocks of images depicting common objects (16 s per block) alternating with blocks containing scrambled versions of the same objects. Each images was presented for 250 msec with a blank interval of 550 msec between items. Each of four stimulus types was presented with balanced order in four different epochs during each functional run. The two stimulus conditions were pairwise in two-condition paradigm of INTACT - SCRAMBLE. Subjects performed a fixation task and judged whether the current presentation was familiar or not in order to maintain attention.

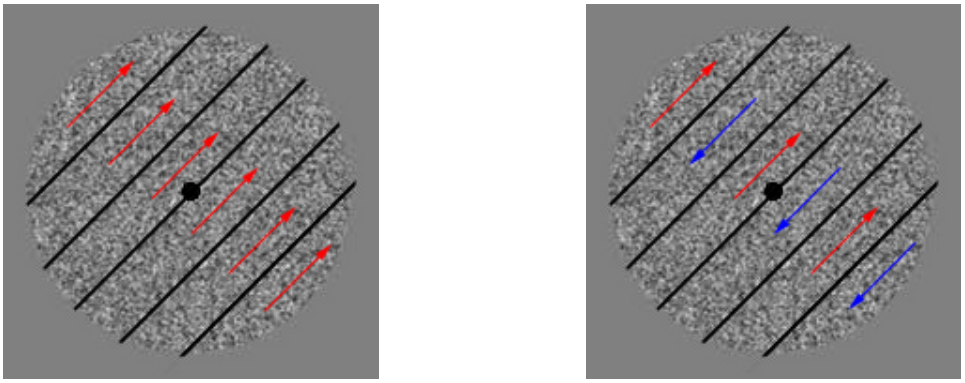

(a) UNI condition (b) GKIN condition

Figure B.3 Schematic illustration of RTP stimuli for KO/V3B Localizer

B.3 Localization of ROIs in dorsal areas

Random texture patterns (RTP) used for localizing KO/V3B area were exactly the same as those used in the studies of Dupont et al. (1997) and Van Oostende, Sunaert, Van Hecke, Marchal, and Orban (1997) with exception of motion parameters. as shown in Fig. B.3. The standard diameter measured 3 deg. Stimuli were centered on the fixation point. They were generated by modulation of random textured patterns (50 % white and dark pixel of 1 arc min) and the stripes differed in motion direction. Pixels moved at 4 deg/sec. The direction of motion was always parallel to the kinetic boundary. Pixels moved along horizontal, vertical and both oblique (45°and 135°) axes. In these stimuli, the direction of motion reversed every 427 ms, while a new axis of motion was randomly selected every 854 ms. In the kinetic gratings, this change was coupled to the change in motion axis since the pixels always moved parallel to the kinetic boundary. It should be noted that locally the motion was exactly the same in the two conditions; the rate of change in motion direction was also the same in these two types of stimuli. In the two conditions, shape cannot easily be disentangled since comparing kinetic gratings with uniform motion isolates shape. The two stimulus conditions

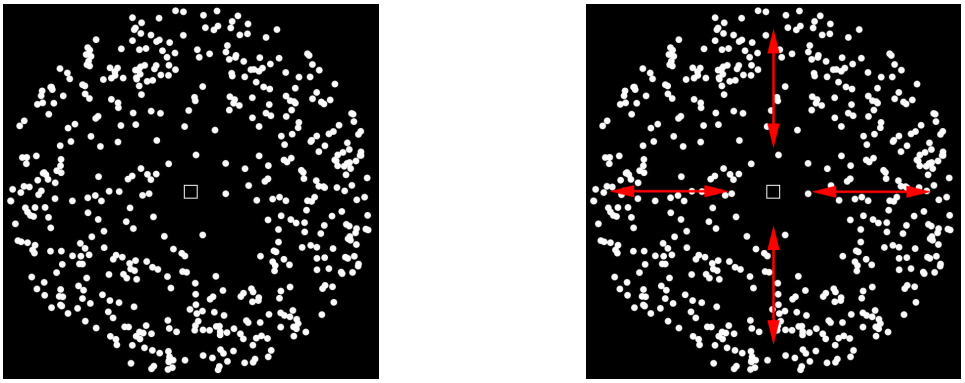

(a) STATIC condition (b) MOTION condition

Figure B.4 Schematic illustration of visual stimuli for hMT+/V5 Localizer

were pairwise in two-condition paradigm of GKIN - UNI. Subjects performed a fixation task and remained passive to the stimuli.

hMT+/V5 area was functionally identified based on reponses to stimuli that alternate in time between moving and stationary dot pattern as shown in B.4. The stimuli were almost the same as those used by Huk, Dougherty, and Heeger (2002). Moving dots traveled toward and away from fixation (8 deg/sec) within a 21 deg diameter circular aperture, alternating direction once per two seconds (white dots on a black background; dot diameter of 0.25 deg).

The localizer was performed using a block-design fMRI localizer scan. There was a field switch every 18 sec between moving and stationary dot for hMT+/V5 localizer. This moving/stationary cycle was repeated seven times in each fMRI time series. The two stimulus conditions were pairwise in two-condition paradigm of MOTION - STATIC. Subjects performed a fixation task and remained passive to the stimuli. Each run started and ended with a 16-s fixation interval so as to avoid noise data introduced into stimulus epoch due to instability of MRI scanner.

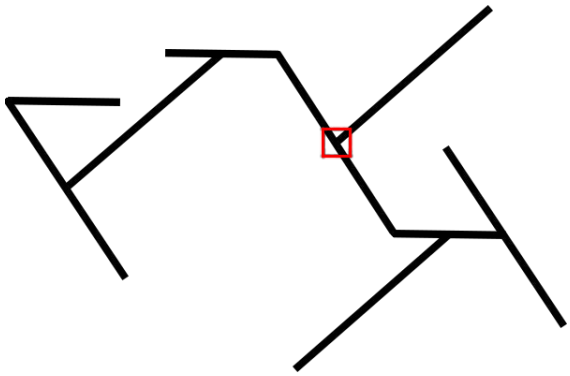

Figure B.5 Schematic illustration of RLP stimuli for localizing SFM-related areas

B.4 Localization of SFM-related ROIs in IPS areas

To localize SFM-related areas, we presented exactly the same type of monocular stimuli as in the study of Orban, Sunaert, Todd, Van Hecke, and Marchal (1999) and Vanduffel et al. (2002). These random line pattern (RLP) consisted of nine interconnected line segments, which, when appearing three-dimensional, formed rectangular angles. There were also two conditions of three-dimensional rigid displays, with one condition (SFS) only involving static cue for 3D structure perception while the other (SFM) condition containing both static and motion cues. In contrast to the previous studies, the stimuli moved in fixation plane during the SFS condition, including translating along horizontal and vertical axis as well as rotating along depth axis. In SFM condition, the stimuli also moved in fixation plane including translation along horizontal and vertical axes. Moreover, the stimuli rotated in depth for 3D shape from motion, including rotation along horizontal and vertical axes. Here, all the motion was three-dimensional rigid display. The translation and rotation of the rigid object were always at the same speed but in randomly selected direction. The two stimulus conditions were pairwise in two-condition paradigm of SFM - SFS. Subjects performed a fixation task and remained passive to the stimuli.

Appendix C

List of Abbreviations

A	ADI, p. 97
ACC	Average_Concave condition in Experiment 1, p. 27
ACV/FS	Average_Concave/Fixed_Size condition in Experiment 1, p. 27
ADI	average disparity information, p. 11
AE	adaptation effects, p. 75
AF	Average_Flat condition in Experiment 1, p. 27
ANOVA	analysis of variance, p. 33
BOLD	blood oxygenation level-dependent signal, p. 67
D	disparity, p. 97
DIPS	dorsal intraparietal sulcus, p. 61
DPSI	Dynamic_PSI condition in Experiment 2.3, p. 44

DS Dynamic_Size condition in Experiment 1, p. 27

FA flip angle, p. 66

fMRIa functional magnetic resonance imaging adaptation, p. 61

FOV field of view, p. 66

FWHM full width at half maximum, p. 73

GLM general linear model, p. 73

hMT+/V5 human middle temporal complex, p. 119

ISI inter-stimulus interval condition, p. 29

ITI inter-trial interval, p. 71

KO/V3B kinetic occipital region, p. 118

LO lateral occipital cortex, p. 60

LOC lateral occipital complex, p. 116

MFDP MoveFixDynamicPSI condition in Experiment 3, p. 70

MFDS MoveFixDynamicScale condition in Experiment 3, p. 70

MFSS MoveFixStaticStim condition in Experiment 3, p. 70

nAE normalized adaptation effect, p. 76

P PSI, p. 97

POIPS parieto-occipital intraparietal sulcus, p. 61

PSC percent signal change, p. 75

PSE point of subjective equality, p. 32

PSI primitive shape index, p. 14

RDS random-dot stereograms, p. 27

RLP random line pattern, p. 120

ROIs regions of interest, p. 66

RTP random texture pattern, p. 118

S shape curvature, p. 97

sCAE stereo-curvature aftereffect, p. 19

sDAE stereo-depth aftereffect, p. 19

SFDP StaticFixDynamicPSI condition in Experiment 3, p. 70

SFDS StaticFixDynamicScale condition in Experiment 3, p. 70

SFM shape from motion, p. 120

SFSS StaticFixStaticStim condition in Experiment 3, p. 70

SI shape index, p. 13

sSAE stereo-slant aftereffect, p. 19

TE time to echo, p. 66

TR time to repeat, p. 66

VIPS/V7* ventral intraparietal sulcus, p. 61

VP ventral posterior cortex, p. 58

References

Adams, W. J., Banks, M. S., & Van Ee, R. (2001). Adaptation to three-dimensional distortions in human vision. *Nature neuroscience*, *4*(11), 1063–1064.

Anderson, B. L. (1992). Hysteresis, cooperativity, and depth averaging in dynamic random-dot stereograms. *Perception & Psychophysics*, *51*(6), 511-528.

Andresen, D. R., Vinberg, J., & Grill-Spector, K. (2009). The representation of object viewpoint in human visual cortex. *NeuroImage*, *45*(2), 522-536.

Balch, W., Milewski, A. E., & Yonas, A. (1977). Mechanisms underlying the slant aftereffect. *Perception & Psychophysics*, *21*(6), 581–585.

Ban, H., Preston, T. J., Meeson, A., & Welchman, A. E. (2012). The integration of motion and disparity cues to depth in dorsal visual cortex. *Nature Neuroscience*, *15*(4), 636-643.

Berends, E. M., & Erkelens, C. J. (2001a). Adaptation to disparity but not to perceived depth. *Vision research*, *41*(7), 883–892.

Berends, E. M., & Erkelens, C. J. (2001b). Strength of depth effects induced by three types of vertical disparity. *Vision Research*, *41*(1), 37-45.

Berends, E. M., Erkelens, C. J., & Van Ee, R. (2000). Adaptation to oscillating disparity. In *Perception ECVP abstract supplement* (Vol. 29, p. 27). Pion Ltd.

Berends, E. M., Liu, B., & Schor, C. M. (2005). Stereo-slant adaptation is high level and does not involve disparity coding. *Journal of Vision*, *5*(1), 71–80.

Bergman, R., & Gibson, J. J. (1959). The negative after-effect of the perception of a surface slanted in the third dimension. *The American Journal of Psychology*, *72*(3), 364–374.

Blakemore, C. B., & Julesz, B. (1971). Stereoscopic depth aftereffect produced without monocular cues. *Science*, *171*, 286–288.

Boynton, G. M., & Finney, E. M. (2003). Orientation-specific adaptation in human visual

cortex. *Journal of Neuroscience*, *23*(25), 8781-8787.

Brainard, D. H. (1997). The Psychophysics Toolbox. *Spatial Vision*, *10*(4), 433–436.

Cadieu, C. F., Kouh, M., Pasupathy, A., Connor, C. E., Riesenhuber, M., & Poggio, T. A. (2007). A model of v4 shape selectivity and invariance. *Journal of Neurophysiology*, *98*(3), 1733-1750.

Champion, R. A., Simmons, D. R., & Mamassian, P. (2004). The influence of object size and surface shape on shape constancy from stereo. *Perception*, *33*(2), 237-247.

Chandrasekaran, C. F., Canon, V., Dahmen, J. C., Kourtzi, Z., & Welchman, A. E. (2007). Neural correlates of disparity-defined shape discrimination in the human brain. *Journal of Neurophysiology*, *97*(2), 1553-1565.

Cottereau, B. R., Ales, J. M., & Norcia, A. M. (2014). The evolution of a disparity decision in human visual cortex. *NeuroImage*, *92*, 193-206.

Cottereau, B. R., McKee, S. P., Ales, J. M., & Norcia, A. M. (2012). Disparity-specific spatial interactions: Evidence from eeg source imaging. *Journal of Neuroscience*, *32*(3), 826-840.

DeAngelis, G. C., & Uka, T. (2003). Coding of horizontal disparity and velocity by mt neurons in the alert macaque. *Journal of Neurophysiology*, *89*(2), 1094-1111.

Domini, F., Adams, W. J., & Banks, M. S. (2001). 3D after-effects are due to shape and not disparity adaptation. *Vision research*, *41*(21), 2733–2739.

Duke, P. A., & Wilcox, L. M. (2003). Adaptation to vertical disparity induced-depth: implications for disparity processing. *Vision Research*, *43*, 135–147.

Dupont, P. J., De Bruyn, B., Vandenberghe, R. R. C., Rosier, A. M., Michiels, J. L. P., Marchai, G. J., et al. (1997). The kinetic occipital region in human visual cortex. *Cerebral Cortex*, *7*(3), 283-292.

Durand, J. B., Peeters, R. R., Norman, J. F., Todd, J. T., & Orban, G. A. (2009). Parietal

regions processing visual 3d shape extracted from disparity. *NeuroImage*, *46*(4), 1114-1126.

Eger, E., Ashburner, J. S., Haynes, J. D., Dolan, R. J., & Rees, G. (2008). fmri activity patterns in human loc carry information about object exemplars within category. *Journal of Cognitive Neuroscience*, *20*(2), 356-370.

Epstein, W. (1972). Adaptation to uniocular image magnification: Is the underlying shift proprioceptive? *Perception & Psychophysics*, *11*, 89–91.

Epstein, W., & Morgan, C. L. (1970). Adaptation to uniocular image magnification: Modification of the disparity-depth relationship. *The American Journal of Psychology*, *83*(3), 322-329.

Freud, E., Ganel, T., & Avidan, G. (2013). Representation of possible and impossible objects in the human visual cortex: Evidence from fmri adaptation. *NeuroImage*, *64*(1), 685-692.

Georgieva, S. S., Peeters, R. R., Kolster, H., Todd, J. T., & Orban, G. A. (2009). The processing of three-dimensional shape from disparity in the human brain. *Journal of Neuroscience*, *29*(3), 727-742.

Gibson, J. J. (1933). Adaptation, after-effect and contrast in the perception of curved lines. *Journal of Experimental Psychology*, *16*(1), 1-31.

Grill-Spector, K., Henson, R. N. A., & Martin, A. (2006). Repetition and the brain: Neural models of stimulus-specific effects. *Trends in Cognitive Sciences*, *10*(1), 14-23.

Grill-Spector, K., Kushnir, T., Edelman, S. Y., Avidan, G., Itzchak, Y., & Malach, R. S. (1999). Differential processing of objects under various viewing conditions in the human lateral occipital complex. *Neuron*, *24*(1), 187-203.

Grill-Spector, K., & Malach, R. S. (2001). fmr-adaptation: A tool for studying the functional properties of human cortical neurons. *Acta Psychologica*, *107*(1-3), 293-321.

Howard, I. P., & Rogers, B. J. (2012). *Perceiving in Depth* (Vol. 2). Oxford University Press.

Huk, A. C., Dougherty, R. F., & Heeger, D. J. (2002). Retinotopy and functional subdivision of human areas mt and mst. *Journal of Neuroscience*, *22*(16), 7195-7205.

Janssen, P., Vogels, R., & Orban, G. A. (2000). Three-dimensional shape coding in inferior temporal cortex. *Neuron*, *27*(2), 385-397.

Kleiner, M., Brainard, D. H., & Pelli, D. G. (2007). What's new in psychtoolbox-3? In *Perception ECVP abstract supplement* (Vol. 36). Pion Ltd.

Knapen, T. H. J., & Van Ee, R. (2006). Slant perception, and its voluntary control, do not govern the slant aftereffect: Multiple slant signals adapt independently. *Vision Research*, *46*(20), 3381-3392.

Koenderink, J. J. (1990). *Solid shape*. Cambridge, MA, USA: MIT Press.

Köhler, W., & Emery, D. A. (1947). Figural After-Effects in the Third Dimension of Visual Space. *The American Journal of Psychology*, *60*(2), 159–201.

Konen, C. S., & Kastner, S. (2008). Two hierarchically organized neural systems for object information in human visual cortex. *Nature Neuroscience*, *11*(2), 224-231.

Kourtzi, Z., & Kanwisher, N. G. (2000). Cortical regions involved in perceiving object shape. *Journal of Neuroscience*, *20*(9), 3310-3318.

Kourtzi, Z., & Kanwisher, N. G. (2001). Representation of perceived object shape by the human lateral occipital complex. *Science*, *293*(5534), 1506-1509.

Larsson, J., & Smith, A. T. (2012). Fmri repetition suppression: Neuronal adaptation or stimulus expectation? *Cerebral Cortex*, *22*(3), 567-576.

Leopardi, P. C. (2006). A partition of the unit sphere into regions of equal area and small diameter. *Electronic Transactions on Numerical Analysis*, *25*, 309–327.

Long, N., & Over, R. (1973). Stereoscopic depth aftereffects with random-dot patterns.

Vision Research, *13*(7), 1283 - 1287.

Mack, A., & Chitayat, D. (1970). Eye-dependent and disparity adaptation to opposite visual-field rotations. *The American Journal of Psychology*, *83*(3), 352-371.

Mendola, J. D., Dale, A. M., Fischl, B. R., Liu, A. K., & Tootell, R. B. H. (1999). The representation of illusory and real contours in human cortical visual areas revealed by functional magnetic resonance imaging. *Journal of Neuroscience*, *19*(19), 8560-8572.

Mitchell, D. E., & Baker, A. G. (1973). Stereoscopic aftereffects: evidence for disparity-specific neurones in the human visual system. *Vision research*, *13*(12), 2273–2288.

Murray, S. O., Boyaci, H., & Kersten, D. J. (2005). The emergence of object size invariance in the human visual cortex. *Journal of Vision*, *5*(8).

Neri, P., Bridge, H., & Heeger, D. J. (2004). Stereoscopic processing of absolute and relative disparity in human visual cortex. *Journal of Neurophysiology*, *92*(3), 1880-1891.

Noest, A. J., Van Ee, R., & Van Den Berg, A. V. (2006). Direct extraction of curvature-based metric shape from stereo by view-modulated receptive fields. *Biological Cybernetics*, *95*(5), 455-486.

Orban, G. A. (2008). Three-Dimensional Shape: Cortical Mechanisms of Shape Extraction. In *The senses: A comprehensive reference* (pp. 245–274). Oxford: Elsevier Press.

Orban, G. A., Sunaert, S. G., Todd, J. T., Van Hecke, P. E., & Marchal, G. J. F. (1999). Human cortical regions involved in extracting depth from motion. *Neuron*, *24*(4), 929-940.

Pelli, D. G. (1997). The VideoToolbox software for visual psychophysics: transforming numbers into movies. *Spatial Vision*, *10*(4), 437–442.

Poggio, G. F., González, F. J. P., & Krause, F. (1988). Stereoscopic mechanisms in monkey visual cortex: Binocular correlation and disparity selectivity. *Journal of Neuroscience*, *8*(12), 4531-4550.

Poom, L., & Börjesson, E. (1999). Perceptual depth synthesis in the visual system as revealed by selective adaptation. *Journal of Experimental Psychology: Human Perception and Performance*, *25*(2), 504-517.

Preston, T. J., Kourtzi, Z., & Welchman, A. E. (2009). Adaptive estimation of three-dimensional structure in the human brain. *Journal of Neuroscience*, *29*(6), 1688-1698.

Preston, T. J., Li, S., Kourtzi, Z., & Welchman, A. E. (2008). Multivoxel pattern selectivity for perceptually relevant binocular disparities in the human brain. *Journal of Neuroscience*, *28*(44), 11315-11327.

Pribram, K. H. (1991). *Brain and perception : holonomy and structure in figural processing.* Lawrence Erlbaum Associates.

Prince, S. J. D., Cumming, B. G., & Parker, A. J. (2002). Range and mechanism of encoding of horizontal disparity in macaque v1. *Journal of Neurophysiology*, *87*(1), 209-221.

Rogers, B. J., & Cagenello, R. (1989). Disparity curvature and the perception of three-dimensional surfaces. *Nature*, *339*(6220), 135-137.

Rohaly, A. M., & Wilson, H. R. (1994). Disparity averaging across spatial scales. *Vision Research*, *34*(10), 1315-1325.

Ryan, C. L., & Gillam, B. J. (1993). A proximity-contingent stereoscopic depth aftereffect: evidence for adaptation to disparity gradients. *Perception*, *22*, 403–418.

Sawamura, H., Georgieva, S. S., Vogels, R., Vanduffel, W. V., & Orban, G. A. (2005). Using functional magnetic resonance imaging to assess adaptation and size invariance of shape processing by humans and monkeys. *Journal of Neuroscience*, *25*(17), 4294-4306.

Sayres, R. A., & Grill-Spector, K. (2006). Object-selective cortex exhibits performance-independent repetition suppression. *Journal of Neurophysiology*, *95*(2), 995-1007.

Sereno, M. I., Dale, A. M., Reppas, J. B., Kwong, K., Belliveau, J. W., Brady, T. J., et al. (1995). Borders of multiple visual areas in humans revealed by functional magnetic

resonance imaging. *Science*, *268*(5212), 889-893.

Smallman, H. S., & MacLeod, D. I. A. (1997). Spatial scale interactions in stereo sensitivity and the neural representation of binocular disparity. *Perception*, *26*(8), 977–994.

Smith, A. T., & Wall, M. B. (2008). Sensitivity of human visual cortical areas to the stereoscopic depth of a moving stimulus. *Journal of Vision*, *8*(10).

Tanabe, S., Doi, T., Umeda, K., & Fujita, I. (2005). Disparity-tuning characteristics of neuronal responses to dynamic random-dot stereograms in macaque visual area v4. *Journal of Neurophysiology*, *94*(4), 2683-2699.

Taya, S., Sato, M., & Nakamizo, S. (2005). Stereoscopic depth aftereffects without retinal position correspondence between adaptation and test stimuli. *Vision research*, *45*(14), 1857–1866.

Te Pas, S. F., Rogers, B. J., & Ledgeway, T. (1997). A curvature contrast effect for stereoscopically-defined surfaces. *Perception*, *26*, 30.

Tyler, C. W., Likova, L. T., Kontsevich, L. L., & Wade, A. R. (2006). The specificity of cortical region ko to depth structure. *NeuroImage*, *30*(1), 228-238.

Van Der Kooij, K., Domini, F., & Te Pas, S. F. (2011). Surface boundaries do not constrain a depth aftereffect. *Vision research*, *51*(1), 138–146.

Vanduffel, W. V., Fize, D., Peuskens, H., Denys, K., Sunaert, S. G., Todd, J. T., et al. (2002). Extracting 3d from motion: Differences in human and monkey intraparietal cortex. *Science*, *298*(5592), 413-415.

Van Oostende, S., Sunaert, S. G., Van Hecke, P. E., Marchal, G. J. F., & Orban, G. A. (1997). The kinetic occipital (ko) region in man: an fmri study. *Cerebral Cortex*, *7*(7), 690-701.

Vreven, D. L. (2006). 3d shape discrimination using relative disparity derivatives. *Vision Research*, *46*(25), 4181-4192.

Weiner, K. S., Sayres, R. A., Vinberg, J., & Grill-Spector, K. (2010). fmri-adaptation and category selectivity in human ventral temporal cortex: Regional differences across time scales. *Journal of Neurophysiology*, *103*(6), 3349-3365.